INVESTIGATION OF TRACE U-236 CONTENT VARIATION IN WORLD-WIDE GEOLOGIC URANIUM DEPOSITS

A Dissertation

by

COREY C. KEITH

Submitted to the Office of Graduate and Professional Studies of
Texas A&M University
in partial fulfillment of the requirements for the degree of

DOCTOR OF PHILOSOPHY

Chair of Committee,	William Charlton
Committee Members,	Craig Marianno
	Sunil Chirayath
	Brent Miller
Head of Department,	Yassin Hassan

May 2016

Major Subject: Nuclear Engineering

ABSTRACT

Nuclear signatures, whether for forensics or safeguards applications, utilize two broad classes: comparative and predictive. While comparative methods analyze a sample against a database of previously measured samples, predictive signatures utilize the underlying physics of the system to draw conclusions about the origin of the sample. Both sets of signatures would ideally be used for any thorough analysis; however, for uranium ore concentrate (UOC) the use of predictive signatures has been scarce. This work evaluates the potential use of ^{236}U variation in uranium ores as a predictive signature for UOC.

Improvements in accelerator mass spectrometry (AMS) have allowed variations to be seen in measurements of ^{236}U for a variety of ore samples. Work was done to evaluate the current capabilities/limitations of AMS systems in regards to ^{236}U measurements. The abundance sensitivity was shown to be the primary limitation for AMS measurements, as some evaluated systems have a cutoff above the natural range of ^{236}U. Improvements in sensitivity can lower precision, and further work is needed to determine potential bias between AMS systems. The physics of ^{236}U production was evaluated next, and it was determined that the primary production pathway was neutron capture of ^{235}U. A model was created to simulate the variations in neutron capture whether through changes in neutron yield and flux. Benchmarking of the model was performed against a set of measured samples, with an average deviation of approximately 40%.

Data analysis was performed using Bayesian methods, due to the incorporation of uncertainty in the parameters and use of additional data through prior distributions. Class selection was performed for uranium mineralization and deposition. In both cases, true positive results were only found for a fraction of the samples. However, the analysis indicated a low false positive rate (important in nuclear forensics). Parameter estimation was also evaluated and showed promise in individually analyzing an element of interest, although computation time and model error will be limiting factors. While each of these capabilities shows promise, work needs to be performed to validate the techniques by utilizing a larger and better characterized data set.

ACKNOWLEDGEMENTS

Numerous individuals deserve recognition for the part they played in the completion of this research. I would like to thank Dr. William Charlton for the years of advice and wisdom he has provided as my advisor. I would also like to thank my other committee members: Dr. Sunil Chirayath, for his time and assistance on this research and in many other areas of nuclear engineering; Dr. Craig Marianno, who's teaching and advice has provided many opportunities in my future career; and Dr. Brent Miller, who provided a foundation in geology. I appreciate all the input and advice each one of you have given. I would also like to thank Claudio Gariazzo, who has allowed me to gain valuable experiences while traveling the world; as well as all the professional staff and students of NSSPI, who's support was invaluable to the completion of my research.

Conclusion of this work would also not have been possible without the staff at LLNL. Specifically, Dr. Scott Tumey who was an integral part for the measurement campaigns to be conducted and Dr. Ian Hutcheon who provided UOC samples to be measured.

Finally to my parents, Rob and Liz: my deepest appreciation for the innumerable sacrifices that have been made to help me to this point in my life.

TABLE OF CONTENTS

LIST OF FIGURES

Page

Page

Page

LIST OF TABLES

Page

Page

I. INTRODUCTION

Uranium ore concentrate (UOC), a product of uranium ore that is mined and milled prior to conversion, is a fungible commodity that is traded on the worldwide market for beneficial civilian purposes. It can also be an attractive material for diversion or illicit trafficking, with several such incidents being recorded by the International Atomic Energy Agency (IAEA) [1]. Due to these concerns, analysis techniques are being developed to regulate the use and movement of UOC around the world. Nuclear forensics, which attempts to identify source information for an unknown nuclear sample, can be an important component of the analysis.

Nuclear forensics for UOC primarily evaluates signatures (i.e. physical, chemical, or nuclear) that could potentially distinguish source information about the ore. This may include information about the geologic setting, deposition geochemistry, or mining/milling methodology among others. Several types of signatures are being investigated: elemental and anionic impurity content [2],[3],[4],[5], isotopics of common decay chains [6],[2],[7], and uranium isotopics [8]. It is important to note that not one unique signature currently being investigated is sufficient to identify a specific mine with complete certainty, and rather it is important to develop a range of signatures that can be utilized for an unknown UOC sample. The primary goal of this research is to determine the feasibility of including uranium isotopic signatures, specifically ^{236}U, in a nuclear forensics methodology to help narrow down the source location. In general, two approaches exist to utilize ^{236}U signatures in UOC: comparative and predictive.

I.1. Comparative/Predictive Approach

The comparative approach for UOC includes matching characteristics of the ore for the unknown sample to the same characteristics of a known sample set. Identifying the unknown sample involves either a point-to-point comparison or a point-to-population comparison using comparative signatures [9]. Point-to-point comparisons are uncommon, and typically only used to rule out a specific known source. Ideally, point-to-population comparisons would be used, utilizing a database of samples from a range of mines and production sites with the desired material characteristics measured. Once the database is developed, statistical

methods can be deployed to match an unknown signature of the sample to a subset of known samples. By extension, depending on the subset size, the location of the unknown sample can be inferred to correlate with the subset sample locations. The advantage of the comparative approach is that the mechanisms governing variation of UOC signatures do not need to be fully understood. It also offers the highest potential to identify the production location, providing the database includes a sample from that location. The disadvantage of this approach is the impossibility of including relevant data for every potential mine (whether it be dormant, operating, or speculative) in the database. In the case where an unknown sample location is not included in the database, this approach will fail.

The objective of the predictive approach is to calculate the signatures of the UOC through an understanding of the production mechanisms and pathways. The mechanisms evaluated can comprise of isotopic and chemical fractionation, particle capture and fission reactions, and radioactive decay among others [9]. Predictive signatures of an unknown sample, through an understanding of the underlying mechanisms, can be used to estimate characteristics of the production site. The advantage of the predictive approach is that samples from a specific mine/production site do not need to be measured to be included in the analysis. It effectively fills in the gaps that are inherent in the comparative approach. One disadvantage of the predictive approach, however, is that significant work needs to be done to model and validate the production of the signatures of interest to be properly utilized. Another disadvantage is that this approach only evaluates characteristics of the source mine that influence the predictive signatures, rather than the mine itself. In most cases, the predictive approach can only narrow the source location to a subset of mines that potentially all share similar characteristics. Comparisons between comparative and predictive approaches suggest both are complimentary to each other. Ideally any nuclear forensics analysis would utilize a mixture of both comparative and predictive approaches.

I.2. Research Goals

The objective of this work was to assess the feasibility of using the content of ^{236}U in an unknown uranium ore concentrate (UOC) to determine its origin. A number of factors needed to be evaluated to determine if ^{236}U can be used as an isotopic tracer. The first step

was to characterize relevant uranium ore bodies to determine relationships between geochemical properties and measured ^{236}U content. From there, it could be determined if uranium deposits have unique $^{236}U/^{238}U$ ratios (isotopic signatures), and if the content variation is large enough for measurements to be able to distinguish. The next goal was to define the production/loss mechanisms for ^{236}U production and to construct a model for the nuclide production in a natural uranium ore body. Simulations using the model are performed to predict ^{236}U concentrations for various ore bodies for which samples exist, and comparisons are made. This step can be iterated on when more data becomes available to refine the model. The ^{236}U measurement capabilities of AMS systems also need to be evaluated. The abundance sensitivities and potential bias for inter-laboratory comparisons between systems would ideally be quantified (factoring in sample preparation techniques and different measurement methodologies). Finally, different analysis procedures were investigated, including Bayesian analysis, to determine uranium deposit attributes (uranium mineralogy, deposit classification, parameter fluctuations, etc.) from the ^{236}U measurements.

I.3. Previous Efforts

The idea of using uranium isotopics as nuclear forensics signatures is not a unique concept for this work. Variations in both the ^{234}U and ^{235}U content for uranium ores have been investigated for the potential use in nuclear forensics [8], [10]. Primarily, work has gone into using the $^{234}U/^{238}U$ ratio as part of a suite of signatures for UOC databases including: trace anion analysis [4], lead and strontium isotope ratios [7], and rare earth element (REE) signatures [5]. However, the issues related to utilizing only the comparative approach (dependence on a complete database) have not been adequately addressed in the open literature. Some authors have identified the use of ^{236}U, through AMS measurement campaigns, as a possible predictive signature [11], [12]. Specifically, work has been performed by Wilcken to measure ^{236}U concentrations in selected UOC samples [13]. Estimations of subsurface production were also evaluated for ^{236}U, to evaluate possible parameters accounting for the variation.

The need for estimation of subsurface production rates for various radionuclides dates back many years. Use of radionuclides for age dating and tracing hydrogeologic processes can not

only be limited by detection capability, but by uncertainties in subsurface production estimates. In 1988, significant work was performed by Fabryka-Martin to estimate production rates of radionuclides in the subsurface, specifically ^{36}Cl and ^{129}I [14]. Analytical calculations were used to estimate neutron and radioisotope production rates, utilizing energy independent cross sections, which provided the foundation for the work done on the current model. Advances in the analytical estimations for radioisotope production rates in the subsurface have also been updated as recent as 1992, for use in the Alligator Rivers Analogue Project [15]. Improvements consisted of use of evaluated cross sections through MCNP [16], although calculations for neutron sources were not significantly altered. Variations of the same calculations have also been performed with similar results [17], [18].

While significant work has gone into comparative nuclear forensics signatures for UOC, little has been done to investigate possible predictive signatures as a compliment. Indications of using ^{236}U as a predictive signature has shown promise, through measurement campaigns and calculated production rates. However, a systematic method for analysis of UOC samples through an integrated production model and sophisticated data analysis techniques has not been fully explored. The objective of this work is to demonstrate the feasibility of such a system and to identify gaps and obstacles for full implementation.

II. BACKGROUND

II.1. Properties of Uranium Ores

Uranium consists of four naturally occurring isotopes (^{238}U, ^{235}U, ^{234}U, and ^{236}U), with multiple oxidation states. Variations in uranium isotopics are unique in that both chemical (redox interactions) and nuclear processes (decay and volume-fractionation) play an important role. The uranium chemistry will affect the speciation (uranium mineralogy), and consequently, the elemental concentrations influencing the neutron flux in the ore. The isotopics of the uranium, as well as the daughter products, also impact the natural neutron flux in the ore. It is therefore important to understand the unique geochemical and nuclear properties of uranium ores in order to properly model ^{236}U production.

II.1.1. Chemical Properties

Four oxidation states are known for uranium ions in aqueous solutions (+III to +VI) which usually exist as U^{+3}, U^{+4}, UO_2^{+}, and UO_2^{+2} [19]. Under oxidizing conditions, uranium is primarily present in the hexavalent (VI) state, which can form highly mobile soluble complexes (primarily with carbonates) [20]. In a reducing environment, however, uranium will primarily occur in the tetravalent (IV) state. U^{+4} tends to form relatively insoluble complexes and have higher sorption kinetics compared to the hexavalent state [20].

This multivalence nature of uranium (along with the high solubility of hexavalent uranium) can lead to the formation of a high number of uranium minerals. Uranium mineralogy is typically grouped into two main categories: primary mineralization and secondary mineralization [21]. The two categories of minerals are based on the dominating valence state of uranium in the chemical species. Primary uranium minerals have tetravalent uranium as the dominant valence state while secondary uranium minerals have hexavalent uranium as the valence state [21]. Table II.1 shows the common primary and secondary uranium minerals that can be present in ore deposits.

Table II.1: Types of uranium minerals [22].

Uranium Ore Mineral Type	**Chemical Composition**
Primary (predominantly tetravalent uranium)	
Uraninite	Ideally UO_2
Pitchblende	$UO_{2.2}$ - $UO_{2.67}$
Coffinite	$U(SiO_4)_{1-x}(OH)_{4x}$
Brannerite	UTi_2O_6
Davidite	$(REE)(Y,U)(Ti,Fe^{3+})_{20}O_{38}$
Thucholite	Uranium-bearing pyrobitumen
Secondary (predominantly hexavalent uranium)	
Autunite	$Ca(UO_2)_2(PO_4)_2 \cdot$ 8-12 H_2O
Carnotite	$K_2(UO_2)_2(VO_4)_2 \cdot$ 1–3 H_2O
Gummite	gum like amorphous mixture
Seleeite	$Mg(UO_2)_2(PO_4)_2 \cdot 10$ H_2O
Torbernite	$Cu(UO_2)_2(PO_4)_2 \cdot 12$ H_2O
Tyuyamunite	$Ca(UO_2)_2(VO_4)_2 \cdot$ 5-8 H_2O
Uranocircite	$Ba(UO_2)_2(PO_4)_2 \cdot$ 8-10 H_2O
Uranophane	$Ca(UO_2)_2(HSiO_4)_2 \cdot 5$ H_2O
Zeunerite	$Cu(UO_2)_2(AsO_4)_2 \cdot$ 8-10 H_2O

II.1.2. Geological Characteristics

A detailed discussion of uranium ore genesis can be found in "Genesis of Uranium Deposits" [23]; however, the mobility and speciation of uranium in geologic environments is an important influence on this research. The geologic behavior of uranium in natural ore systems is mainly influenced by the pH of the precipitating solution, the redox potential at the deposition site, and the presence of various complexing agents (such as sulfate ions). The distribution of uranium complexes (under a variety of conditions) can be calculated using a speciation software EQ3/6 [24] utilizing a specific database. The accuracy of the speciation software EQ3/6 can be limited due to potentially significant missing thermodynamic data

(causing the need for model assumptions and data fitting). Also if the system being explored is not well characterized, the uncertainty in the parameters can propagate through the model. It can still be useful to use in evaluating relative changes in speciation of one parameter (such as temperature). Figure II.1 and Figure II.2 show the change in speciation due to an increase in temperature for a standard $U\text{-}O_2\text{-}CO_2\text{-}H_2O$ system, utilizing the database developed for the Yucca Mountain Project.

It can be seen from Figure II.1 and Figure II.2 that even a small change in temperature can impact the uranium speciation and deposition. In the natural pH range (around 7), $(UO_2)_2CO_3(OH)_3^-$ is the main uranium species present at close to 90% uranium mass. With an increase in temperature, the dominance of that species decreases both in magnitude and dominant pH range. Depending on the geologic conditions, this change in the speciation can lead to changes in the mineralization (different uranium complexes due to changes in the charge state of the species).

The uranium species will also depend on the complexing agents present in solution. Uranium sulphate and carbonate complexes, for example, are soluble and can be transported by groundwater to the deposition site (deposited along with the uranium when reduced). The following uranium species have been shown to dominate with the following complexing agents: $Ca_2UO_2(CO_3)_{3(aq)}$ at pH = 7.1 in carbonate and Ca-containing groundwater; $UO_2(CO_3)_3^{4-}$ at pH = 9.8 in carbonate-containing and Ca-poor groundwater; and $UO_2SO_{4(aq)}$ at pH = 2.6 in sulphate-rich groundwater [25].

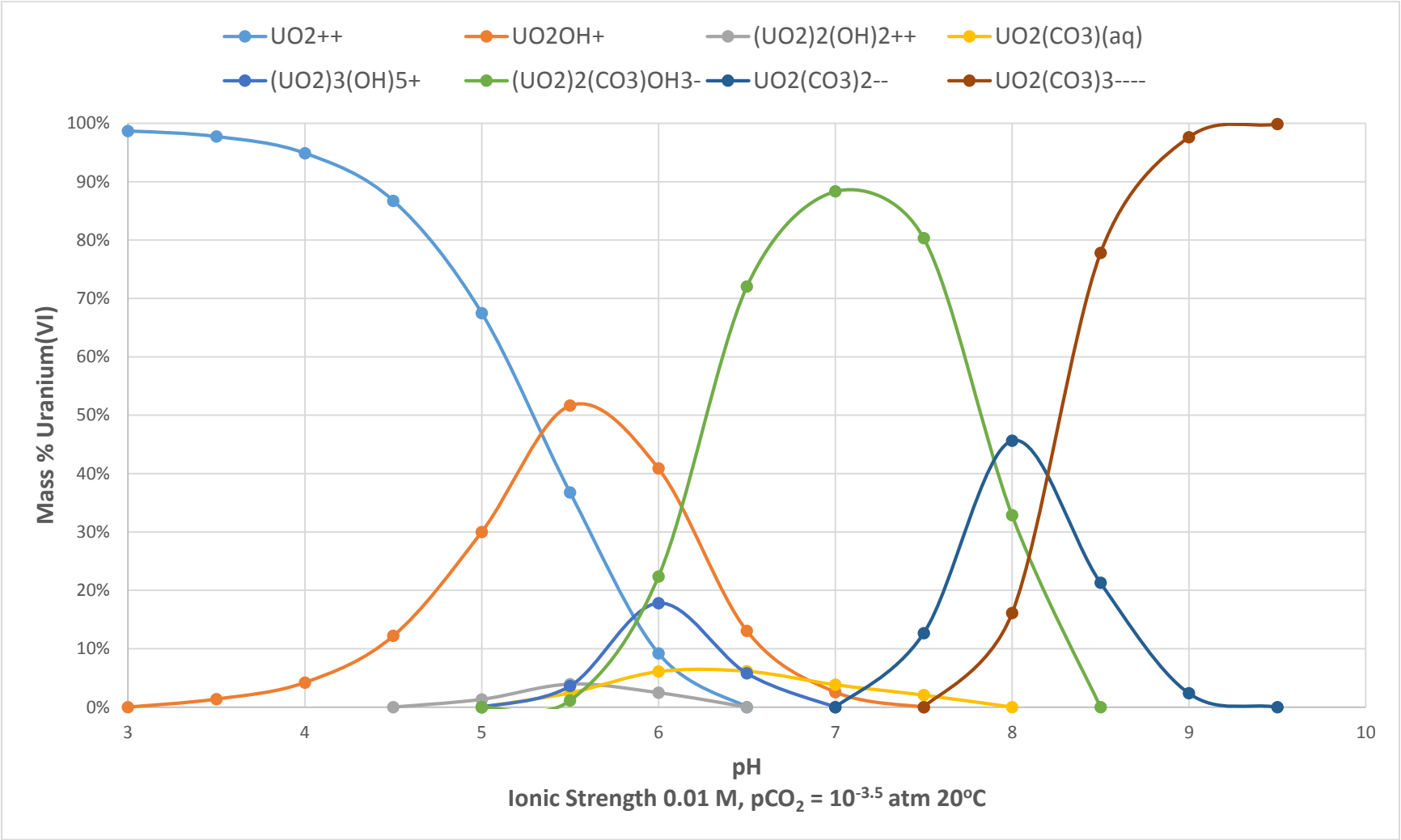

Figure II.1: Uranium speciation under a U-O_2-CO_2-H_2O system at standard temperature (ionic strength of 0.01M, pCO_2 of $10^{-3.5}$ atm., and uranium concentration of 500 ppm) [26].

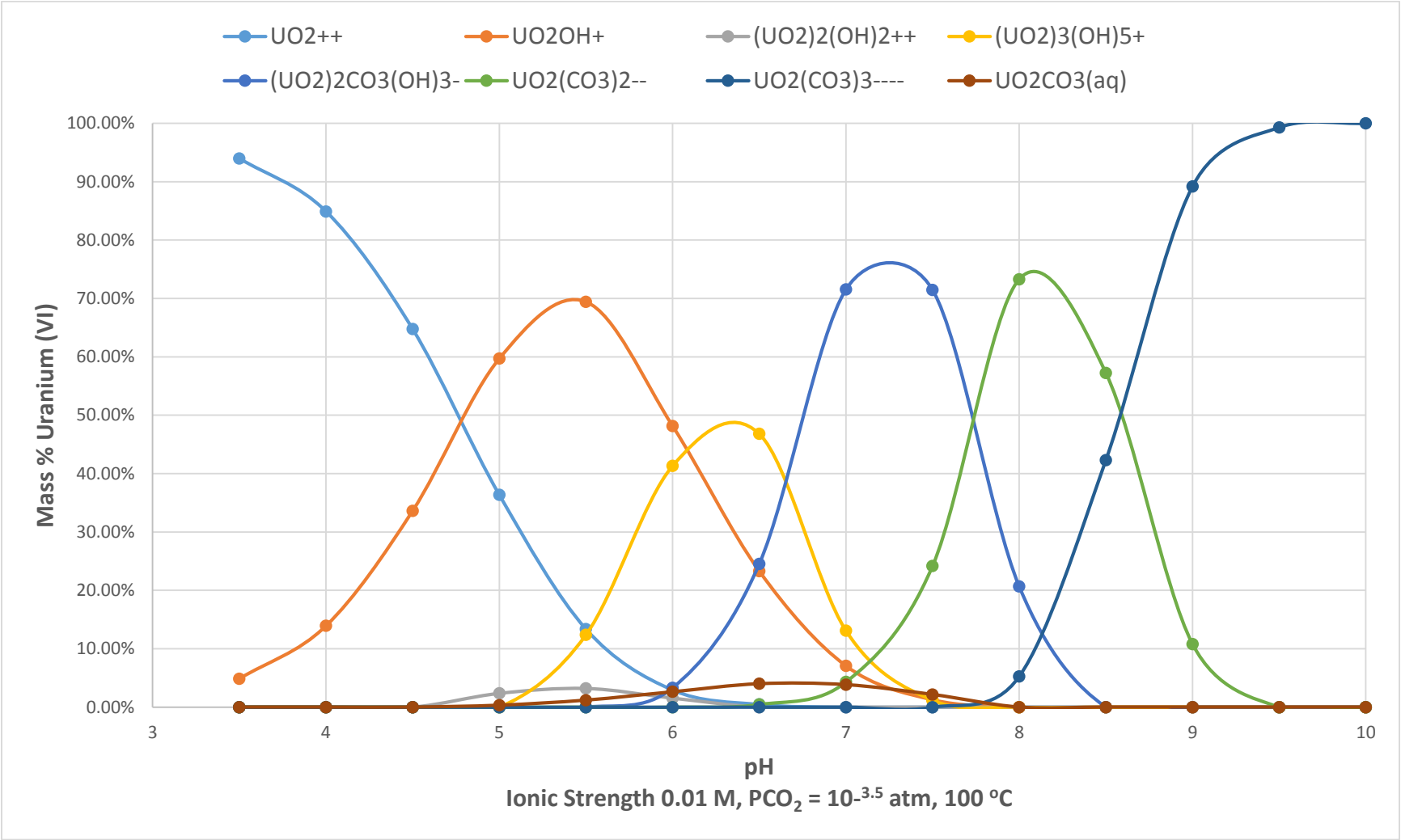

Figure II.2: Uranium speciation under a U-O_2-CO_2-H_2O system at 50°C (ionic strength of 0.01 M, pCO_2 of $10^{3.5}$ atm., and uranium concentration of 500 ppm) [26].

II.1.3. Uranium Ore Isotopics

With an increase in measurement capabilities, all three isotopic ratios (relative to ^{238}U) have been shown to naturally vary in some degree due to various factors. The first uranium isotopic that was discovered to have natural variation was $^{234}U/^{238}U$, the increased abundance of ^{234}U in seawater (~15%) perhaps being the best example [27]. Variations in ^{234}U are primarily a consequence of an increased mobility of ^{234}U relative to other uranium isotopes due to redox interactions. Production of ^{234}U occurs through α-decay of ^{238}U, which subsequently results in extensive damage to the crystal lattice. The ^{234}U containing crystal sites damaged by α-recoil are more susceptible to oxidation to the hexavalent state compared to ^{238}U [28]. Preferential leaching of ^{234}U will consequently result from these α-damaged crystal sites. Uses of ^{234}U disequilibrium have been investigated since, such as the application of dating secondary uranium mineralization in the ore [29],[30],[31]. This could be useful in providing a time estimate for uranium deposits in nuclide production models.

Compared to ^{234}U, variations in ^{235}U isotopics is a relatively recent discovery. It was first proposed that uranium isotopes were too heavy to undergo mass-fractionation to any significant degree, resulting in an invariant ratio of $^{238}U/^{235}U$ (137.88). It was later theorized that fractionation of uranium isotopes should occur during redox reactions due to an isotopic fractionation mechanism termed the nuclear volume effect [32]. With heavy elements, such as uranium, differences in the nuclei volume between the isotopes results in differences in the electric charge distribution [32]. Due to these effects, ^{238}U tends to be preferentially enriched over ^{235}U in the precipitating uranium mineral phases [10]. Figure II.3 presents the variations in uranium isotopics measured by various sources.

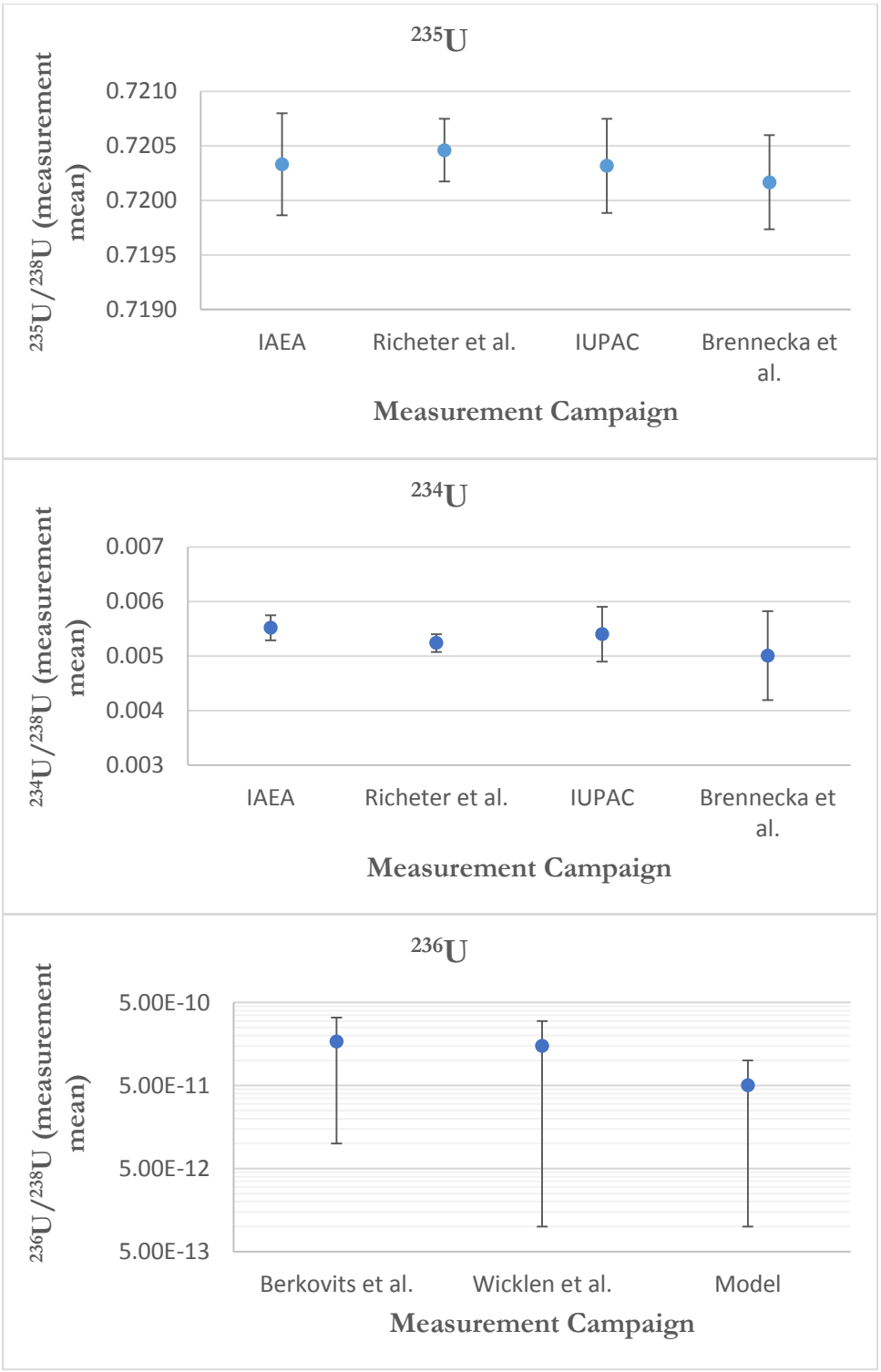

Figure II.3: Modeled (this work) and reported (IAEA[33], Richter[34], IUPAC[35], Brennecka [8], Berkovits [11], Wilcken [13]) ranges of isotopic variation relative to ^{238}U were measured in natural uranium samples.

Uranium-236 is naturally present in uranium ores at very low concentrations (~10^{-10} atom percent). With the increasing precision of mass spectroscopy, specifically accelerator mass spectroscopy (AMS), variations in ^{236}U concentration have been able to be distinguished. Variations in ^{236}U abundance of natural uranium samples are known to exist due to various physical, chemical, or even biological processes including mass fractionation, redox transitions, radioactive decay, radioactive disequilibrium, alpha-recoil, and neutron capture [35]. One of the mechanisms for production of ^{236}U in the environment is through neutron capture of ^{235}U. These captures occur due to the very low levels of naturally occurring neutron fluxes present in uranium ore bodies. Unique to ^{236}U, neutron capture is the primary production mechanism. Significantly, it results in ^{236}U having the largest variation potential due to considerable changes in neutron flux between differing geologic deposits.

II.2. Uranium Ore Classification Scheme

Due to the redox chemistry of uranium, specifically the high mobility of the hexavalent oxidation state compared to the tetravalent, there exist numerous settings of uranium deposits. A classification scheme is needed to distinguish between different geologic ore deposits and draw inferences on the variability of ^{236}U. Using a classification scheme will also allow similar deposits to be grouped, and the factors that cause ^{236}U variations easier to realize. Several classification schemes exist, from genetic ore deposit classifications to purely descriptive schemes [36],[37],[38],[39],[40]. Genetic ore deposit classifications tend to contain more information on mineralization processes, but are hindered by the variability of those processes from multiple sources [41]. Another consideration to be made is in the number of deposit groups in each classification scheme. While a greater number of groups tends for a more detailed scheme, the complexity in classification increases. Also with the number of uranium deposits invariant, large number of groups in a scheme leads to less potential sample size between the groups.

Two classification schemes will be considered in this work, the World Distribution of Uranium Deposits (UDEPO) classification scheme [37] and a depositional scheme [8]. Based on the depositional scheme, uranium deposits can be divided into three foremost settings

based on the redox environment and temperature during the deposition. The three settings include:

Low Temperature, Redox Sensitive: Mineralization occurs in this type below the water table. Low-temperature fluids carrying soluble hexavalent uranium will come in contact with a reducing agent, precipitating the insoluble U^{+4}.

High Temperature, Redox Sensitive: Mineralization still occurs through a redox reaction ($U^{+6} \rightarrow U^{+4}$), except at higher temperatures usually related with igneous processes.

Non-Redox: These deposits include all mineralization occurring without a redox interaction. This setting consists primarily of quartz-pebble conglomerate deposits, which formed prior to the oxygenation of the atmosphere and consequently not formed through a redox interaction.

The benefit of using this scheme is the ability to potentially constrain the impact that oxidation and temperature have on fractioning ^{236}U from ^{238}U, allowing a more careful consideration of the neutron capture mechanism. Also with only three groups, sample sizes will be larger leading to more statistically significant results. The disadvantage is that the settings are general and do not realistically provide enough information for using ^{236}U as an isotopic "fingerprint". A possible solution is for scoping work to be done based in a depositional classification scheme, then transition to the UDEPO scheme. Based on UDEPO classification, uranium deposits can be assigned on the basis of their geological settings. The major deposits with brief descriptions are provided below [37]:

Unconformity deposits: These deposits are associated with an unconformable contact which divides a crystalline basement altered by overlying clastic sediments. These can be further divided by fracture controlled and clay bounded unconformity deposits.

Sandstone deposits: These deposits occur in sandstones deposited in a continental fluvial or marginal marine sedimentary environment. These can have sub-types of roll-front and tabular deposits.

Hematite breccia complex: These deposits occur in hematite-rich breccias and contain uranium in association with copper, gold, silver and rare earths.

Quartz-pebble conglomerate: These deposits are found in quartz-pebble conglomerates deposited as basal units in fluvial to lacustrine braided stream systems.

Vein deposits: The mineralization of these deposits fill fractures of varying thicknesses and consisting typically of carbonates and quartz.

Intrusive deposits: These deposits are associated with intrusive or anatectic (differentially or partially melted) rocks of different chemical compositions.

Volcanic deposits: These deposits are typically located within/nearby volcanic caldera, where mineralization is largely controlled by structures and occurs at several levels of volcanic and sedimentary units found in fractured granite and in metamorphites.

Metasomatite deposit: These deposits are confined to the areas of tectono-magmatic activity and are related to near-fault alkali metasomatites, developed upon different basement rocks.

Surficial deposit: These deposits are loosely defined as young, near-surface uranium mineralization in soil. They are primarily associated with weathered, uranium-containing granites.

Collapse breccia pipe deposits: These deposits occur in circular, vertical pipes filled with fragments, with mineralization concentrated mainly as uraninite in a permeable breccia matrix.

Phosphorite deposits: These deposits are associated with large quantities of phosphorite, and are typically of a very low uranium grade. Uranium is typically recovered in these deposits as a by-product of phosphate production.

II.3. Production Mechanisms in Ore Bodies

The mechanisms for subsurface production of radionuclides need to be evaluated before any model can be developed. A general equation can be used that evaluates the change in concentration of a specific radionuclide in a closed system

$$\frac{dN}{dt} = \sum_j P_j - \lambda N$$

where N is the atomic concentration of a specific radionuclide, P_j is the production rate of a mechanism and radionuclide, and λ the decay constant for the radionuclide. The assumption of a closed system removes other loss terms that could be present in the system, including chemical and physical fractionations (redox chemistry, nuclear volume effect, etc.). Another assumption is that loss pathways through particle capture of ^{236}U are negligible, which was verified in scoping studies. The sensitivity of the model in not including these loss terms can be evaluated by examining the geologic system. The previous equation can be integrated to the following to evaluate the concentration of radionuclide (i).

$$N(t) = \sum_j P_j \lambda^{-1}\left(1 - e^{-\lambda t}\right) + N_0 e^{-\lambda t}$$

Depending on the timescale of the ore body relative to the decay constant of the radionuclide, an assumption of equilibrium can be applied.

$$\lim_{t \to \infty} N = \sum_j P_j \lambda^{-1}$$

There are several mechanisms for production of isotopes in a subsurface environment, either in a primary or secondary role. This research evaluated three main types of production mechanisms: decay/fission of radionuclides, nuclide spallation, and particle-capture reactions.

II.3.1. Decay / Fission of Radionuclides

Decay/fission of radioelements can directly or indirectly produce nuclides in a subsurface environment. The best examples of decay products in the subsurface are from the ^{238}U, ^{235}U,

and ^{232}Th α-decay series. Uranium-234 is directly produced from the ^{238}U series, which can be an isotopic signature. Also, α-decay from the three decay series can have an influence on particle-capture reactions, or be a cause of disequilibrium among products in the series. Fission, whether spontaneous or induced, can be a source of nuclide production such as ^{81}Kr, ^{85}Kr, ^{99}Tc, and ^{129}I. Fission also will produce neutrons, which can have an impact on particle-capture reactions. Production of nuclides by exotic fission processes can occur, such as ternary fission (three fragment emission) or rare emission of ^{14}C nuclei (during decay of radium and radon isotopes) [14].

The direct production of ^{236}U through decay of primordial isotopes is essentially nonexistent, due to ^{236}U belonging to the thorium (4n) decay series. The nuclides above ^{236}U in the thorium decay series all have half-lives shorter then 1E8 years, causing ^{236}U not to be present through this pathway. Several secondary decay pathways in regards to ^{236}U production are theoretically possible and shown below.

$$^{238}U \underset{(\gamma,n)}{\overset{(n,2n)}{}} {}^{237}U \xrightarrow{\beta^-} {}^{237}Np \underset{(\gamma,n)}{\overset{(n,2n)}{}} {}^{236}Np \xrightarrow{EC} {}^{236}U$$

$$^{238}U\ (n,\gamma)\ {}^{239}U \xrightarrow{\beta^-} {}^{239}Np \xrightarrow{\beta^-} {}^{239}Pu\ (n,\gamma)\ {}^{240}Pu \xrightarrow{\alpha} {}^{236}U$$

The production pathways for ^{237}Np and ^{239}Pu can theoretically be numerous, although the probable pathway is shown. To simplify the production pathways, the upper ^{237}Np and ^{239}Pu concentrations can conservatively be evaluated for uranium ores.

$$^{237}Np \underset{(\gamma,n)}{\overset{(n,2n)}{}} {}^{236}Np \xrightarrow{EC} {}^{236}U$$

$$^{239}Pu\ (n,\gamma)\ {}^{240}Pu \xrightarrow{\alpha} {}^{236}U$$

Atomic concentration ratios of ^{237}Np/^{238}U were measured for several uranium ores with an upper limit of approximately 2.0 x 10^{-12} [42]. Other measurements were done to evaluate the ^{239}Pu/^{238}U concentration ratio with an approximate upper limit of 6 x 10^{-12} [43].

II.3.2. Nuclide Spallation

Spallation in which particles (protons, neutrons, or light nuclei) with high kinetic energy (~100 MeV to several GeV) interact with a target nuclei, causing the emission of large numbers of hadrons or fragments [44]. Typically these energies are only found naturally in cosmic rays, and as a consequence become negligible below near surface depths. Spallation can produce light nuclides such as ^{14}C and ^{36}Cl, as well as produce additional particles that will influence particle-capture reactions. The only impact spallation has on ^{236}U production is through influencing the natural neutron flux in the ore body.

II.3.3. Particle-Capture Reactions

The particle-capture production mechanism is the primary mode evaluated in this research, with the other mechanisms indirectly influencing the particle source term. The main reactions in the subsurface environment involve the capture of neutrons, muons, and α-particles. The production rate of particle-capture (P_i) will depend on the atomic density of the target nuclei (N_t), the energy dependent cross section $\sigma_t(E)$, and the particle flux as a function of energy $\Phi(\mathrm{E})$:

$$P_i = N_t \int_0^{E_{max}} \sigma_t(E)\Phi(\mathrm{E})\, dE$$

Muon capture is primarily based on the simple semi-leptonic reaction which occurs via the charged current of the weak interactions [45].

$$\mu^- + p \rightarrow n + \nu_\mu$$

When a muon is captured by a heavy nucleus, the nucleus formed is in a highly excited state (with de-excitation occurring essentially through neutron emission) [46]. To produce ^{236}U through muon capture, a neptunium target would be needed

$$^{237,238,\ldots}Np\left(\mu^-, \nu_\mu\right)^{237.238,\ldots}U^* \rightarrow {}^{236}U + X_n$$

where X_n is the number of neutrons emitted depending on the target nuclide. The concentrations of neptunium coupled with the estimated muon flux [14] in uranium ore

bodies result in a negligible contribution to ^{236}U production. Capture reactions involving α-particles for production of ^{236}U can be of the form:

$$^{232}Th\ (\alpha,\gamma)\ ^{236}U$$
$$^{233}Th\ (\alpha,n)\ ^{236}U$$
$$^{233}Pa\ (\alpha,p)\ ^{236}U$$

The primary flux of α-particles in an ore body are due to the decay of the radionuclides present, which typically have energies less than 10 MeV. The α-particle reactions listed previously are all essentially threshold reactions (around 8 – 10 MeV), so no production of ^{236}U occurs through this pathway. Incident α-particle cross sections were evaluated using the TALYS-based evaluated nuclear data library [47].

Neutron capture reactions are essentially the only mechanism to directly impact ^{236}U production, in terms of particle-capture reactions. Numerous neutron capture reactions are possible, depending on the residual particle (γ, p, α, etc.). However, in regards to the target abundance in uranium ore only the following reactions are considered

$$^{235}U\ (n,\gamma)\ ^{236}U$$

$$^{238}U\ (n,3n)\ ^{236}U$$

For neutrons, sources of a naturally occurring flux can be found from a variety of mechanisms, including fission and α-capture. The initial neutrons can be slowed down in the rock median and captured or cause secondary particles through fission and scattering. An important example on neutron capture in this work is on ^{235}U, leading to the reaction ^{235}U(n,γ)^{236}U. Muons, specifically negative muons, can also play an important role for nuclide production. Nuclear capture of negative muons results in an excited product nucleus, which may de-excite by emitting neutrons, charged particles, and/or neutrinos [48]. Muon capture and muon-induced photodisintegration reactions can also produce secondary neutrons which would indirectly influence production rates [48]. Nuclide production can also be induced by photon-capture reactions, with the absorption of a high-energy gamma-ray causing the emission of a neutron or proton [14]. These reactions can be represented in the same form as particle capture, and are evaluated in the production model.

III. AMS MEASUREMENT SYSTEM

III.1. Obstacles and Interferences

To be able to benchmark the ^{236}U production model, as well as evaluate future unknown UOC samples, a measurement capability of natural ^{236}U needs to be accessible. Measurements on naturally occurring ^{236}U in ore bodies is problematic, and is a driving factor in why little research exists in this area. Measurements are limited by the low concentrations of ^{236}U in ore bodies and, until AMS, was unreliable. Even with AMS, obstacles exist for ^{236}U measurements which can be influenced based on the choice of system and protocols.

III.1.1. Pre Tandem Accelerator Interferences for ^{236}U

For a heavy element like uranium, there are no stable isobars that exist naturally that can interfere with measurements of ^{236}U. In comparison, ^{36}Cl will have isobars (^{36}S, etc.) that will have to be separated before any measurements can be made. The main interferences for ^{236}U measurements are due to the more abundant ^{235}U and ^{238}U ions that can reach the detector of the AMS system. A schematic of the possible routes that the ^{235}U and ^{238}U ions can take to reach the detector is shown in Figure III.1.

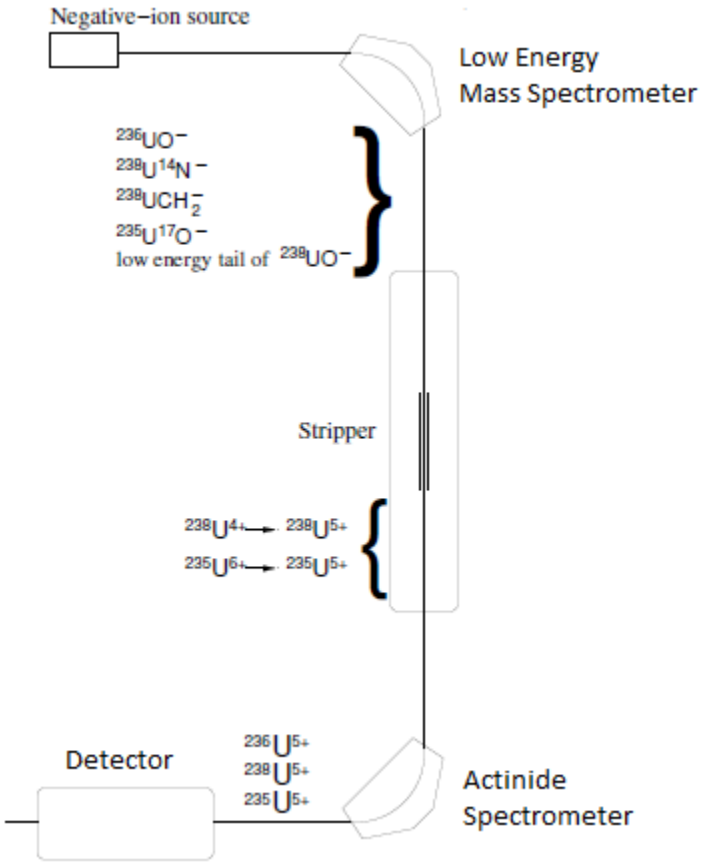

Figure III.1: Background interferences of the ^{236}U measurement present at difference stages in a typical AMS setup. [13]

The low energy mass spectrometer (a combination of an electrostatic analyzer and magnetic injection) limits what gets introduced to the accelerator by selecting molecular ions of mass 252. The ions that will be selected primarily consist of $^{238}UN^-$, $^{238}UCH_2^-$ and $^{235}U^{17}O^-$, along with the ion of interest $^{236}UO^-$. It is also possible that a part of the low energy tail of $^{238}UO^-$ and the high energy tail of $^{235}UO^-$ presented to the injection magnet will also enter the accelerator.

A cesium sputter source is used to generate the negative ions from the sample cathode shown in Figure III.2. Cs vapor is pumped into a near-vacuum chamber between the cooled cathode (a) and the heated ionizing surface (d) through an external oven (f). The cesium cloud will partially condense on the front of the cathode while being ionized by the hot surface. The

cesium coating on the cathode surface is important to increase the efficiency of ionization. The ionization potential of the sample surface is dependent on a low work function, which can be altered with the adsorption of a cesium layer. The charged Cs^+ ions will then accelerate towards the cathode, sputtering sample particles through the condensed cesium layer. For a full description of the ion source characteristics at CAMS see Southon and Roberts [49].

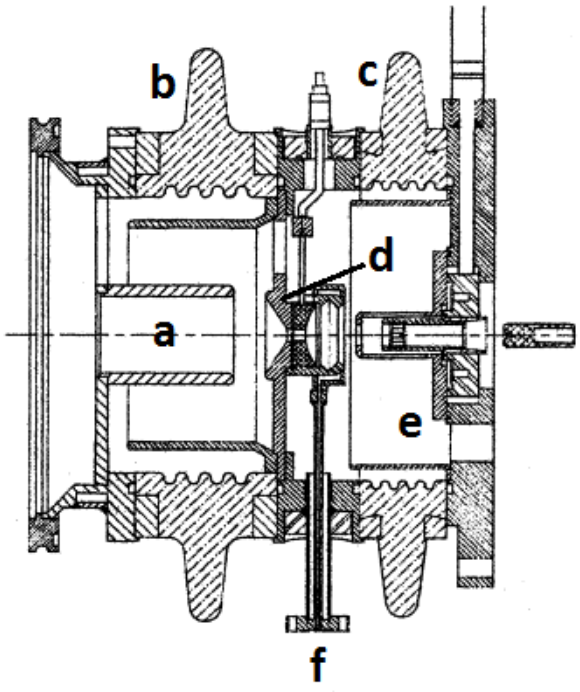

Figure III.2: The present source at CAMS design modified from [49] where: (a) extraction electrode; (b) extraction insulator; (c) cathode insulator; (d) ionizer and Cs beam-forming electrode; (e) immersion lens and sample holder; (f) Cs reservoir and feed tube.

The Cs^+ ions (which are used for the sputtering ion source) transfer energy to the uranium oxide (UO) clusters during the ionization process. The energy transferred is not mono-energetic and is associated with a similar energy distribution as that of carbon atoms [50]. Although not specific for the sample and source characteristics, the same behavior is expected to exist (consisting of a peak ionization energy with a low and high energy tail distribution) for uranium ions. The high energy tail would also be limited, and is characterized by an energy equal to the maximum energy of the Cs^+ ions subtracted by the surface work function and

pre-acceleration potentials. The low energy tail can theoretically reach thermal energies (although is difficult to measure) by undergoing multiple collision reactions. The following are all thought to contribute to the low energy distribution of the ions before entering the tandem accelerator: The creation and ensuing fragmentation of short lived molecular species within the ion field; the fragmentation of longer lived molecular species within the free regions of the beam transport system (within the low energy mass spectrometer); and the scattering of the ion current from the residual gas and beam components [50].

With the ionization energy distribution, it becomes possible that a portion of the $^{235}UO^-$ and $^{238}UO^-$ currents will have the same magnetic rigidity (allowing it to be selected in the low energy mass spectrometer) as that of the $^{236}UO^-$ ions. Magnetic rigidity describes the effect of a particular magnetic field would have on a given charged particle, which is defined by its momentum divided by particle charge. The low energy mass spectrometer allows ions with the same magnetic rigidity to be selected for the tandem accelerator. On the basis of momentum (same charge ion currents), the $^{235}UO^-$ ions would need to obtain a 0.4% higher ionization energy relative to the magnetic rigidity of the $^{236}UO^-$ ions. A similar calculation finds that a 0.8% reduction in energy would be needed for $^{238}UO^-$ ions to be selected. Although the $^{238}UO^-$ ions require a larger change in energy (due to mass difference), it is thought to be the dominating background interference relative to the $^{235}UO^-$ ions. Although never quantified, the reduction in current due to ion energy changes (+0.4% and -0.8%) has been shown to be comparable in other cases [50]. It is therefore believed that the two order more magnitude natural abundance of ^{238}U would offset any potential reduction in current relative to $^{238}UO^-$.

III.1.2. Post Tandem Accelerator Interferences for ^{236}U

Some ^{235}U and ^{238}U ions will be inserted into the accelerator as molecular isobars of $^{236}UO^-$ (mass 252). The secondary accelerator stage would normally remove the ^{235}U and ^{238}U ions, but they can pass through changes in the charge state (through collisions with residual gas) and achieve the correct magnetic rigidity [51]. The most likely molecular isobars at mass 252 are thought to be $^{238}UN^-$, $^{238}UCH_2^-$, and $^{235}U^{17}O^-$ in addition to a low energy tail of $^{238}UO^-$ which can enter the accelerator and contribute to charge changing collisions [11].

Specifically, the atoms that are injected as molecules are stripped to a distribution of positive charge states. A calculation was done to estimate the charge state distribution (1+ to 7+) of ^{236}U for a 6.5 MV voltage and is presented in Figure III.3 (see section III.1.3.2). It was assumed in the calculation that the thickness of gas was enough for the charge state distribution to reach equilibrium (independent on target thickness and initial charge state distribution). Even though the relative intensity of the charge states indicates 3+ would be an ideal selection, beam transport limitation of the system dictate the 5+ charge state be selected for uranium.

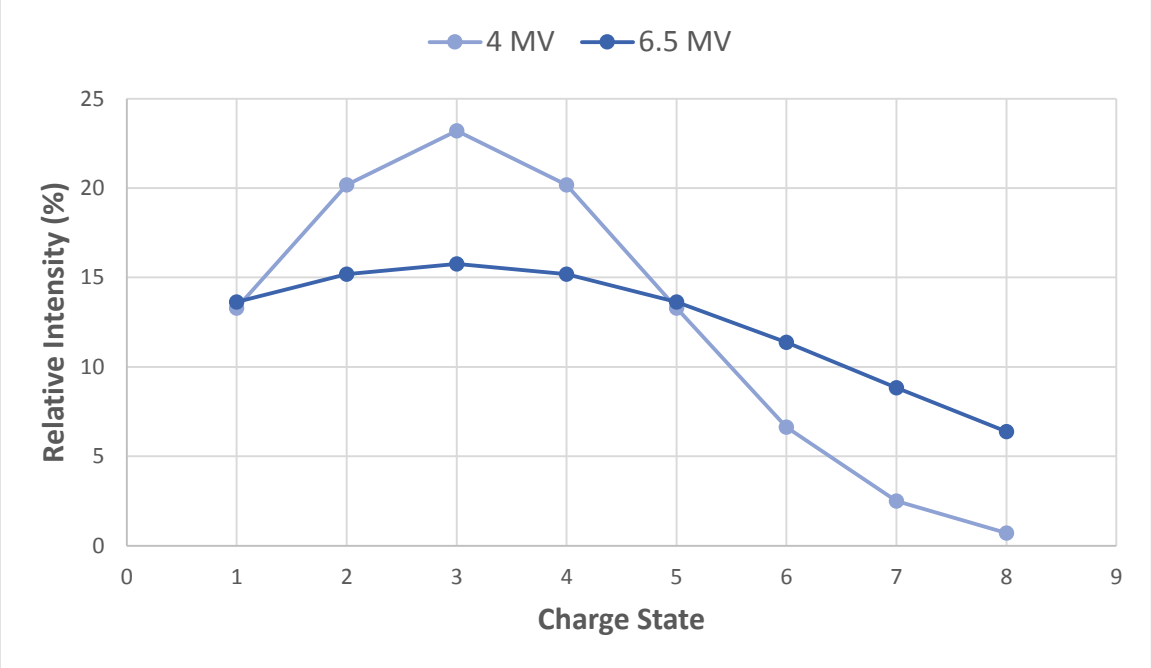

Figure III.3: An estimated charge state distribution of ^{238}U and ^{236}U (oxygen stripper) for both 4 MV and 6.5 MV acceleration potential.

The acceleration potential allows the uranium atoms to have a distribution of exit energy based on the charge state. To obtain the correct magnetic rigidity (a combination of charge state and energy), charge changing collisions have to occur at a specific point in the accelerator for select ions. Ions of ^{238}U will need to have an increase in energy (due to the higher mass),

that is accomplished through an increase in charge state at a specific point. Charge changing collisions from $^{238}U^{4+}$ ions to $^{238}U^{5+}$, must occur after approximately 5% of the second accelerator stage to have the correct energy to be selected. Secondary collisions can cause $^{238}U^{3+}$ ions to also change to the appropriate charge state with the correct energy, although is thought to have a negligible probability. For ^{235}U ions, a decrease in energy is needed which can be accomplished through a charge changing collision ($^{235}U^{6+}$ to $^{235}U^{5+}$) occurring after around 2.5% of the second accelerator stage. The two factors that determine the probability of these mechanisms is the stripping yield (the uranium abundance at the stripping stage of the accelerator) and the charge changing probability for a collision.

The relative background for ^{236}U AMS measurements can now be considered as a function of the following parameters: the contribution of molecular isobars into the tandem accelerator ($^{238}UN^-$, $^{238}UCH_2^-$, $^{235}U^{17}O^-$, and energy tails of the more abundant $^{235}UO^-$ or $^{238}UO^-$), the abundance of given uranium species introduced, and the efficiency yields of the stripping / charge changing collisions. The amount of background in AMS measurements will directly inhibit the sensitivity (which is vital in ^{236}U measurements). On the contrary, reductions in the background ion beam can also negatively impact the efficiency of the ^{236}U ion beam in the system. Possible reductions to these interferences can be used in AMS systems, such as time of flight [13] which reduces background interferences in the detection system. The disadvantages of using time of flight methods is due to a deviation of beam efficiency between the measured ^{236}U and ^{238}U ions (this can be hard to quantify the associated uncertainty). The addition of further magnetic and energy analyzers can also reduce the background, without significantly changing the beam efficiency (however with cost disadvantages compared to time of flight). A description of the AMS system, specifically the sensitivity of the system with regards to efficiency, is therefore needed.

III.1.3. AMS Efficiency

As in any measurement system, efficiency considerations are needed to convert the detection signal to a physical quantity (such as mass). The benefit of measuring isotopic ratios is that the absolute efficiency is not needed in most cases. However, any deviations in efficiency between the ions and over small time periods needs to be characterized sufficiently.

Decreases in system efficiency can also have a direct impact on the sensitivity and bias in the measurement (longer count times, more sample needed, etc.). Understanding how changes in the AMS design can influence efficiency is important, especially for inter-laboratory comparisons of samples utilizing differing AMS systems. In general, the overall efficiency of the AMS system can be a function of the following parameters: negative ion yield, beam transmission, and ion/current detection.

III.1.3.1. Negative Ion Yield

In general, ionization efficiency of the sample (negative ion yield) is a critical factor for mass spectrometry. Ionization yields from Cs sputter sources can be approximately 1%, with both the sample matrix and chemical form significantly affecting the yield for uranium. The use a metallic matrix for the sample (i.e. niobium) can result in better thermal and electric conductivity, increasing the yield[52]. The addition of iron oxides as part of the matrix has been hypothesized to increase the availability of oxygen, increasing the probability of forming negative uranium oxides. The sample matrices for uranium targets at CAMS utilize both niobium and iron oxide additions (see section 3.2.2). In contrast, metallic silver (with no iron oxide) was added to the sample matrices for AMS measurements at ANSTO. Differences between target preparation procedures have not been fully investigated in terms of ion yield and beam stability. A measurement bias can potentially be introduced that should be evaluated.

III.1.3.2. Transmission Efficiency

Beam transmission (optical losses) is primarily dependent on the physical dimensions of the system. The addition of a given element along the beamline (slits, drift, magnet, stripper, etc.) and the properties that govern the element (size, position, strength, etc.) can significantly affect the transmission efficiency. At the CAMS facility, for example, the addition of a low energy injection magnet with a large pole gap has significantly increased the transmission efficiency on the system [12]. The stripping process has a substantial impact on efficiency due to the charge state distributions. Theoretical calculations were performed on the charge

distribution of uranium ions in AMS system at CAMS utilizing the following semi empirical formulas [53]:

$$Y = (2\pi d^2)^{-.5} e^{-\frac{(Z-q)^2}{2d^2}}$$

$$d = Z^{0.27}(0.76 - 0.16\frac{v}{3.6E8 * Z^{0.45}})$$

where Y is the full-stripping probability, v is the ion velocity, Z is the ion atomic number, q is the charge state, and d is the empirical distribution width. The previous equations were utilized to calculate the relative charge state distribution for 6.5 MV seen in Figure III.3. While not intended to be an exact calculated distribution, it allows the yield to be evaluated over given accelerator energies. Since the velocity of the charge particles affects only the distribution width, an increase in voltage potential increases the charge distribution. Consequently, the efficiency for selecting a particular charge state relative to the energy of the accelerator can be compared for different AMS systems.

III.1.3.3. Detector Efficiency

The detection efficiency is based on the system used to measure the ion current and pulse counts for the ^{238}U and ^{236}U respectively. The reference current in AMS systems commonly utilize faraday cups for measurements, however can also employ pulse counting measurements (used when the ^{238}U current is to low). In the AMS system at CAMS, a two-anode, longitudinal field gas ionization detector is used to measure the pulse counts from ^{236}U. The efficiency of the ionization detectors can be characterized by the geometric acceptance of the detector and the conversion to electronic signal. Due to the directional bias and energy/mass of the ion current, the detection efficiency can be approximated to 100% given ideal conditions. Dead time corrections can be an important factor to consider in regards to efficiency, and the associated uncertainty is usually the upper limit for abundance sensitivity in the system. Other factors can reduce the efficiency of the detector such as pile-up and entrance foil scattering (thickness of foil). However, even when considering potential losses for ion detectors, the difference in detection efficiency between ^{238}U and ^{236}U can be

assumed to be negligible (assuming the isotope abundance is not exceeded). Therefore, no real normalization is needed for the isotopic ratio (in regards to detector efficiency).

The real difficulty in utilizing an ion chamber system is the low energy separation between ^{236}U and ^{238}U. Other systems have been considered to increase energy resolution, such as time-of-flight (used for the ANU sample measurements). Time-of-flight detection utilizes differences in velocity between isotopes with the same magnetic rigidity (passes the analyzing magnet). The velocity differences can be measured through flight times over a long enough distance. The disadvantage of such a system is a reduction in efficiency, which is due to losses through ion transmission across the start detector (typically a combination of accelerating grid and carbon foil). Depending on the setup, estimates in efficiency range from 30 to 50%, with a high uncertainty in the estimation. Losses in efficiency between ^{238}U measured using a faraday cup and the ^{236}U measured with time-of-flight make normalization of the isotopic ratio problematic.

III.2. Methodology

Advances have been made in measurement precision in many areas of mass spectrometry. However, the precision needed to distinguish variations of ^{236}U in natural UOC have only been shown for accelerator mass spectrometry measurements [12]. Several key characteristics differentiate AMS from other techniques in regards to trace actinide measurements. These characteristics include high efficiency, low interferences, low susceptibility to changes in sample matrix, and high dynamic range which will all be discussed in more detail.

Most of the measurements done for this research was at the Center for Accelerator Mass Spectrometry (CAMS) at Lawrence Livermore National Laboratory (LLNL) [54]. The CAMS facility was selected for measurements due in part to the development and recent improvements of the heavy isotope AMS beam line.

III.2.1. CAMS Setup and Procedures

The following setup and procedure methods were based on guidance on CAMS staff [54] and on previous actinide measurement campaigns [55]. The configuration of the actinide beam

line used at CAMS for all measurements is shown in Figure III.4. A high intensity cesium sputter source was used to produce approximately 40 keV negative oxide ions from the sample targets. The negative ions were then energy selected by the 90° spherical electrostatic analyzer (ESA). The 90° injection magnet provides fast switching cycling between the ion of interest $^{236}U^{16}O^-$ and the reference ion $^{238}U^{16}O^-$ by changing the potential of the insulated vacuum box. The three components mentioned constitute the low energy mass spectrometer, which reduces the amount of background ions. These background ions can consist of other uranium isotopic oxides or other contaminants in the sample [see section III.1.1].

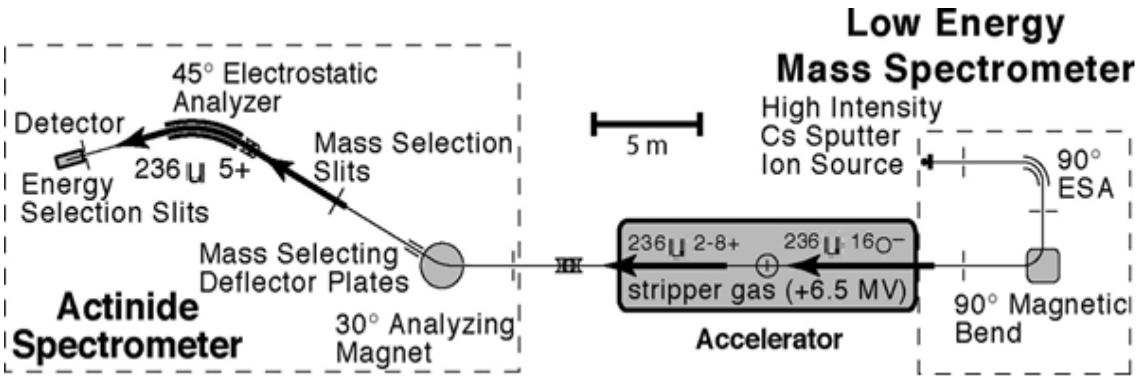

Figure III.4: Schematic of AMS actinide measurement system at CAMS, modified from Brown et al. [55].

The beam then continues into the 10-MV FN tandem Van de Graaff accelerator. The molecular ions are accelerated using a 6.5 MV terminal voltage and stripped (molecular bonds broken) in the stripper canal (oxygen gas stripper) at the center of the accelerator. The molecular ions that were injected into the accelerator are stripped to positive atomic ions with a distribution of charge states

The next set of components are referred to as the actinide spectrometer, which consists of a series of electrostatic and magnetic selectors to further reduce background interferences due to charge changing collisions [see section III.1.2]. The actinide spectrometer was set to transport the ion of interest $^{236}U^{5+}$ and the reference ion $^{238}U^{5+}$ with a 39 MeV energy to the

detector. The atomic ion beam exiting the tandem accelerator enters a 30° analyzing magnet, fast-switching electrostatic (mass selecting) deflector plates, image (mass selection) slits, and finally a 45° cylindrical electrostatic analyzer (ESA) before entering the detector. Similar to the 90° injection magnet, the fast-switching electrostatic deflector plates at the exit of the 30° analyzing magnet enable isotope switching with the actinide spectrometer. The reference isotope $^{238}U^{5+}$, for example, was selected at the image slits when the deflector plates were set to zero volts. The capability of both the low energy mass spectrometer and actinide spectrometer to swiftly switch ions of interest allows quasi-continuous normalization to a reference isotope (in this case $^{236}U/^{238}U$). This is accomplished by synchronizing the cycling of the electrostatic plates (between ^{236}U and ^{238}U) with that of the change of the injected ion mass in the low energy mass spectrometer. A two anode, longitudinal field gas ionization detector was used for the detection of the ions of interest. The measurement operations were automated to cycle between a count time of 0.4 s to measure $^{236}U^{5+}$ and a count time of 0.1 s to measure the reference isotope $^{238}U^{5+}$. The timed cycling between the two isotopes is repeated for a given sample until the desired statistical uncertainty for each sample is reached. Sub-second cycling is performed to enable quasi-continuous normalization and to minimize potential bias due to non-uniformity in beam current over time.

III.2.2. Sample Preparation

Most samples, depending on the measurement technique, need to undergo some chemical and/or physical processes prior to any measurements being taken. These processes can significantly improve the precision of the measurement by either reducing interferences in the sample, producing a more homogenous sample, and/or placing the sample in an ideal form for the measurement technique. The sensitivity of the measurements in regards to sample preparation can also depend on many factors, such as the measurement technique and the isotope being measured.

One of the main concerns in preparing uranium ore concentrate samples for ^{236}U measurements, is ensuring a homogeneous distribution. To reduce potential uncertainty, it is important to maintain a stable ion beam current. Heterogeneous pockets in the sample target can potentially cause disturbances in the ion beam, which needs to be minimized. Typically

this is accomplished through chemically separating out the uranium from the ore concentrate, and reducing to a uranium oxide. One of the benefits of measuring ^{236}U, is that it is commonly measured against the ^{238}U current (resulting in an isotopic fraction of $^{236}U/^{238}U$). It is therefore not necessary to know the yield of uranium during the chemical separation. In contrast, measuring ^{239}Pu requires the yield to be known with a high degree of precision (typically accomplished through the addition of an isotopic tracer) during chemical separation. While the uranium yield can be variable in regards to measurement precision, it is still good practice to strive for complete extraction from the ore concentrate.

Another common reason for preparing samples prior to measurement is to reduce potential interferences from molecular isobars. Purifying the sample through chemical extraction is one way to limit these interferences. However, reducing potential molecular isobars of ^{236}U is not a critical process prior to the measurement. Background interferences caused by the more abundant isotopes ^{235}U and ^{238}U is by far the primary obstacles of quantifying ^{236}U in uranium ores. Furthermore, molecular isobars are less likely to cause interferences in AMS measurements due to the stripping process discussed previously.

For these reasons, a sample preparation procedure for uranium was developed in order to quantify the concentrations of natural ^{236}U. It is important to understand the chemical properties and geologic setting of the sample whenever a preparation procedure is being developed. Accordingly, a detailed description the sample preparation procedures is based on the geochemical properties discussed in the following sections. The sensitivity of AMS allowed the use of less than 1 g samples with the condition that the samples were relatively rich in uranium (greater than 10% U). A detailed description of the protocol is presented in the following sections.

III.2.2.1. Digestion

Uranium samples were received as uranium ore concentrate, and an aliquot of approximately 100 mg was removed from each. Although the efficiency of extraction is not necessarily an issue due to the intrinsic $^{236}U/^{238}U$ ratio of the ore, it was still preferred to have complete

dissolution. The solubility of uranium ore concentrate will also be affected by the geochemical properties of the uranium compounds and is shown in Table III.1.

Table III.1: Solubility of selected uranium compounds in various solvents [56].

Uranium Compound	**Formula**	**Solubility**	
		Water	**Solvents**
Uranium metal	U	Insoluble	Acids
Uranium dioxide	UO_2	Insoluble	HNO_3
Uranium trioxide	UO_3	Insoluble	HNO_3, HCL
Triuranium octaoxide	U_3O_8	Insoluble	HNO_3, H_2SO_4
Uranium tetrafluoride	UF_4	Slightly Soluble	Concentrated acids
Uranium hexafluoride	UF_6	Decomposes	CCl_4, chloroform
Uranium tetrachloride	UCl_4	Soluble	Ethanol
Uranyl fluoride	UO_2F_2	Soluble	Ethanol
Uranyl acetate dehydrate	$UO_2(CH_3COO_2)_2 \cdot 2H_2O$	7.7g/100 cm^3 at 15°C	Ethanol
Uranyl nitrate hexahydrate	$UO_2(NO_3)_2 \cdot 6H_2O$	miscible in water at 15°C	Ethanol
Ammonium diuranate	$(NH_4)_2U_2O_7$	Insoluble	Acids
Uranium peroxide	UO_4	Decomposes	

There also exists a possibility of deviations in the $^{236}U/^{238}U$ ratio between different uranium minerals, which leads to the requirement of total digestion of any uranium-bearing minerals. Uranium is incorporated into the structure of minerals with relatively low solubility: such as zircon, apatite, titanite, and allanite [57]. Consequently, normal leaching methods that utilize just HNO_3 or aqua regia do not meet these requirements with the inability to dissolve silicates for example. Work has been done by various authors to compare various dissolution techniques in regards for minimizing the uranium left in the residue for various soil samples.

Specifically, Jurečič et al. compared the following dissolution techniques: wet dissolution with mixtures of the acids HNO_3, $HClO_4$ and HF; closed-vessel microwave dissolution using HNO_3 and HF followed by open-vessel dissolution with $HClO_4$; and alkaline fusion with Na_2CO_3 and Na_2O_2 in a glassy carbon crucible followed by mineralization with HNO_3, HCl, HF and H_2SO_4 [57]. The results of the study indicated that conventional wet ashing had the least uranium left behind in the residue, and was justified for use in the dissolution protocol [57].

The samples were first ashed at 650 ^oC in a furnace to remove organic matter. Up to 1 g (depending on the uranium percentage) of each sample was added to an HF resistant (Teflon) beaker. Chemicals are prepared new from ultrapure reagent stocks and <18 Megohm high-purity deionized water. Five milliliters of concentrated HNO_3 were added twice to the Teflon beaker followed by the addition of two times the following mixture: 5 ml of concentrated HNO_3 10 ml of concentrated $HCLO_4$ and 10 ml of concentrated HF. The uranium ore was allowed to dissolve in the solution while being heated just below boiling over a hot plate. After dissolution the samples were heated to approximately 200 ^oC until near dryness. The dry samples were then dissolved in 10 ml of 3 M HNO_3. The dry-down steps were repeated to ensure the removal of any fluorides created with the addition of HF. The addition of perchloric acid was looked into to aid in the expulsion of fluorides (such as silicon tetrafluoride), but it has been shown to reduce yield [43]. Finally any residue still left over was separated from the solution through centrifugation and the supernatant was collected.

III.2.2.2. Uranium Separation and Purification

The isolation and purification of uranium isotopes protocols for measurement by AMS is taken from the standardized methodology used by researchers from the Center for Accelerator Mass Spectrometry (CAMS) (Energy and Environment Directorate) and the Environmental Radiochemistry Group (Chemistry and Materials Science Directorate) at the Lawrence Livermore National Laboratory (LLNL) [58]. An aliquot (approximately 10 mg uranium) of the sample in 3 M HNO_3 is transferred to a Teflon vial, where a small amount of concentrated HNO_3 is added. The sample is then heated to near dryness and rehydrated

in 10 ml of 3 M HNO_3 – 1 M $Al(NO_3)_3$ solution, ideally forming hexavalent uranium nitrates. The aluminum nitrate is added as a salting agent, which adds additional nitrate ions (to ensure saturation in regards to the uranium ions) without having to concentrate the nitric acid. The uranium extraction yield for a given system has been shown to increase with the addition of a salting agent such as aluminum nitrate [59]. The added aluminum can also effectively tie up other matrix ions, such as phosphate, removing their effect on actinide retention. Phosphate anions can readily complex with tetravalent actinides (not extracted by the UTEVA resin), although this effect is more significant for neptunium and thorium (uranium is mostly present as IV and VI) [60].

The sample is passed through a UTEVA column which was preconditioned with 6 mL of 3M HNO_3 to place the resin in a nitrate matrix. The UTEVA column were prepared using 2 ml of resin with a 50-100 μm mesh. Gravity flow rates were used with an approximate flow speed of 0.25 ml/min. The extractant in the UTEVA Resin consists of diamyl amylphosphonate (DAAP) which extracts hexavalent uranium according to the following equation:

$$UO_2^{2+}{}_{(aq)} + 2NO_3^-{}_{(aq)} + 2E_{(org)} \leftrightarrow UO_2(NO_3)_2 \cdot E_{2(org)}$$

where E (extractant) represents DAAP and a neutrally extracted U nitrate complex [60]. The formation of these complexes, and consequently the uptake of the actinides, is driven by the concentration of nitrate in the system shown in Figure III.5. The k' is a measure of uptake corresponding to the number of free column volumes relative to the peak maximum.

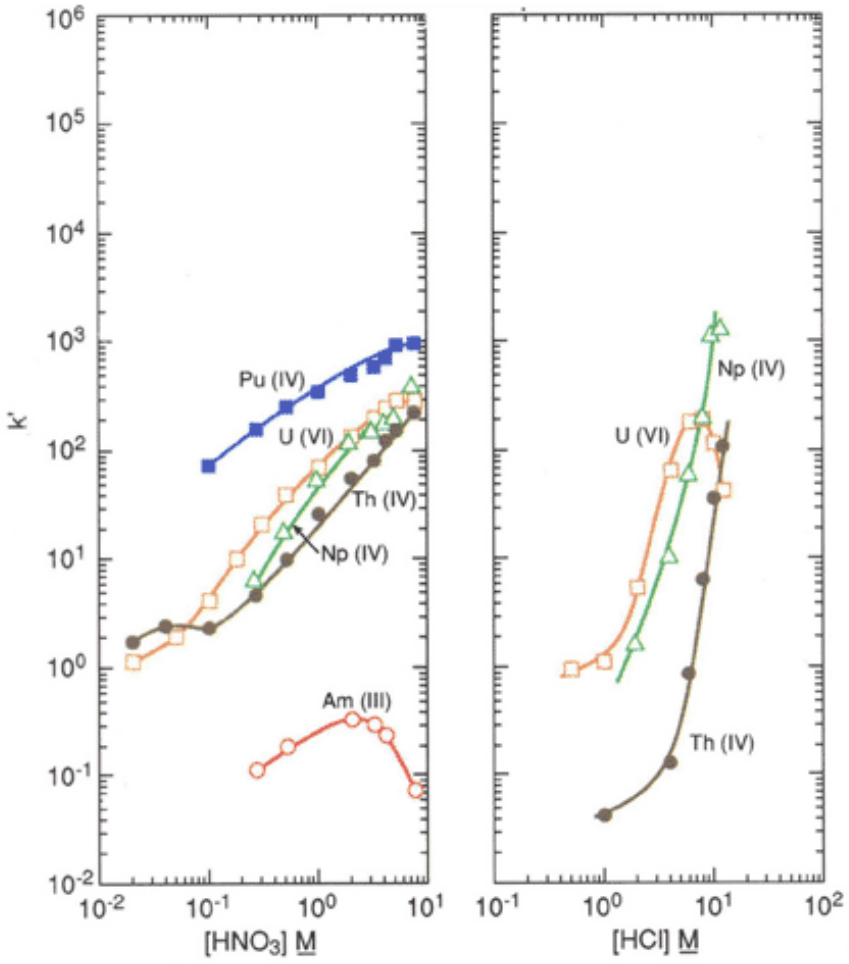

Figure III.5: k' values for actinide adsorption on UTEVA resin in varying nitric and hydrochloric acid concentrations (23 -25 °C) [61].

By using a 3M HNO_3, the hexavalent uranium is retained on the resin while the undesired tertiary ions are eluted through the column. To ensure all the sample is transferred to the column, the Teflon vial is rinsed with two 1 ml aliquots of 3 M HNO_3. To ensure complete elution through the column, another four 5 ml aliquots of 3 M HNO_3 is washed through the resin.

The column resin is then washed with four 5 ml of a 5 M hydrochloric acid – 0.05 M oxalic acid solution. The large difference in k' for uranium and thorium in the 4 – 6 M HCl range, allows for the elution of thorium from the resin. The oxalic acid has a matrix effect on Np

(IV) relative to U(VI) at low concentrations, allowing Np to be stripped with 0.05 M oxalic acid solution without an effect on U elution. Uranium is then eluted into a 30 ml Teflon vial using 20 ml of 0.02M H_2SO_4. Although dilute sulfuric acid was used to extract uranium, it has been recommended that HCl is more efficient at stripping uranium [61]. The collected uranium sample is then slowly evaporated to dryness.

The theoretical maximum loading capacity of UTEVA Resin for uranium is approximately 37 mg/ml of resin bed [61]. However, this assumes all extractant sites are bonded with uranium nitrate. Other anions can fill these sites and the column behavior of the resin does not allow each site to have equal probability to bond with uranium. Therefore, 20% of the resin's theoretical maximum loading capacity was never exceeded (7.4 mg /ml).

A second column step is used to further purify the sample by anion exchange using an AG 1 – X8 resin. The AG 1 resins are strongly basic anion exchangers with four ammonium functional groups attached to the styrene divinylbenzene copolymer lattice [62]. The resin is placed in a chloride matrix by preconditioning the column with 20 ml of 10 M HCl. Again, 2 ml of resin was used for each column and flow was controlled through gravity. The dried sample is then rehydrated with 3 – 5 ml of 10 M HCl to place the uranium in a chloride matrix and loaded onto the column. A rinse solution of the same acidic concentration was used to wash the sample container and transfer pipette to ensure all the uranium was loaded onto the column. A column wash was completed by adding four 5 ml aliquots to the top of the resin bed, allowing the impurities to be captured in the effluent. Uranium was then eluted using 20 ml of 0.5 M HCl, again, capturing the effluent in a Teflon vial and slowly evaporating to dryness.

III.2.2.3. AMS Target Preparation

Once through the double column purification protocols, the samples are ready for processing into AMS targets. Approximately one milligram of uranium oxide is required for the AMS measurement, so the appropriate aliquot is taken of the sample. The dried sample is rehydrated using 2 ml of 3 M nitric acid and carefully transferred to a 15 ml centrifuge tube. Multiple washings were done with 2 ml of the same nitric acid concentration to ensure all of

the uranium was transferred to the centrifuge tube. An iron (III) carrier solution (1 mg iron /g solution) is created, and 0.3 g of the solution is dispensed into the 15 ml centrifuge tube for each sample. The iron carrier solution is added to ensure complete precipitation of the uranium sample (co-precipitation). Co-precipitation is useful when the element of interest (uranium) is too dilute to precipitate by conventional means. Uranium can be then precipitated from solution adsorbed onto iron hydroxide ($Fe(OH)_3$). This can be accomplished using approximately 2 – 4 ammonium hydroxide solution ($NH_4OH \cdot xH_2O$), which is a 1:1 ratio of ammonium hydroxide to deionized water. The volume of the sample solution at this point should not exceed 14 ml, and be approximately the same volume for centrifugation.

The sample precipitate is then allowed to settle, preferably overnight. After which, recovery of the precipitate is done through centrifugation (2000 RPMs for 20 minutes) of the samples. The supernatant liquid is then decanted from the centrifuge tube without disturbing the precipitate pellet. The pellet is then washed with 2 ml of ultra-pure water. It is important to consider the volume of the wash, as the solution should be kept slightly basic to prevent the sample precipitate from dissolving (this is accomplished through the residual ammonium hydroxide). The sample pellet is then broken up (using a disposable pipette), suspending the precipitate in solution to transfer to a quartz crucible. The samples are slowly taken to dryness in the crucibles under an infra-red heat lamp. The intermediary step before calcification is to ensure no significant amounts of liquid are present in the crucibles during the rapid heating process, which could potentially cause sample loss (due to changes in pressure). When the samples are dry, the crucibles can be capped and transferred to a high temperature oven (at 800°C for several hours). Calcification minimizes potential background interferences due to the reduction of nitrogen and carbon from the samples.

Once the samples are done baking, the oven is allowed to cool before carefully removing the crucibles and settle to room temperatures. Approximately 3 mg of niobium metal is added to each crucible, after which a #60 gauge drill stem is used to break up and homogenize each sample with the metal. Niobium is needed due to the fact that most of the sample (including UO_2) are insulators. The sample needs to therefore be dispersed in a conducting matrix to

prevent charge build up under the cesium ion sputter source during measurement, which can cause spatially heterogeneous secondary ion emission from the cathode surface [63]. Consequently it has been shown that a metal matrix (such as copper, silver, or niobium) has dramatically improved the cesium ion sputter source performance [52]. To avoid any possible cross contamination, a unique #60 gauge drill stem is used for each sample (which is first cleaned with acetone to prevent contaminants present during the manufacturing of the drill stems).

For each sample, an aluminum AMS sample holder (cathode) is drilled to a depth of 0.006 inches (calibrated to minimize unconformity) using a #60 gauge drill bit. The dry powder sample can then be transferred to an AMS sample holder, making sure to apply enough pressure until the material is compact (typically creating a smooth, reflective surface). It is important to ensure the sample powder is compact so that the ion sputter source creates a uniform ion beam throughout the measurement. The way the AMS system at LLNL introduces samples is through a sample wheel shown in Figure III.6. The sample introduction system may contain as many as 64 targets. For a measurement run, these 64 slots can potentially include: blank targets prepared from the target matrix materials (iron and niobium), standards containing mixtures of natural uranium and spike concentrations of ^{236}U NIST standards, and the actual sample set.

Figure III.6: The target wheel used for AMS measurements with aluminum cathode targets [64].

III.3. Experimental Results

Two experimental measurements were performed to assess the capability of the AMS system at CAMS for ^{236}U measurements. The first experiment was to evaluate the effects of sample preparation procedures on AMS measurements. The second experimental campaign was to evaluate the ^{236}U concentrations for 17 UOC samples, and if possible, evaluate any bias between different AMS systems. Both measurements utilized the AMS system and procedures described in section 3.2.1.

III.3.1. Sample Preparation Variations.

The benefit of AMS measurements is the suppression of most molecular isobars due to the high energy and stripping process. The minimal molecular interferences theoretically should result in a reduced dependence of sample preparation procedures (which can be significant in other measurement systems). However, sample preparation methods could indirectly impact the stability of the ion current (through heterogeneous inclusions, etc.). Current procedures at the CAMS facility dictate double column purification for uranium samples (see section 3.2.2). The effects of sample preparation procedures for uranium measurements was tested for three uranium reference standards shown in Table III.2. The reference standards were prepared with the following procedures: no column work, UTEVA column purification only, double column purification. The mass of each sample was dictated by the uranium fraction, so that each procedure was for 1 mg U. All of the remaining sample procedures were kept constant, such as AMS target production.

Table III.2: The reference standards used to test sample preparation variations: double column, single column, and no purification.

Sample I.D.	Description	Uranium Fraction
CRM-112A	Natural Uranium Metal	0.99975 g U/g
CRM-129A	Natural Uranium Oxide U_3O_8	0.88 g U/g
BL-5	Low-Grade Concentrate Standard	0.0709 g U/g

Unfortunately, during the AMS measurements, a significant current dependent bias was observed in the repeated measurements of individual samples. This was reported to be an uncommon occurrence in the AMS system, and was most likely caused by the drifting of the calibration of the current integrator box. Consequently, the absolute measurements of the $^{236}U/^{238}U$ atom ratios were biased and therefore not reported in this work. Some initial conclusions can still be made of the relationship between reference standards utilizing different column procedures.

The two certified reference materials (CRMs) were not expected to have a significant change throughout the sample procedures. The dissolution of pure uranium metal in nitric acid would oxidize the uranium ions, such as by the following reaction (though several reaction stoichiometries exist):

$$U_{(s)} + 8\,HNO_{3(aq)} \rightarrow UO_2(NO_3)_{2(aq)} + 6\,NO_2 + 4\,H_2O$$

The oxidation of the uranium metal would result in very little difference between the chemistry for either CRM sample, as the column chemistry procedures should not impact the relatively pure uranium samples. Observations of the variation in raw counts for ^{236}U during measurements seemed to indicate this conclusion, although no quantitative conclusions can be drawn due to bias in measurements.

The BL-5 sample had a significant fraction of impurities (non-uranium species), and was thought to be most impacted by the sample processing procedures. A significant mass reduction was observed for the BL-5 sample between no column and single column procedures (~ 90% mass reduction). The difference between the single and double column procedures had a minimal impact on mass, with variations being within measurement error. The result follows the initial estimate that the double column work (relative to single) has an insignificant impact on AMS measurements. The main purpose with the addition of AG resin is to further separate the minor actinide content, and is used primarily in plutonium analysis. However, the goal for uranium sample procedures is to reduce current fluctuations by producing a homogeneous distribution between AMS targets. The initial low concentrations of minor actinides in the samples, and the high separation yields for UTEVA resins, lead to

an insignificant impact for secondary AG resins on the sample distribution. While far from conclusive, the raw count measurements seemed to indicate a similar assessment, with the majority of variation seen between the no and single column procedures.

The UOC sample measurements were performed simultaneously with the sample preparation experiments. As a result, double column purification was used for the UOC sample procedures at CAMS (which kept consistency with other CAMS uranium measurements). However, the initial conclusions of this work was that UTEVA resin was sufficient for sample purification (although not conclusive). The purification procedures for various facilities (i.e. CAMS and ANU) should result in little variation between the ^{236}U measurements, assuming a sufficient reduction in the ore matrix. This study primarily focused on the variations due to differing purification procedures, however future work can examine influences based on target preparations (additions of a metal matrix, iron oxide carrier, etc.).

III.3.2. Measured ^{236}U Concentrations

The ^{236}U concentrations were measured with AMS in a variety of UOC samples. The uranium concentrations in the samples, as well as the location (when available), is presented in Table III.3. Data for the UOC samples was limited due to proprietary issues at LLNL, and the location data for only a select number of samples was known. The samples were prepared using double column purification procedures through UTEVA and AG resins (see section 3.2.2). Due to similar measurement problems with the previous experiment (see section 3.3.2), only a portion of the UOC samples had ^{236}U concentrations available for analysis. The CAMS [54] measured $^{236}U/^{238}U$ ratio is included in Table III.3 when available.

Table III.3: The UOC prepared samples with uranium fraction estimates and ^{236}U concentrations [54] when available.

Vendor	Name	Uranium Fraction	$^{236}U/^{238}U$	Relative Error
Agency	NUFCOR	~ 10%		
Agency	NUFCOR	~ < 1%		
Agency		~ 10%		
Agency		~ 10%		
Agency		~ < 1%		
Agency		~ 10%		
Agency		~ 10%		
STANDARD		~ < 1%		
STANDARD		~ 10%		
Commercial	Cotter	~ 10%		
Commercial	Belgian Congo	~ 10%		
Commercial	Belgian Congo	~ 10%		
Commercial	Czech	~ 10%	3.44×10^{-9}	1.11%
Springfield	ESI, USA	~ 10%	1.13×10^{-11}	72.70%
Springfield	Randstadt, Sweden	~ 10%	5.12×10^{-9}	2.54%
Springfield	El Mesquite, USA	~ 10%	2.06×10^{-11}	5.83%
Springfield	Kerr McGee, USA	~ 10%	7.23×10^{-9}	1.37%
Springfield	Falls City, USA	~ 10%	1.70×10^{-11}	4.48%
Springfield	Beaverlodge, Canada	~ 10%	2.89×10^{-10}	3.29%
Springfield	Sunnar, Canada	~ 10%		

The $^{236}U/^{238}U$ ratio for the CAMS measured samples ranges from approximately 1 x 10^{-11} to 7 x 10^{-9} relative to uranium concentrations approximately around 10%. In comparison, ANU measured samples obtained $^{236}U/^{238}U$ ratios ranging from 1 x 10^{-12} to 3 x 10^{-10} relative to uranium concentrations between 1% and 75%. The counting statistics for the CAMS measurements for most of the samples were within a few percent (although the ESI sample had upwards of 70% uncertainty). Similar counting statistics were obtained with ANU measurements, with the majority of samples being within several percent with one or two outliers.

It is interesting to note the magnitude increase for the range of CAMS measurements relative to ANU measurements. Although no duplicates exist between the sample sets, the CAMS measurements indicate higher ^{236}U concentrations then has been measured elsewhere. One possibility is due to differences in the abundance sensitivity between the AMS systems. It has been stated that the limit for CAMS $^{236}U/^{238}U$ measurements is on the order of 10^{-11}, compared to the predicted ANU limit of 10^{-12} (although at a cost of increased uncertainty though time-of-flight measurements). The effect of the CAMS limit on ^{236}U measurements is particularly evident in comparison to the ANU samples (with a majority of measurements below this ratio).

III.3.3. Conclusions

The feasibility of using ^{236}U as a nuclear forensics signature can be directly impacted by the capabilities of the AMS measurement systems. More specifically, the precision and accuracy of ^{236}U AMS measurements, specifically between systems, had to be investigated. Key differences between two AMS systems were evaluated:

- The CAMS system implemented additional magnetic analyzers to reduce interfering ions. Sample preparation was performed with double column purification, niobium matrix with iron carrier.
- The ANU system utilized a time-of-flight measurement system to reduce interfering ions. Sample preparation was performed with single column purification, silver matrix with no oxide carrier.

The precision for AMS systems is dictated by beam stability over the measurement time, and by the efficiency of the system (as it relates to counting statistics). Beam stability can be impacted by heterogeneous inclusions in the target, which is reduced through sufficient sample preparation. Differences in sample purification, with no real differences in beam stability noticed between the single and double column purification procedures. The difference between metal matrix (niobium vs. silver) and additions of an iron carrier were not investigated with regards to ionization efficiency.

The accuracy for AMS systems depends on systematic errors that can be introduced in the sample or through equipment performance. Of particular concern for this work was the systematic errors introduced through different AMS setups. Specifically, the use of time-of-flight detection in an AMS system compared to utilizing additional mass/energy selectors. Standards are commonly used to determine the accuracy of a measurement system (or between systems); however, a universal standard for natural ^{236}U has not been developed. General observations were therefore made between two sets of measurements for UOC samples. The abundance sensitivity for ^{236}U was indicated to be a critical factor in AMS measurements. In order for a complete analysis of ^{236}U signatures, the sensitivity limit needs to be below 1×10^{-12}. The abundance sensitivity can be costly to achieve with use of mass/energy selectors alone. Time-of-flight has been shown to perform well, but an assessment of the efficiency errors associated with this system was not performed. Before implementation of ^{236}U as a nuclear forensics signature, a more thorough evaluation needs to measure the same set of samples targets (with identical preparations) to assess any bias between AMS system measurements.

IV. ^{236}U PRODUCTION MODEL

IV.1. Neutron Source Term

Although other mechanisms for ^{236}U production in natural ore bodies were considered (see section II.4.1), neutron radiative capture of ^{235}U was believed to be the most significant. It was determined that the most likely sources of neutrons in an ore body would be due to atmospheric radiation (evaporation, muon-capture, photo-neutrons, etc.) and radioactive decay of primordial isotopes (spontaneous fission, induced fission, and (α,n) reactions). Analytical work (discussed in more detail) was done to evaluate the approximate magnitude of these sources of neutrons for a variety of uranium ore deposits. The ^{235}U radiative capture cross section, however, is not dominated by a specific energy as shown in Figure IV.1 [65]. Calculations were needed on the neutron energy spectra of the various sources as well as the magnitude.

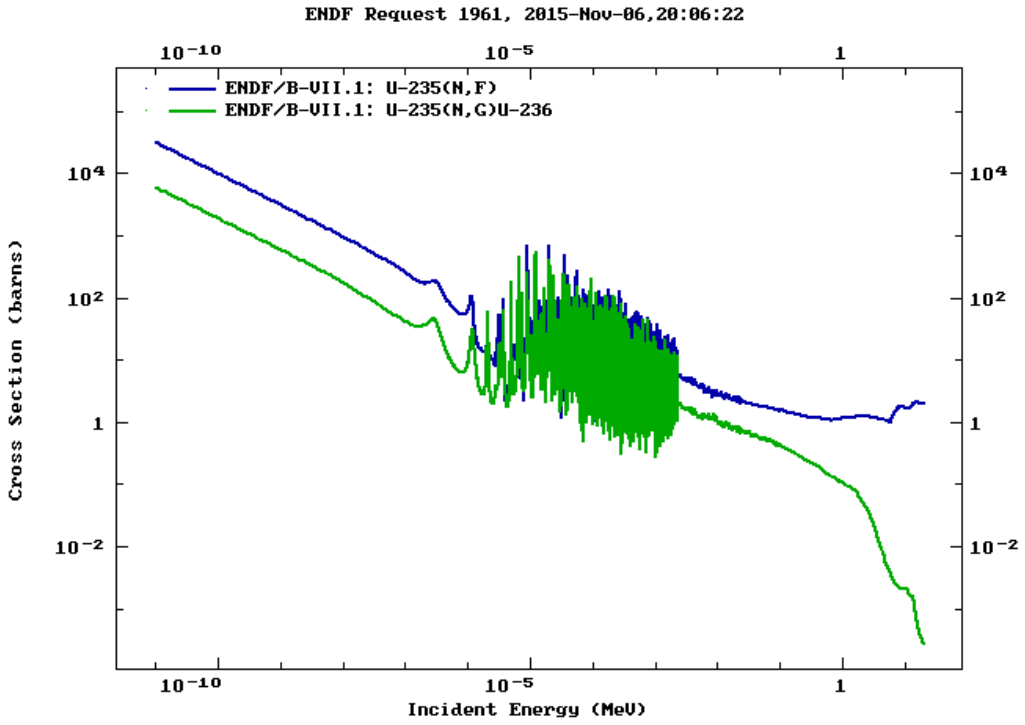

Figure IV.1: A plot of the radiative capture (n,γ) cross section (barns) as a function of incident neutron energy. Data was taken from the ENDF/B-VII.1 library [65].

IV.1.1. Atmospheric Neutron Source

Cosmogenic radiation can be a source of neutron producing reactions at the surface – atmosphere interface. The three main types of reactions are: spallation / evaporation neutrons from cosmic ray nucleons, photonuclear reactions (γ,n), and muon-capture reactions [14]. These neutron sources can be significant in the shallow subsurface, but are greatly attenuated with increasing depth. To be able to compare reaction rates for different ores independent of the density of the rock, depths described hereafter are normalized to the depth of water with the same mass:

$$d = h\,(\rho_b/\rho_w)$$

in which h is the absolute depth (m), ρ_b is the bulk density, and ρ_w is the density of water.

One approach to calculate cosmic neutron fluxes in the subsurface is to empirically measure a standard neutron production rate at the land /atmosphere interface. Factors can then be applied (adjusting the production rate for a given case) and the thermal neutron flux can be directly derived from the high-energy production rate [66], [14]. A significant limitation to this approach is that it neglects intermediate energy interactions. Improvements have been added to this approach by accounting for moderation of the epithermal neutron flux, allowing for a two-group (thermal and epithermal) energy solution which is derived from the fast neutron production rate [17]. This research used a combination of the two methods [17], [14] to empirically solve for the neutron production rate due to cosmic radiation as a function of depth. To solve for the neutron flux, however, the transport code MCNPX was used (see section IV.2).

IV.1.1.1. Spallation and Evaporation Neutrons

The production rate of spallation and evaporation neutrons $(P_n)_{evap}$ can be estimated in the subsurface:

$$(P_n)_{evap} = K_L\,K_E\,K_D\,(P_0)_{evap}$$

where $(P_0)_{evap}$ is the production rate of neutrons at the interface. The other terms are factors that adjust for variation in neutron surface production due to geomagnetic latitude (K_L), atmospheric pressure/elevation (K_E), and cosmic ray nucleon attenuation (K_D).

The production rate can then be normalized to a measured neutron production rate (2000 neutrons g^{-1} yr^{-1}) for a surface (K_D=1) exposed at sea-level (K_E=1) with a geomagnetic latitude of ≥ 60° (K_L=1) [14],[67]. For the scope of this research, variations in neutron production due to the latitude and elevation of the ore body are ignored (K_L, K_E = 1). These effects are thought to negligible relative to the total neutron production, but could be assessed in future work. The value of K_D can approximated by:

$$K_D = \exp\left(-\frac{d}{\Lambda_{n,ss}}\right)$$

where d is the mass depth (g cm^{-2}) below the surface and $\Lambda_{n,ss}$ is the effective attenuation length in the sub-surface for cosmic ray nucleons. The effective attenuation length has been empirically determined to range from 140 to 170 g cm^{-2} [68], [17], and consequently this work will use a value of 155 g cm^{-2}.

IV.1.1.2. Negative Muon Capture

The production of neutrons through negative muon capture (μ^-, xn) reactions can be estimated in the subsurface using:

$$(P_n)_u = K_L\, K_E\, I_u(d) \sum_i (f_c\, f_d\, Y_n)$$

where $I_u(d)$ is the stopping rate of negative muons relative to sub-surface depth, estimated using data from Charalambus [69]; K_L and K_E are factors to account for the effects of geomagnetic latitude and atmospheric pressure/elevation; f_c is the fraction of muons stopped by the target element i; f_d is the fraction of muons stopped by target element i that are captured by the nucleus, and Y_n is the average neutron yield per captured muon. Calculating the adjustment factors for latitude and elevation was beyond the scope of this research and a

conservative solution was to assume the effects were negligible (K_L, K_E = 1) relative to the total neutron production.

IV.1.1.3. Photonuclear Reactions

Another potential source of neutrons can be produced through photonuclear (γ, xn) reactions. The source of gamma rays in the subsurface was thought to be due primarily through bremsstrahlung produced by fast muons. Other gamma sources are present but predominantly have energies inadequate for photonuclear reactions (see section II.4.3). Neutron production through this mechanism can be estimated as a function of depth based on the following empirical equation: [14],[70]

$$(P_n)_\gamma = (7.9 * 10^{-6})\ \ln(8d)\ j_g(d)$$

where j_g(d) is the fast-muon flux as a function of depth. The empirical equation is based on using the following average parameter values: mass number of the ore (25), absorption cross-section (2.5E-26 cm^{-2}), and gamma energy due to bremsstrahlung produced by fast muons (20 MeV). Average parameter values were used due to negligible changes in neutron production when accounting for natural variations in the ores.

IV.1.2. Geologic Neutron Source

Neutron sources are present in all ore bodies, but particularly in uranium ores, due to spontaneous-fission (SF) decay of primordial isotopes and from the interaction of decay alpha particles (from the primordial isotopes or that of their decay daughters). Analytical calculations were initially used to estimate neutron yields for various ore samples. The analytical estimates consisted of using tabulated energy independent mass stopping power and neutron yields. The tabulated data was taken from work compiled by Fabryka-Martin [14]. By utilizing the atmospheric source equations as well (see 4.1.1), an estimate of the neutron production rate could be evaluated. Figure IV.2 represents the analytical estimation for neutron production rate as a function of depth (elemental data was used from UOC sample ANU-103). Depth is represented by mass water equivalent as a means for density normalization between samples. While variations of Figure IV.2 were calculated for many of the UOC samples available in the literature, the general trend remained constant. The

geologic neutron sources was repeatedly shown to significantly dominate the production rate for uranium ore concentrates.

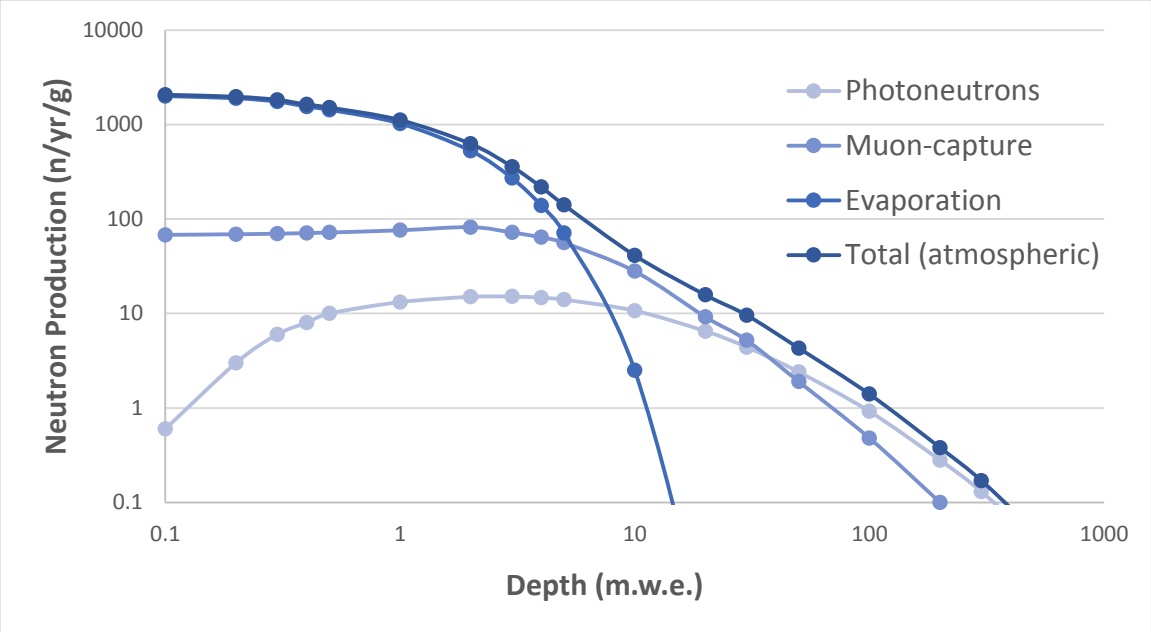

Figure IV.2: Production rate of neutrons from different reactions for UOC sample ANU-103 in a high-Ca granite matrix as a function of depth, depths are relative to a rock surface exposed at sea level at a geomagnetic latitude > 60°

Due to the relative significance of spontaneous fission and (α,n) reactions, more rigorous calculations were needed for the energy spectra (specifically spectra from (α,n) reactions). Multiple techniques were evaluated to solve this issue but ultimately the computer code SOURCES 4C [71] was utilized. SOURCES 4C is a code that can determine neutron production rates and spectra due to spontaneous/induced fission and (α,n) reactions. One advantage over the previous analytical calculations is that it can solve the neutron spectrum for up to 750 energy groups (linearly interpolated between a user-defined maximum and minimum energy). This is a vast improvement to the 1 group energy spectra previously calculated analytically. The output of the spectra from the code can also be adjusted for easy coupling to the transport code MCNP (see VI.2) due to the output structure.

Another advantage is the code is capable of calculating (α,n) source rates and spectra for a variety of geometries including: homogeneous media, two-region interface problems, three-region interface problems, and mono-energetic beam of α-particles incident on a slab of target material. One of the main difficulties in calculating (α,n) reactions in ore bodies is the modeling the distribution of elements or minerals in the ore matrix [14],[13]. Typically, a homogeneous distribution is assumed for the elements in the ore which can be a considerable over-simplification. Elements typically exist as mineral phases in the ore, which have a specific structure that is not representative of a homogenous mixture. The range of α-particles is also on the scale of tens of micrometers, which leads the mineral matrix of the ore to play a bigger role in the reaction rate. The production of neutrons can depend more on the composition of the uranium phase and the elements bordering on the uranium mineralogy then on the bulk composition. The ability of SOURCES 4C to model an interface geometry potentially could be used to estimate more accurate neutron source rates and spectra due to (α,n) reactions. New assumptions were needed to utilize the interface geometry, however, which could possibly lead to greater error in the calculations. To evaluate the better approach for SOURCES 4C, comparisons were made with both the homogeneous media and the two-region interface geometries against several experimental test cases.

IV.1.2.1. Homogenous Geometry

A full description of the theory and methodology of the code can be found in the very well written manual for SOURCES 4C [71], but a brief summary of the mechanics is as follows. For all geometries, the spontaneous fission spectra are calculated for 43 actinides using half-life data, spontaneous fission branching ratios, and Watt spectrum parameters. The (α,n) spectra are calculated by assuming a center-of mass system with an isotropic angular distribution. Data is included for the α-particle spectra from 89 source nuclides as well as measured and/or evaluated (α,n) cross sections and product nuclide level branching fractions from 24 target nuclides. The functional α-particle stopping cross sections were included for up to $Z < 106$. The delayed neutron spectra were taken from an evaluated library of 105 precursors.

A homogeneous mixture problem assumes the source material (α-emitting material) and the target material (low-Z target material). Another assumption is that the target material is thick (relative to the range of the α-particles) and therefore all α-particle tracks are within the mixture. To assess the geometric assumptions, as well as the ability of SOURCES 4C to reasonably estimate neutron production rates, experimental measurements were needed.

There exists limited measurement data of neutron production rate in ores, which is somewhat due to the difficulty of the measurements. In-situ measurements would need to employ downhole neutron probes and track detectors, but then have the difficulty of obtaining source and target composition. Measurements of the flux in drillcore samples can be done using coincidence counting to distinguish the source of neutrons (spontaneous fission and α induced neutrons). However, drillcore samples disturb secular equilibrium and therefore have biased (α,n) measurements. A full validation of the SOURCES 4C code in regards to uranium ore (α,n) calculations would use a combination of the different measurement methods. In the scope of this research, measurement data from Fabryka-Martin et al. (drillcore samples) were used to compare to S.F. and (α,n) calculations from SOURCES 4C [15]. The data was collected on primary ore samples from the following ore deposits: Koongarra, Key lake, Cigar lake, and Oklo (along with UOC reference standards). The bulk elemental composition of the ores were included with the neutron production rates, making it possible to compare to rates calculated through SOURCES 4C based on a homogenous geometry. The calculated and measured neutron production rate and the percent deviation is shown in Table IV.1.

Table IV.1: Total neutron production rate measurements and calculations (SOURCES 4C in a homogenous geometry) are compared in a suite of uranium ores.

Sample	***Calculated*** ***(n yr^{-1} g^{-1}U)***	***Measured*** ***(n yr^{-1} g^{-1}U)***	***Fraction*** **(calc/meas)**
Koongarra			
G2698	7.52E+05	8.99E+05	0.837
G4674	8.70E+05	9.25E+05	0.941
Key lake			
KL785	7.67E+05	9.97E+05	0.769
KL756	5.50E+05	8.52E+05	0.645
Cigar lake			
CS235L	7.54E+05	9.06E+05	0.833
W83A	6.47E+05	7.76E+05	0.834
W83C	6.74E+05	7.48E+05	0.901
Oklo			
Z9-05	7.72E+05	6.66E+05	1.159
Z9-28	7.71E+05	6.56E+05	1.175
Standard UOC			
NBL-6	5.67E+05	8.93E+05	0.635
Reference Mat			
Metal	4.27E+05	4.58E+05	0.933
UO_2	4.75E+05	5.08E+05	0.934
U_3O_8	4.84E+05	5.43E+05	0.892

IV.1.2.2. Interface Geometry

Interface problems occur when an α-emitting material (such as uranium) forms a boundary with a low-Z or target material as shown in Figure IV.3. In the case for uranium ore, the two-region interface geometry allows the consideration of the uranium mineral (for example U_3O_8) to interface against the other mineralogy of the ore (^{17}O, ^{18}O, ^{23}Na, ^{27}Al, etc.). Region 1 materials emit α-particles that travel across the interface junction into the Region 2 material

where (α,n) reactions can occur and produce a neutron source. The thickness of the two regions is assumed to be significantly larger than the range of the α-particles, which simplifies the calculations. Another assumption is the α-particle tracks are linear (straight line trajectory) from the point of emission.

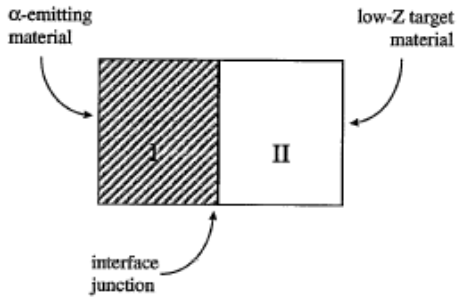

Figure IV.3: A schematic of the interface geometry solved for in SOURCES 4C [71].

The interface geometry solution was tested against the same suite of UOC samples taken from the Koongarra, Key lake, Cigar lake, and Oklo ore deposits [15]. The calculated and measured neutron production rate and the percent deviation for the interface geometry was evaluated utilizing a suite of uranium ores shown in Table IV.2.

Table IV.2: Total neutron production rate measurements and calculations (SOURCES 4C in an interface geometry) are compared in a suite of uranium ores.

Sample	***Calculated*** ***(n yr^{-1} g^{-1}U)***	***Measured*** ***(n yr^{-1} g^{-1}U)***	***Fraction*** **(calc/meas)**
Koongarra			
G2698	7.95E+05	8.99E+05	0.884
G4674	8.82E+05	9.25E+05	0.954
Key lake			
KL785	7.85E+05	9.97E+05	0.787
KL756	6.09E+05	8.52E+05	0.715
Cigar lake			
CS235L	7.68E+05	9.06E+05	0.848
W83A	6.87E+05	7.76E+05	0.885
W83C	6.90E+05	7.48E+05	0.922
Oklo			
Z9-05	7.81E+05	6.66E+05	1.173
Z9-28	7.63E+05	6.56E+05	1.163
Standard UOC			
NBL-6	6.61E+05	8.93E+05	0.740
Refence Mat			
Metal	4.27E+05	4.58E+05	0.933
UO_2	4.75E+05	5.08E+05	0.935
U_3O_8	4.84E+05	5.43E+05	0.892

The interface solution resulted in an improvements to the calculated neutron yield for the majority of the cases. The average increase between the homogenous and interface geometries for neutron yield was approximately 4%, with a maximum increase of 10% calculated for sample NBL-6. While the magnitude improvements were not substantial, the effects on the neutron spectrum were more pronounced. A comparison of homogenous and interface solutions for sample G4674 is shown in Figure IV.4. The difference in neutron

spectrum is primarily a function of the (α,n) reactions (although slight perturbations are possible for S.F. due to attenuation). The lower shift in average energy can be attributed to the lower energy distribution (due to the interface junction) of the alpha particles relative to the target atoms. The shift in the spectrum for interface solutions is more likely a better representation due to the grain structure of the uranium ores. All subsequent source calculations utilized the interface geometry as a result.

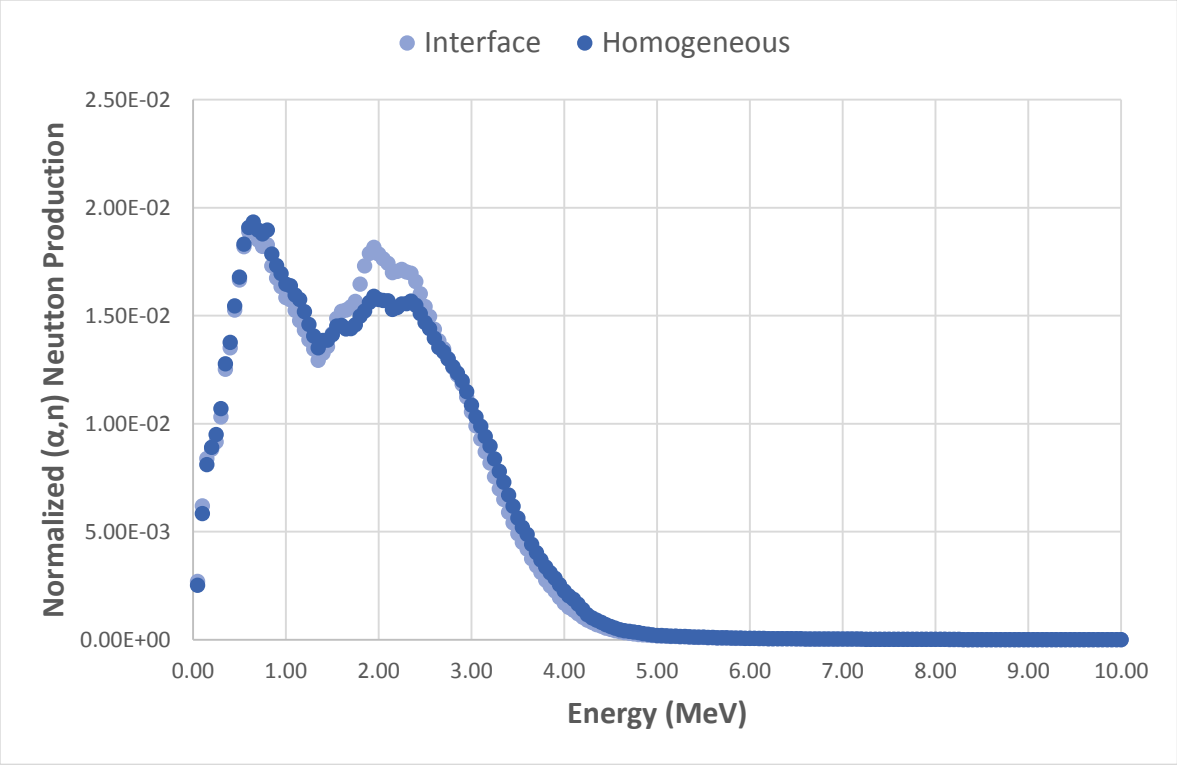

Figure IV.4: The homogeneous and interface SOURCES 4C calculated energy spectrum for (α,n) neutrons utilizing UOC sample ANU-103 (200 energy groups).

IV.2. MCNP Model

Once the source term was found, a model was developed to account for neutron transport and capture in a given ore body. The objectives in developing the model was to estimate ^{236}U production in various ore samples and to identify sensitive or critical parameters influencing

production rates. A Monte-Carlo code (MCNPX2.7) was used over analytical methods in order to utilize 3-D geometric representation and continuous energy/angular calculations. Characteristics of the ore (elemental composition, density of the media, neutron sources, etc.) can all be specified in the model to calculate neutron capture for specific nuclides.

Limitations of the MCNP production model are largely based on the inability to accurately model the ore body with partial information. A detailed mineral distribution and geometric structure within the ore body will never be known completely, however, the model can utilize the bulk nature of mineralization. Based on the mean neutron path length, the ore body can be assumed to have a degree of homogeneity. Since the production rate (or particle flux) is evaluated over the entire ore deposit, variations existing at different points in the heterogeneous ore deposit may be averaged out. In this way, the error associated with a homogeneous model can be reduced.

The MCNP modeled ore body will need the following variable inputs: the particle source term, the elemental composition (mineralogy), and the water content (porosity/inclusions). The input parameters will be estimated, and minimum/maximum boundaries are used to account for potential variability in the estimations. The output of the neutron source model (neutron production rate and energy spectrum) was used as the source term, for various depths. The mineralogy of the uranium deposit, obtained from mining databases, was used to account for neutron scattering and absorption. The ore geometry was modeled using several bounding cases, such as infinite ore (no leakage) and planar (high leakage).

IV.2.1. Properties of the Model

IV.2.1.1. Elemental Content

The elemental compositions of the uranium ore concentrate is required for the MCNP production model. The elemental analyses of the UOC samples was obtained from several sources[15],[13], which utilized differing measurement techniques. The elemental composition of all the samples, as well as the measurement analysis, is provided in Appendix VI.1. Wavelength spectroscopy and x-ray diffraction were mostly used for the major elemental (Na, Mg, Al, Si, etc.) analyses. The minor elemental (Gd, Sm, Th, etc.) analyses

mostly used laser ablation inductively coupled plasma mass spectrometry (ICP-MS). To combine the measurement methods, considerations were made for the sensitivity and uncertainty analyses. This allowed bounds to be placed on the elemental composition (related to the accuracy/precision of the measurement technique) in order to represent the biased uncertainty in the model.

IV.2.1.2. Uranium Content

Measurements of the uranium isotopics was used in the model when available. The measurements were typically preformed using alpha spectroscopy[15]. However for most cases it was assumed that the isotopics (specifically ^{234}U) had no variations from that of equilibrium. The sensitivity of the production model for variation in ^{234}U and ^{235}U was examined in a scoping study (see section IV.3.3).

IV.2.1.3. Porosity and Inclusions

Hydrogen (water content) was difficult to obtain for the UOC. Hydrogen is present with any hygroscopic minerals, with sorb water molecules either through surface processes or though inclusions (water trapped within the crystal structure of the mineral). This adsorption is disturbed with the removal and processing of the UOC, which can remove water content that is present in-situ. On the contrary, hygroscopic minerals in UOC samples that are exposed to the atmosphere (during processing, storage, etc.) will naturally sorb water that might not have been present or available in the ore body. Estimations of the hydrogen content was therefore calculated based on the mineralogy of the ore samples. Two processes were considered for the introduction of water content in the uranium mineralogy: water filled porosity of the mineralization, and sorption of water in the mineral phase through inclusions. To calculate the water content as a function of porosity the following relation was used:

$$H_{por} = \phi \rho_{bulk} \Big/ \sum_{i=mineral} \frac{M_i}{M_t} \rho_{particle,i}$$

where ϕ is the porosity, ρ_{bulk} is the bull density of the ore, and $\rho_{particle,i}$ is the particle density of the specific mineral. The minerals considered were UO_2, PbO_2, NiAsS (sulfides: sum of sulfur, copper, nickel, arsenic), FeOOH, and silicates (chlorite, illite, kaolinite). It was

assumed for the purposes of this estimation all of the elemental content of the sample falls under one of the mineral categories. Using the particle densities of the mentioned minerals (Table IV.3) and the range of 1% to 5% porosity, the range of hydrogen content can be estimated as a function of porosity.

The hydrogen content due to inclusions in the mineral phase were found through the following relation:

$$H_{incl} = \sum_{i=mineral} \frac{M_i}{M_t} I_i$$

where I_i is average water present in inclusions for the specific mineral. The data for the water inclusions was averaged from several sources [72],[73],[74] and is shown in Table IV.3. Since silicates constitute a large percentage of minerals, the data table was broken up into a minimum (assume silicates are a mixture of muscovite, kaolinite, illite) water content and maximum (assume silicates are primarily chlorite) water content. This helps account for the uncertainty associated with the estimation.

Table IV.3: Grain density and fluid inclusions for the set of minerals obtained from several sources [72],[73],[74].

Mineral Phase	Grain Density (g/cm3)	Min H Fluid Inclusion	Max H Fluid Inclusion
UO_2	7.5	0.0014	0.0014
PbO_2	7.5	0	0
NiAsS	6	0	0
FeOOH	4	0.0075	0.0075
Silicates	2.5	0.0075	0.013

IV.2.1.4. Geometry

The goal of the model was not to simulate the exact structure of the uranium ore body. The level of detail needed is not feasible for UOC samples, and adds complexity to the model that does not necessarily improve the results. However, depending on the specific sample, some geometric considerations are needed. The geometric modeling of the UOC was conducted for two types of geometries: infinite model and borehole model.

The infinite model assumes no neutron leakage from the uranium mineralogy. The model consists of a sphere with mirror boundaries (the elemental composition and bulk density of each sample are used for the material properties). The neutron source is evenly distributed throughout the sphere. The mirror boundaries placed on the sphere allow particles to be reflected back into the material, simulating an infinite geometry. Typically the UOC samples are obtained from high uranium grades (i.e. the material surrounding the sample location have lower concentrations of uranium). If this is the case, the infinite model provides an upper limit of ^{236}U production.

Realistically, the uranium mineralization in the ore body is finite. The borehole model attempts to account for neutrons that leave the uranium rich mineralization, and therefore do not contribute to the potential production of ^{236}U. Each sample was modelled as the primary, higher grade material (same material characteristics as the infinite model) surrounded by a lower uranium grade material (i.e. sandstone, quartz, etc.). The geometry of the primary material was cylindrical with dimensions averaged using several uranium mineralization records obtained from the World Distribution of Uranium Deposits (UDEPO) [75]. The majority of UOC samples were obtained through sandstone deposits in this work, so the model is characteristic of those dimensions.

The main assumption in the borehole geometry is that most of the uranium is contained in the cylindrical dimensions used. This provides a lower boundary (not necessarily a minimum) for the production model. If a significant portion of the uranium is outside the dimensions (i.e. surrounding material has a high grade), then the ^{236}U production should approach that of the infinite model. The elemental composition of the surrounding material was determined

using scoping studies. The impact of the bounding material (differences between shale, sandstone, granite, etc.) was not significant (unless secondary uranium mineralization was used for the bounding material) and for consistency, sandstone was used for all samples. Sensitivity studies were performed (see section 4.4.5) to determine the dependency of the model on geometric dimensions, specifically on the neutron leakage outside the model.

IV.3. Comparative Results

A range of uranium ore samples were obtained[13] to assess the accuracy of the MCNP production model. A complete assessment of the accuracy would include analysis of samples evenly distributed across country origin and/or classification. While this work attempted an exhaustive evaluation, two main obstacles were encountered: lack of ^{236}U measurement data and proprietary information. The lack of measurement data is slowly being resolved with more AMS measurement campaigns, including work done in this research. The other obstacle is due to the commercial nature of uranium ore mining. Mining companies are concerned that open information on UOC samples could lead to knowledge of their specific procedures. Due to this concern, access and open data on UOC samples are very limited. A more in-depth discussion and possible resolutions can be found in the future work section. As a consequence of these obstacles, only the samples found in Table IV.4 were able to be used for a comparative analysis of the model.

Table IV.4: UOC Samples used for the comparative analysis of the model, including country origin and classification.

Sample ID	Country Origin	IAEA Class.	Depositional Class.
ANU-103	Australia	Vein	High-Temp Redox
ANU-093	Italy	Volcanic	High-Temp Redox
ANU-094	Italy	Volcanic	High-Temp Redox
ANU-098	Madagascar	Intrusive	High-Temp Redox
ANU-102	Czech Republic	Sandstone	Low-Temp Redox
ANU-097	Australia	Unconformity	High-Temp Redox
ANU-104	Australia	Intrusive	High-Temp Redox
ANU-105	Australia	Intrusive	High-Temp Redox
ANU-83	BL-5 Reference	n/a	n/a
ANU-99	Italy	Volcanic	High-Temp Redox
ANU-101	Czech Republic	Sandstone	Low-Temp Redox
ANU-267	Torbernite	n/a	n/a
ANU-92	France	Vein	High-Temp Redox
ANU-91	Australia	Sandstone	Low-Temp Redox
ANU-100	Zambia	Sandstone	Low-Temp Redox
ANU-096	Zambia	Sandstone	Low-Temp Redox
ANU-108	Gabon	Oklo	n/a
ANU-109	Gabon	Oklo	n/a
ANU-88	BL-3 Reference	n/a	n/a

Table IV.5 shows some of the key parameter data for the samples, such as the uranium, hydrogen, and gadolinium/samarium concentrations. The data used is for the average case and does not show the range used for sensitivity and bounding results. For a complete description of samples used, including elemental composition, see Appendix VI.1.

Table IV.5: The uranium, hydrogen, and gadolinium/samarium concentrations used in the production model for comparative analysis.

Sample ID	Uranium Content	Hydrogen Content	Gd + Sm Content
ANU-103	1.99%	1.31%	0.097%
ANU-093	2.46%	1.40%	0.003%
ANU-094	2.04%	1.47%	0.004%
ANU-098	9.89%	1.32%	0.036%
ANU-102	14.70%	1.26%	0.008%
ANU-097	69.20%	0.47%	0.055%
ANU-104	17.80%	1.07%	0.050%
ANU-105	2.85%	1.33%	0.080%
ANU-83	7.68%	1.34%	0.005%
ANU-99	20.30%	1.00%	0.085%
ANU-101	37.20%	0.91%	0.006%
ANU-267	42.60%	0.80%	0.013%
ANU-92	50.00%	0.74%	0.003%
ANU-91	62.70%	0.56%	0.011%
ANU-100	71.00%	0.45%	0.322%
ANU-096	74.50%	0.40%	0.334%
ANU-88	1.07%	1.47%	0.002%
ANU-108	67.90%	0.49%	0.097%
ANU-109	70.60%	0.45%	0.086%

The MCNP calculated $^{236}U/^{238}U$ atom ratios are compared to the AMS measured values presented in Figure IV.5. The error bars on the measured results are representative of the counting statistics only (effects of biasing not accounted for). The error bars on the simulated results are based off of uncertainties with the elemental measurements in the UOC samples. The range of calculated ratios was predicted to be from approximately 8×10^{-13} to 8×10^{-11} for the UOC samples. The average $^{236}U/^{238}U$ atom ratio was observed to be approximately to 1×10^{-11}, an important consideration for AMS abundance sensitivity.

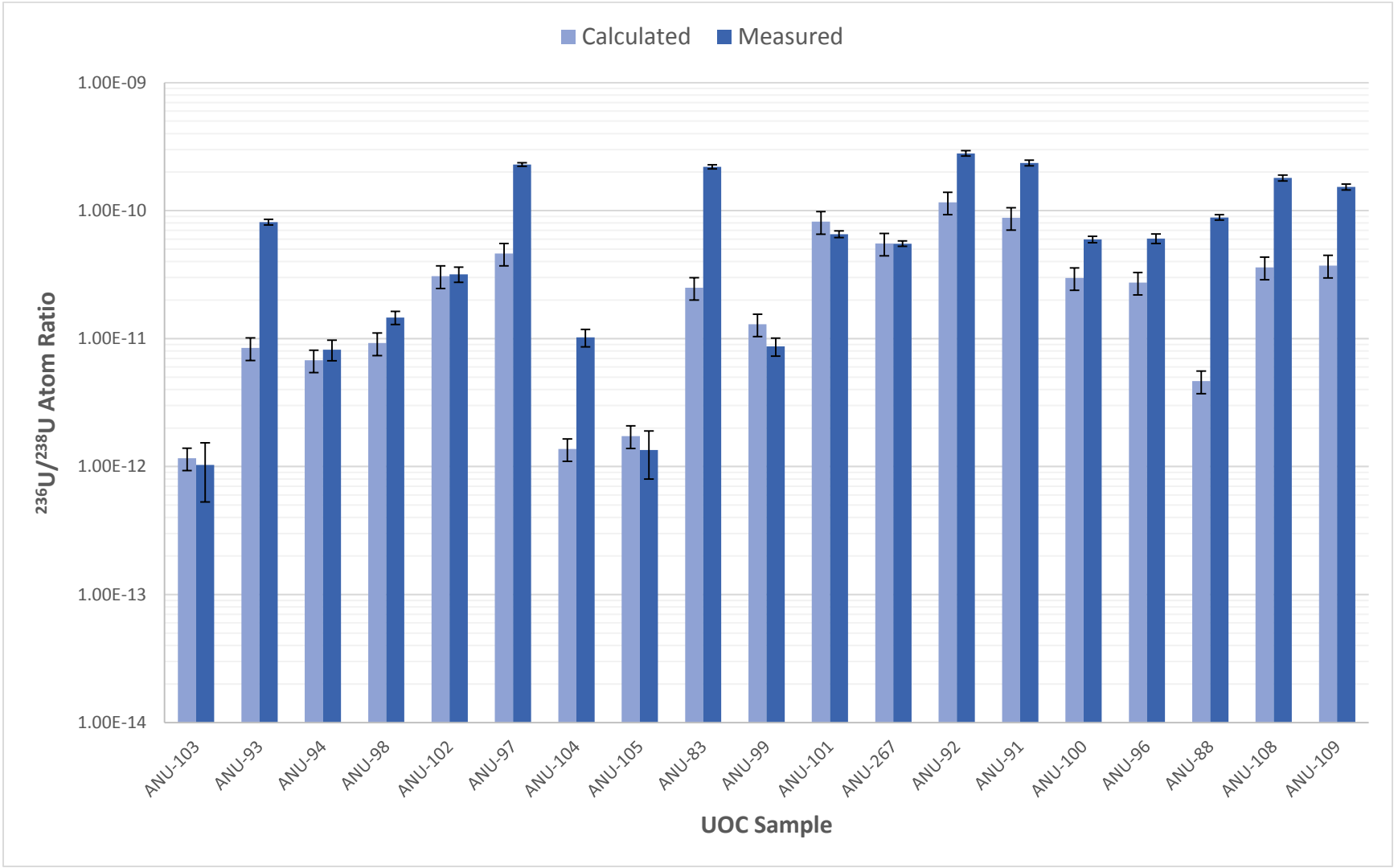

Figure IV.5: A comparison of the calculated to AMS measured $^{236}U/^{238}U$ ratios for various UOC samples.

There is generally very good agreement between the measured and calculated results in Figure IV.5; however, several samples have notably large variations, specifically samples ANU-83, ANU-88, ANU-93, ANU-104. ANU-83 and ANU-88 are reference UOC, meaning it has possibly been homogenized and processed from several source ores. Due to the extensive homogenization and processing, the trace elemental characteristics most likely are not representative of the initial conditions of the ore. Also the infinite geometry might be more appropriate for modeling the reference samples (although still under predicts relative to the AMS measurements). The large variations between calculations and measurements in samples ANU-93 and ANU-104 are more difficult to account for. It is interesting to note that both of these samples have very similar samples counterparts with which the model does significantly better in predicting ^{236}U concentrations. For ANU-93, there is ANU-94 with the same country and ore classification (Italy and volcanic classification), and even closely similar uranium concentration. For ANU-93, there is ANU-94 with the same country (Australia) and the same classification (Intrusive). As discussed previously, the accuracy and precision of ^{236}U AMS measurements is very difficult to estimate (no existing standards). It is entirely possible that the measurements of those two specific samples were biased towards higher concentrations (possible current or contamination bias). Or the estimations of the model parameters might inadequately represent the UOC initial conditions. This could be through the specific processing procedures of the sample that could lead to significant addition or removal or trace elemental content.

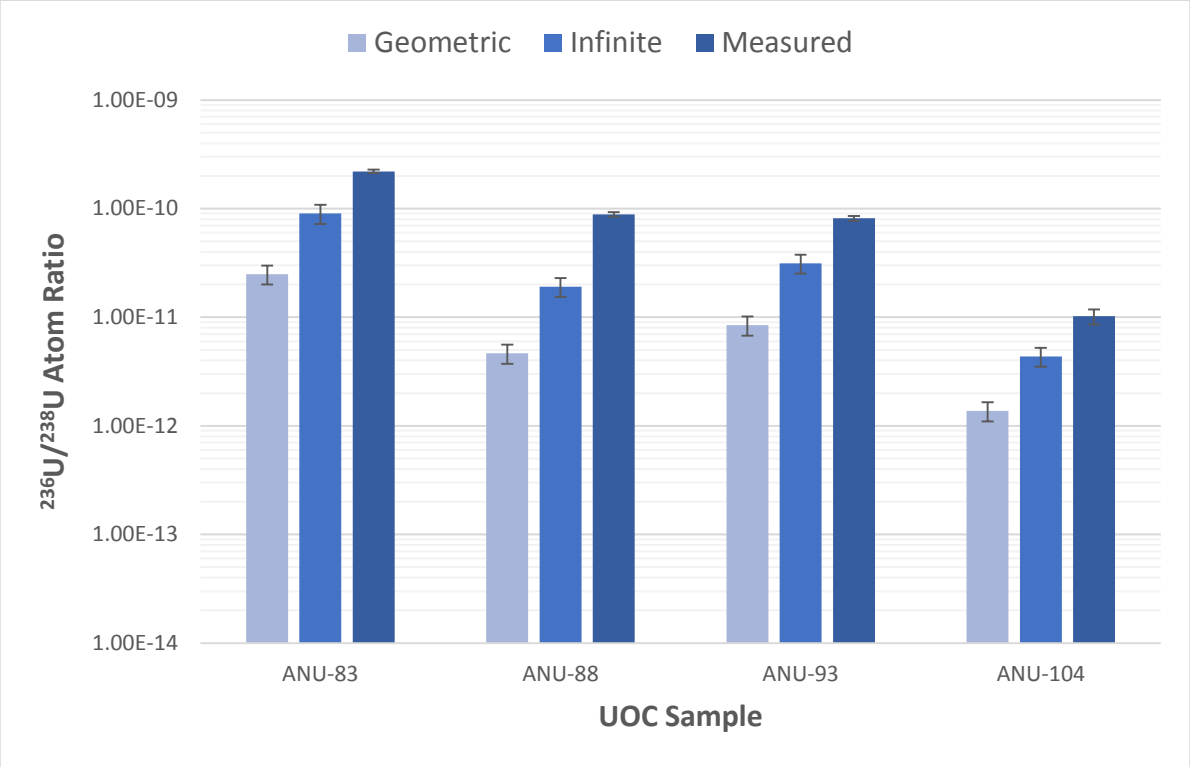

Figure IV.6: A comparison of the $^{236}U/^{238}U$ atomic ratio of the modeled borehole and infinite geometry relative to the AMS measured values.

For highly processed ore concentrates, an infinite geometry can be shown to better represent the ^{236}U production. Figure IV.6 shows samples ANU-83, ANU-88, ANU-93, ANU-104 for both the borehole and infinite geometry in comparison to the measured results. For each of the samples, the comparison to measured results improved by around an order of magnitude.

IV.4. Sensitivity Studies

One of the goals in this study was to determine the primary conditions that influence variations in ^{236}U content. The production model was used to evaluate the sensitivities on multiple variables which can affect the production and transport of neutrons in the uranium ore body. The linear correlation between these parameters can also be tested through the model. The sensitivity of these parameters in regards to ^{236}U content in ore can also be used to assess the uncertainty of the model. No model is without a degree of uncertainty, and

modeling ^{236}U production is no exception. However a model can still be a valuable tool with an understanding of the causes and scale of the biased uncertainty. The sensitivity study focuses on the factors that are difficult to estimate and/or have a predicted high influence including: the content of water through porosity and inclusions, the concentration of gadolinium and samarium, the concentration of uranium in the UOC, effects on the initial neutron energy spectrum, the geometric and temperature parameters, and time influences.

IV.4.1. Water Content

Hydrogen has had a long history of importance as a moderator in neutron reactions. One only has to look at the natural Oklo reactor to appreciate the influence water can have on an environmental neutron flux. As a consequence, it has been predicted by several authors to be a primary factor in variations in ^{236}U concentrations. A secondary concern is the difficulty in estimating the water content that is present in the ore body, as measurement techniques disturb the true value. Also this value is not necessarily a true representation of the average water content during the lifetime of the ore body. The sensitivity of the water content on the model was tested in two phases: one testing the most likely range in water content for each sample estimated through previous works, and the other testing the behavior of the model with a more extreme range of water content (not intended to be representative of the UOC sample). It was important to test the sensitivities of a variety of samples (for each sensitivity parameter) to assess the linear correlation between the different parameters in the model.

Figure IV.7 shows the variation in ^{236}U concentration between that of the estimated range in water content for each sample. The variation in water content is consistent with previous measurements of uranium ores which commonly consist of 1 – 2% hydrogen in the form of water. As can be seen in Figure IV.7, the change in production of ^{236}U relative to hydrogen content can be significant, with an average variation of ~ 20.0% (between the hydrogen bounds).

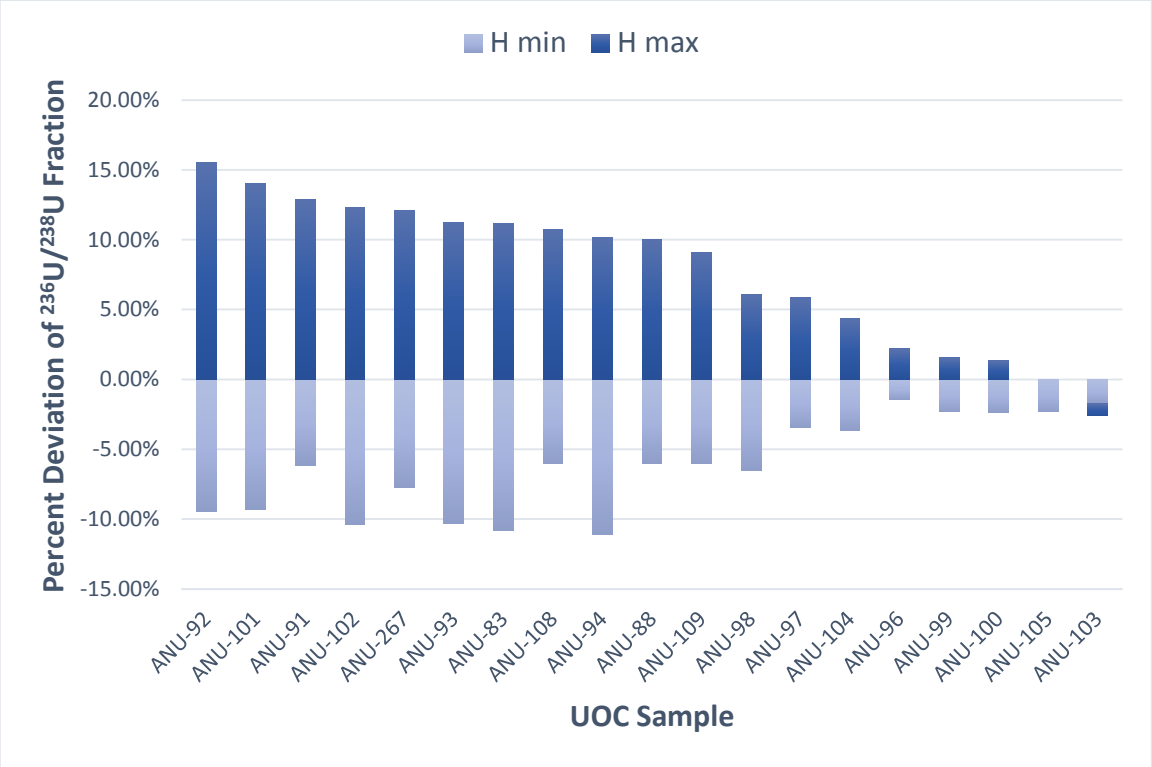

Figure IV.7: The percent deviation of ^{236}U concentration with the minimum and maximum bounds of hydrogen.

Several authors have considered water content to account for the significant portion of ^{236}U variation. At least for the current model, this appears not to be the case. The role hydrogen plays in affecting the ^{236}U production is by acting as a moderator for the neutron flux. The range in hydrogen content (0 to 2.5%), while significant, does not account for the majority of variation in ^{236}U concentrations observed in UOC samples (i.e. orders of magnitude). Also by examining the capture cross section of ^{235}U, the ^{236}U production is not a purely thermal process. The energy dependent capture rate is further investigated in section IV.3.4.

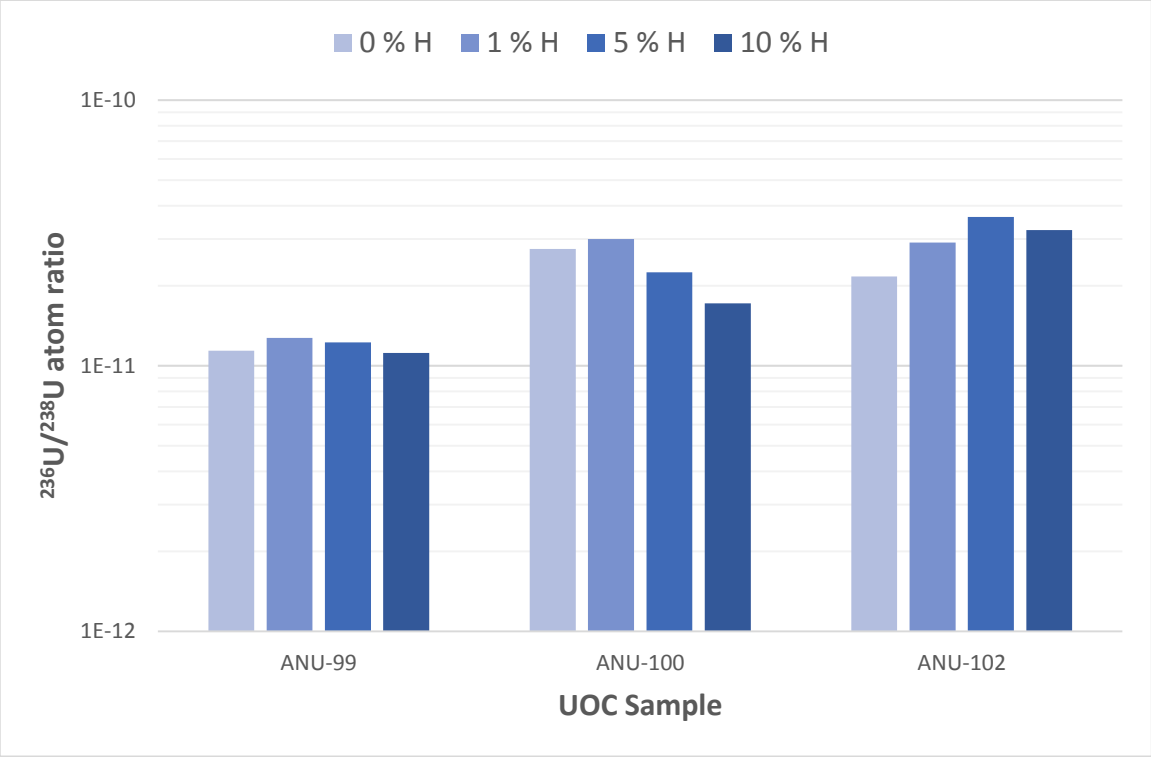

Figure IV.8: The variation in ^{236}U concentration as a function of hydrogen content

Although some variation in ^{236}U can be seen for small changes in water content, a possibility still exists that a UOC sample can have a larger concentration in the ore body. Water is not necessarily the sole contributor to hydrogen content in ore bodies. Organic compounds (such as oil) can lead to increased hydrogen contents around 5 – 10%. Even though these conditions are far less likely for uranium mining ores (one reason this is not accounted for in the model), the effects of a large hydrogen concentration is still explored. Figure IV.8 shows the impact of large changes in hydrogen content for a variety of UOC samples. The hydrogen content was changed to weight fractions of 1, 5 and 10% with the other major elemental concentrations being scaled down accordingly. While the model was tested for large hydrogen ranges, the water content in the UOC samples was more likely within 2 to 3%. Higher water concentrations is thought to be unlikely for significant time periods, due to instability of the uranium ore. Even considering a high concentration of hydrogen (10%) in the ore samples, the average variation in ^{236}U concentration was within 16%. According to

the model, water content is not an influential factor relative to the large variations seen in ^{236}U concentrations.

IV.4.2. Gadolinium / Samarium (Rare Earth Elements)

Gadolinium and samarium both have the potential to have a large impact on the production of ^{236}U in uranium ore. The thermal absorption cross section for gadolinium is approximately 49700 barns, which is four orders of magnitude higher than that of typical major elements found in uranium ores. Samarium also has a high thermal absorption cross section of around 5920 barns (approximately 3 orders of magnitude higher that other ore elements). The variation seen in UOC samples used in this study and from other sources [15] is on the order of 10s to 100s ppm (weight fraction), with several samples measuring in the 1000s of ppm. As a consequence, a large range of both samarium and gadolinium concentration is shown in Figure IV.9 and Figure IV.10 respectively to test the sensitivity of the model. As previously discussed, the elemental concentrations of the samples were scaled accordingly to changes in the rare earth content.

Figure IV.9 and Figure IV.10 show the gadolinium and samarium effects on the ^{236}U production model respectively, for a few select UOC samples. The UOC samples displayed in the figures were selected to represent the full variation in the ^{236}U concentration measured for the study. Very little difference is noted between the use of gadolinium compared to samarium for the same concentrations. For small concentrations (10 ppm), gadolinium relative to samarium resulted in a higher production rate with an average fractional deviation of 1.11. Larger concentrations result in a shift, where gadolinium relative to samarium has a lower average fractional deviation of 0.96 for the samples. However the variance between the deviations indicated that other factors, such as the energy dependent neutron flux, play an influential role.

The effects of either samarium or gadolinium seems to be very dependent on the other conditions of the ore. The UOC samples in both Figure IV.9 and Figure IV.10 were chosen to represent the upper and lower ranges of deviation based on REE concentration. Samples ANU-93 and ANU-102 are representative of UOC that are very sensitive to additions of REE

concentrations. On the other hand, samples ANU-100 and ANU-96 are representative of UOC that are relatively insensitive to REE content. One possible parameter that can control the sensitivity is the energy dependent neutron spectrum. More precisely, the energy dependent ^{236}U production spectrum

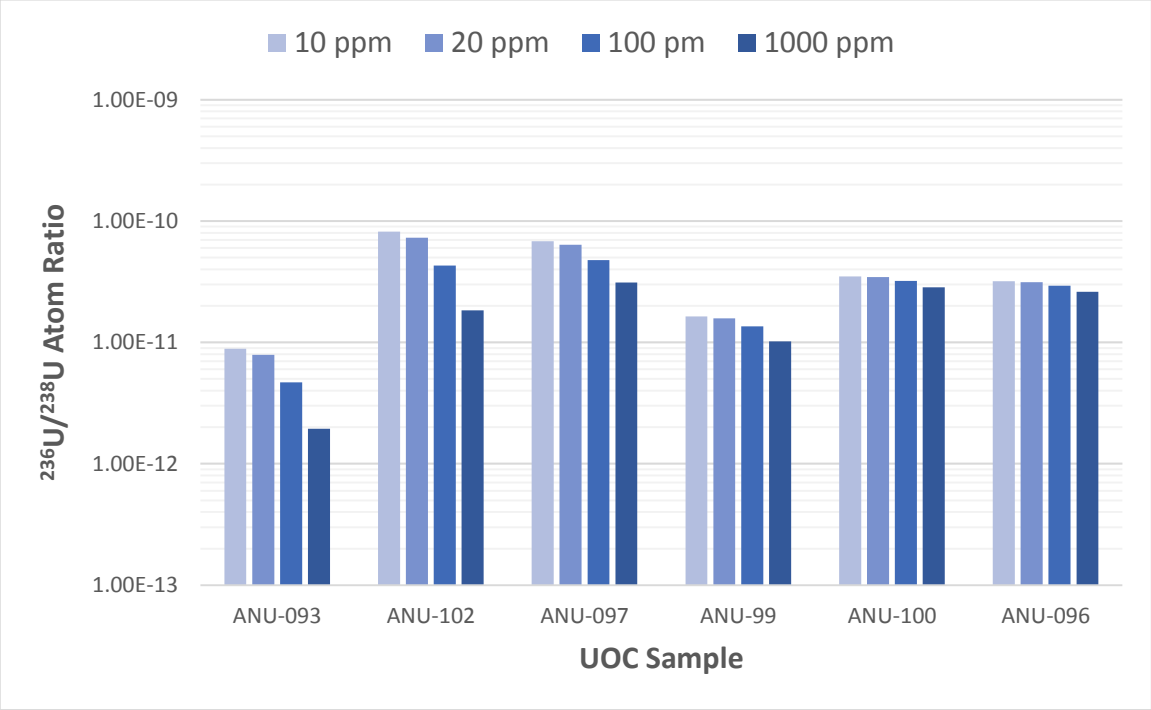

Figure IV.9: The dependence of gadolinium concentration on the ^{236}U production model

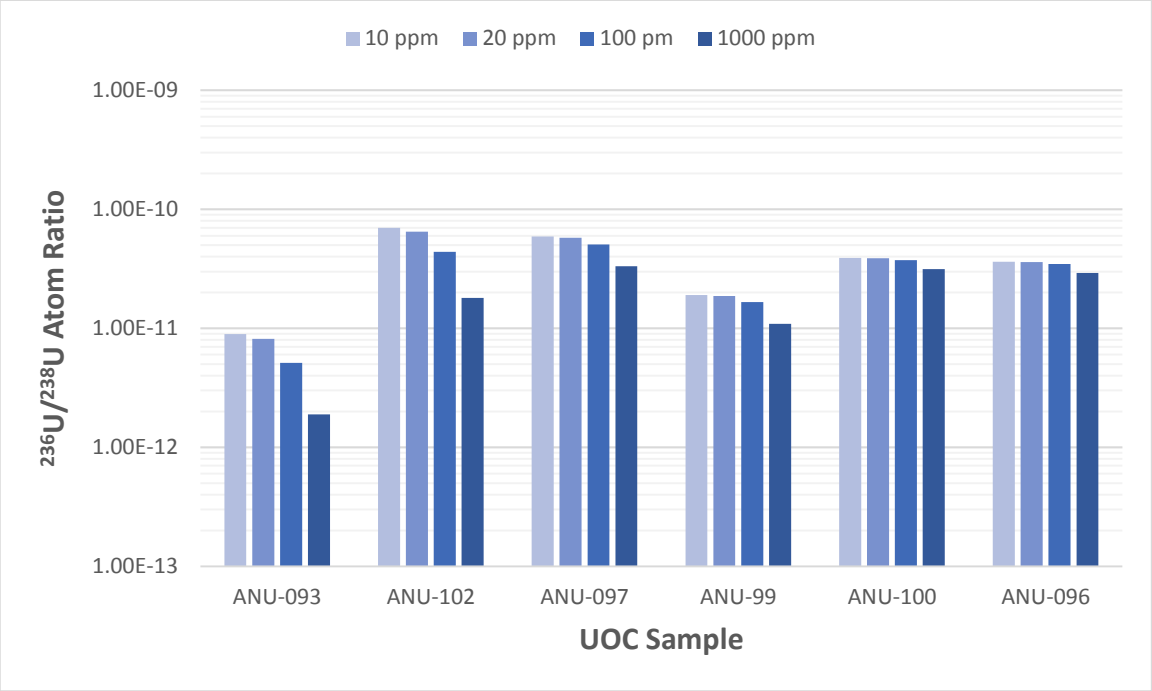

Figure IV.10: The dependence of samarium concentration on the ^{236}U production model

The isotopics of both gadolinium and samarium were assumed to constitute that of natural isotopic abundances found in the 1997 report of the IUPAC Subcommittee for Isotopic Abundance Measurements [76]. The average natural isotopic abundances are not necessarily representative of the specific UOC sample. A great example of this can be seen in the Oklo ore body, where a high neutron flux led to a shifted equilibrium for the isotopics of the rare earths (large neutron absorbing isotopes were burned up due to the high neutron fluence). Simple analytical calculations were performed to approximately assess the potential changes in the REE isotopics:

$$\Delta\frac{^{158}Gd}{^{157}Gd} = \varphi t\sigma^{157}\left[1+\left(\frac{^{158}Gd}{^{157}Gd}\right)_{nat}\right] + \frac{\varphi t\sigma^{155}}{4}\left(\frac{^{158}Gd}{^{157}Gd}\right)_{nat}\left(\frac{^{155}Gd}{^{156}Gd}\right)_{nat}$$

Using the highest predicted neutron fluxes from the samples and a conservative estimation of the age of the ore, the percent change is approximately 5%. Given the relatively small concentration of REE in the sample to begin with, it was thought that a 5% deviation to the gadolinium and samarium (similar equation) isotopics would have a negligible effect on the

model. For completeness, this assumption was tested through perturbation tallies in the MCNP model for up to 10% changes in isotopics. The results of the perturbations are shown in Table IV.6. As was hypothesized, the assumption to use natural abundance isotopics for the REEs was valid and therefore used for all subsequent simulations.

Table IV.6: The deviation in the flux tally due to a gadolinium shift in isotopics (due to burnup)

Percent Deviation	**ANU-99**	**ANU-93**	**ANU-96**
0%	1.36E-03	4.04E-04	4.38E-03
5%	1.37E-03	4.06E-04	4.41E-03
10%	1.38E-03	4.08E-04	4.44E-03

Percent Deviation	**ANU-97**	**ANU-99**	**ANU-100**
0%	6.68E-03	1.36E-03	4.07E-03
5%	6.73E-03	1.37E-03	4.09E-03
10%	6.78E-03	1.38E-03	4.12E-03

IV.4.3. Actinide Content

The actinide concentrations (specifically uranium and thorium) can play a significant role in the production of ^{236}U. Almost all of the neutron fluence can be contributed to the uranium and thorium content in the ore (either directly or indirectly). Variations in the isotopics of the uranium, specifically on ^{234}U through fractionation (variations in ^{235}U are assumed to be negligible), can also potentially influence the production rates. The sensitivity of the model to minor changes in the isotopics and concentration of the actinides was tested. The degree of influence associated with these parameters on the ^{236}U concentration in the UOC can be evaluated through the sensitivity studies.

IV.4.3.1. Uranium Content

The concentration of ^{236}U is quantified as the atomic ratio of $^{236}U/^{238}U$. An increase in the uranium content would not impact the ratio in regards to increasing the number of ^{235}U capture target atoms. This assumptions is valid as long as the $^{235}U/^{238}U$ ratio remains constant with increasing uranium concentrations. Therefore, the only influence uranium concentration should have on the $^{236}U/^{238}U$ ratio is on the neutron flux relative to the ore concentration. To assess the independent sensitivity uranium concentration has on ^{236}U content is difficult. Any artificial change (not representative of the UOC mineralogy) in the uranium weight fraction will have a corresponding impact in the other elemental weight fractions. Methods for scaling of the other elemental concentrations was important to consider. The concentrations of major elements were scaled with the uranium concentration, while water and the rare earth concentrations were kept constant. Figure IV.11 shows the variation of the $^{236}U/^{238}U$ ratio relative to a range of uranium concentrations for a select number of UOC samples.

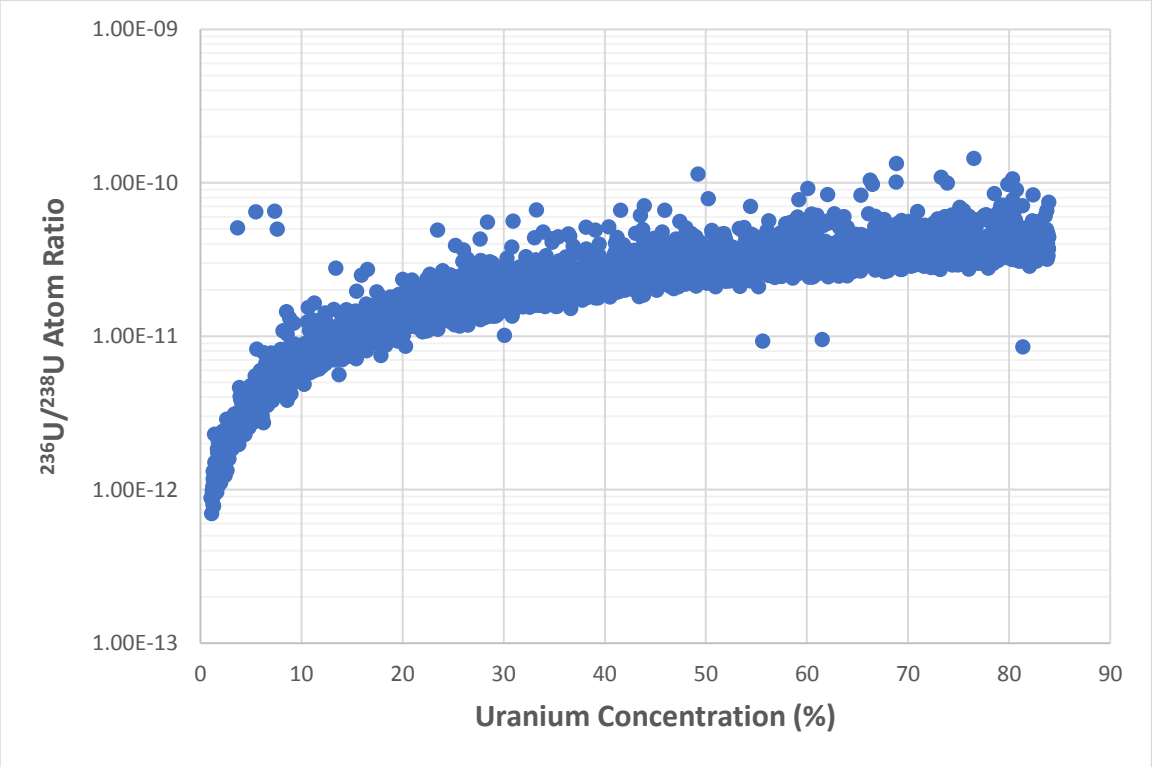

Figure IV.11: The predicted $^{236}U/^{238}U$ ratio with respect to uranium concentration for random ore compositions (3000 data points).

The sensitivity study indicates that a directly linear relationship exists between the concentration of uranium and the $^{236}U/^{238}U$ ratio. Therefore, any uncertainty associated with the uranium measurement can be incorporated into the predicted $^{236}U/^{238}U$ ratio. Since the uranium concentration has a linear relationship in the model, variations in the $^{236}U/^{238}U$ ratio can be factored out. Specifically, the uranium parameter in the model can be considered a linearly uncorrelated variable. This is useful when data analysis is performed, especially for data reduction techniques such as principal component analysis or partial least squares analysis. Parameter relationships in the model for data analysis will be explored further in chapter 5.

While this study assessed artificial changes in uranium concentration (to estimate uncertainties and relationships in the model), it did not consider changes in concentration due to uranium ore processing. UOC consists of uranium ore that has had some processing conducted to

enrich the uranium content. The model is designed to work best with moderate processing of the uranium ore, due to primarily modeling the uranium mineralization. Where it is most likely to fail is that of the two extreme ends of the processing methodology. For uranium ores that have only been crushed and ground mechanically, the elemental composition is more representative of the ore matrix instead of the uranium mineralogy. The assumptions of a homogenous mixture become invalid under those conditions (due to artificially dispersing the uranium and therefore the neutron source). Since the assumption of a homogenous mixture fails for these cases, the model will have a bias that underestimates the ^{236}U concentrations. However, uranium ores that have been processed to the point of near purity (UO_2), lose the elemental contributions in the mineralogy. It is these elemental concentrations in the mineralogy and immediate matrix that result in variations in the ^{236}U concentrations. Since modeling pure uranium oxide will lead to upper bounds of the $^{236}U/^{238}U$ calculations, high processing of the ore can potentially lead to a bias that overestimates the ^{236}U content. The origin of the UOC samples (mining and processing methodologies) was not available, and therefore not tested against the model. However, future work should evaluate the impact that processing UOC (specifically changes in uranium content) has on the model. A parameter could potentially be developed to account for the degree of processing, and to minimize the biasing associated with the ^{236}U estimations.

IV.4.3.2. Uranium Isotopic Fractionation

Isotopic fractionation has been observed to occur for both ^{234}U and ^{235}U with differing degrees of variation. The primary mechanisms controlling the fractionation of the $^{234}U/^{238}U$ and $^{235}U/^{238}U$ ratios are thought to be due to preferential leaching and nuclear volume effects respectively. The same mechanisms were assumed to not significantly affect the variations in ^{236}U directly. The degree of fractionation observed for those mechanisms is relatively insignificant compared to the variation in ^{236}U concentrations. As a consequence, these mechanisms for fractionation were not added to the production model. However the indirect impact on the model, through variations in the $^{234}U/^{238}U$ and $^{235}U/^{238}U$ ratios, needed to be evaluated. The range of fractionation that has been observed in studies for the $^{235}U/^{238}U$ ratios is approximately 1.3% [8]. This range was independently tested in the model, and as

expected did not lead to any significant variations for ^{236}U. The use of a constant value for the current $^{235}U/^{238}U$ ratio (0.007204) was assumed to be valid. The range of fractionation of the $^{234}U/^{238}U$ ratio was more significant, with a maximum range estimated through studies [8] to be approximately 20%. The sensitivity of the production model for the end boundaries observed for ^{234}U fractionation was evaluated. Figure IV.12 shows the normalized ^{236}U variation for the UOC samples with differing $^{235}U/^{234}U$ ratios (125 and 160) relative to the assumed equilibrium (≈ 135).

An increase of the ^{234}U concentration results in an increase of the production rate of ^{236}U in the model. The average change in the ^{236}U concentration was 2% with an upper bound for ^{234}U fractionation (125 $^{235}U/^{234}U$ weight ratio). A lower bound of 160 $^{235}U/^{234}U$ weight ratio (decrease in ^{234}U concentration) resulted in an average 5% decrease in ^{236}U concentration from equilibrium. Figure IV.12 represents the maximum deviation of ^{236}U production due to ^{234}U fractionation. In reality, the majority of uranium mineralization would never have fractionation at the magnitude considered in this study. The influence it has on the production model will therefore be diminished, although uncertainties were still estimated using the maximum range. When available, the true $^{234}U/^{238}U$ ratio was used in the production model for given UOC samples. However, the low uncertainty in the production model associated with ^{234}U fractionation allowed the use of the equilibrium assumption when measurements were not available.

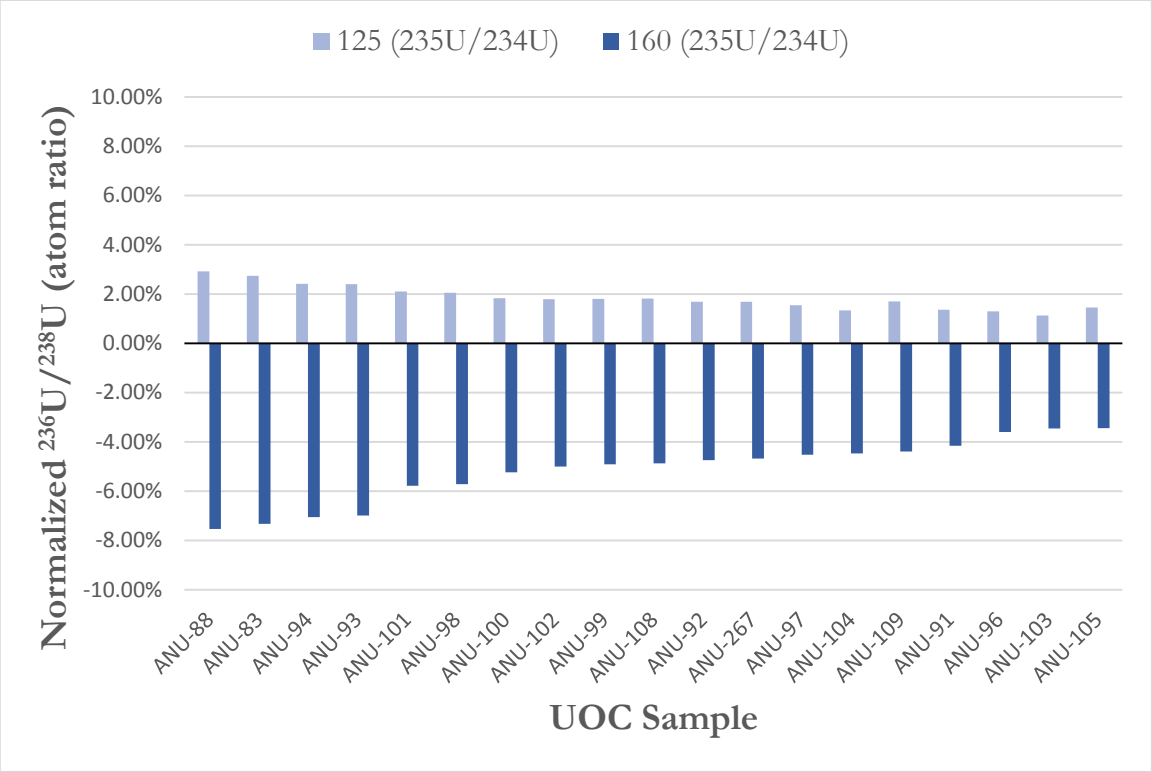

Figure IV.12: The normalized ^{236}U variation for the UOC samples relative to fractionation of the $^{235}U/^{234}U$ ratio (eq. ≈ 135)

IV.4.4. Neutron Spectrum

The energy spectrum of the neutrons produced in the ore is primarily affected through (α,n) reactions. More specifically, by the concentration and ratios of nuclides with significant threshold capture cross sections (isotopes of oxygen, silicon, etc.). While the spontaneous fission of the uranium isotopes does impact the magnitude of the neutron source, it does not account for variation between ore bodies (watts fission spectrum). Since the alpha producing nuclides are in the decay series of the uranium isotopes (and assuming secular equilibrium), the daughter products also have no spectral impact in variation. The concentration of elements such as aluminum and silicon, therefore, will have a direct impact on the initial variation of the neutron spectrum (based significantly on the energy thresholds). It is interesting to note that the potential alpha targets do not contain any isotopes of either Sulphur, nitrogen, or chloride. During processing of the uranium ore for each sample, it is

these three elements that have the highest potential for contamination (increase in content). This is though the additions of a given acid (hydrochloric, nitric, or sulphuric), depending on the processing method, that can lead to unrepresentative elemental concentrations of the ore. Consequently, it is beneficial for those elements to have a low influence on ^{236}U production relative to the alpha target isotopes. Evaluations of the normalized neutron source spectra from each alpha target is shown in Figure IV.13. The results are generated through the code SOURCES 4C, utilizing GNASH cross section and level branching fraction libraries.

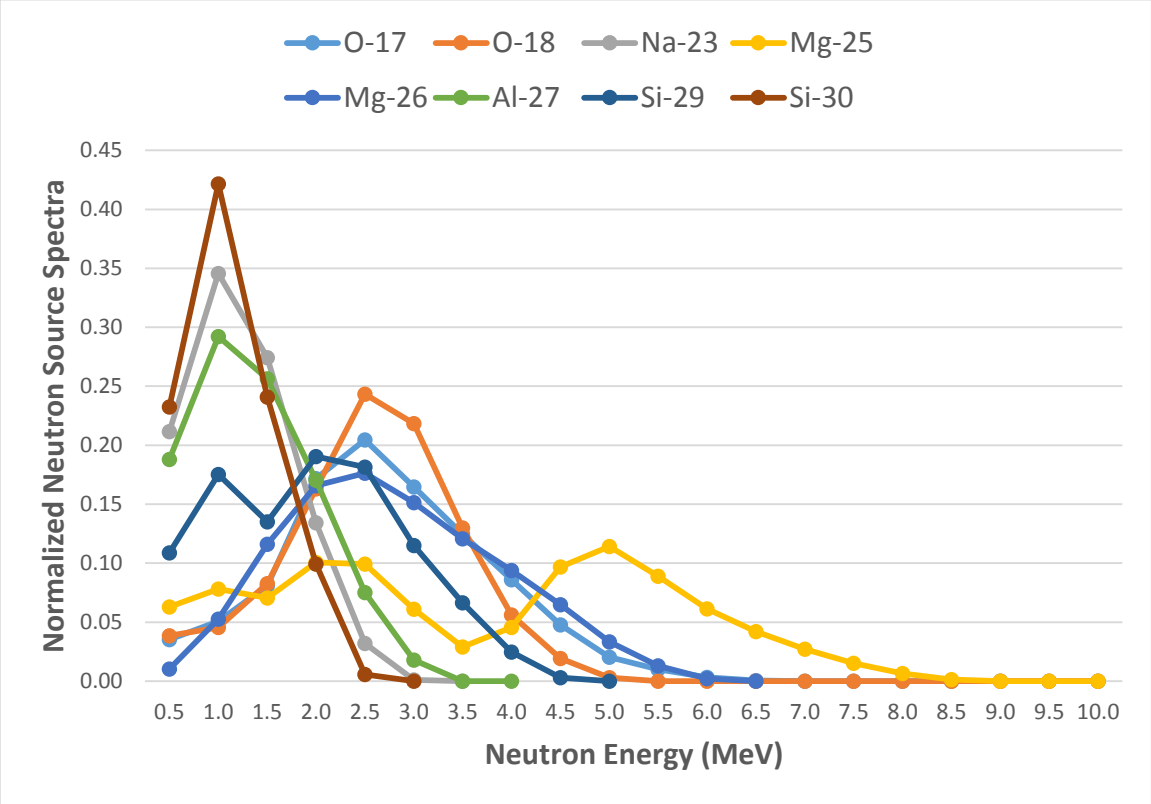

Figure IV.13: The neutron source spectra normalized to each alpha target using SOURCES 4C, a homogenous geometry, and secular equilibrium.

Therefore, ores with a relatively higher concentration of silicon, aluminum, and sodium will typically result in a softer neutron spectrum (dominated by lower energy neutrons). In contrast, ores with a high concentration of magnesium, and to a lesser extent oxygen, will

result in a relatively harder neutron spectrum. It is interesting to note that the production of higher energy neutrons should theoretically decrease the production of ^{236}U through loss terms including escape from the ore geometry and resonance capture in ^{238}U. This is complicated through the neutron transport and the resonance captures of ^{235}U. The sensitivity of the other parameters should also be influenced by variations in the neutron spectrum. For example, the hydrogen content in regards to the moderation potential of the ore will be impacted by the spectra of the source neutrons.

While the variations of the spectra for the source neutrons can be seen in Figure IV.13, the impact of ^{236}U production is not as evident. A given UOC with a high initial neutron spectrum can be affected by energy dependent parameters such as water and REE (gadolinium and samarium) content, as well as scattering off the alpha targets themselves. The addition of thorium (present in several UOC samples) also adds slight perturbations to the neutron spectrum in the ore. To investigate the sensitivity of the model to changes in the concentration of alpha targets, the production rate of ^{236}U was energy binned and evaluated. In this way, the influence of given parameters (such as the concentration of alpha targets) can be evaluated for specific energy regions in ^{236}U production. An example of the energy dependent ^{236}U production can be seen in Figure IV.14 for several UOC samples.

The energy dependent production rates can be used to evaluate the variation in influence between UOC samples. Parameters that impact the thermal energy region, such as REE content, will have a greater impact with UOC samples that have a higher fraction of ^{235}U capture in that energy region. For example, sample ANU-93 (which has a large fraction of thermal capture) has a high sensitivity to REE concentration compared to sample ANU-99. In contrast, the sensitivity to changes in water content will be more pronounced for samples with a larger fraction of resonance ^{235}U captures. Sample ANU-99 had a 20% variation in ^{236}U production for the range of water concentration (0 – 10% H) compared to a 12% variation for sample ANU-100.

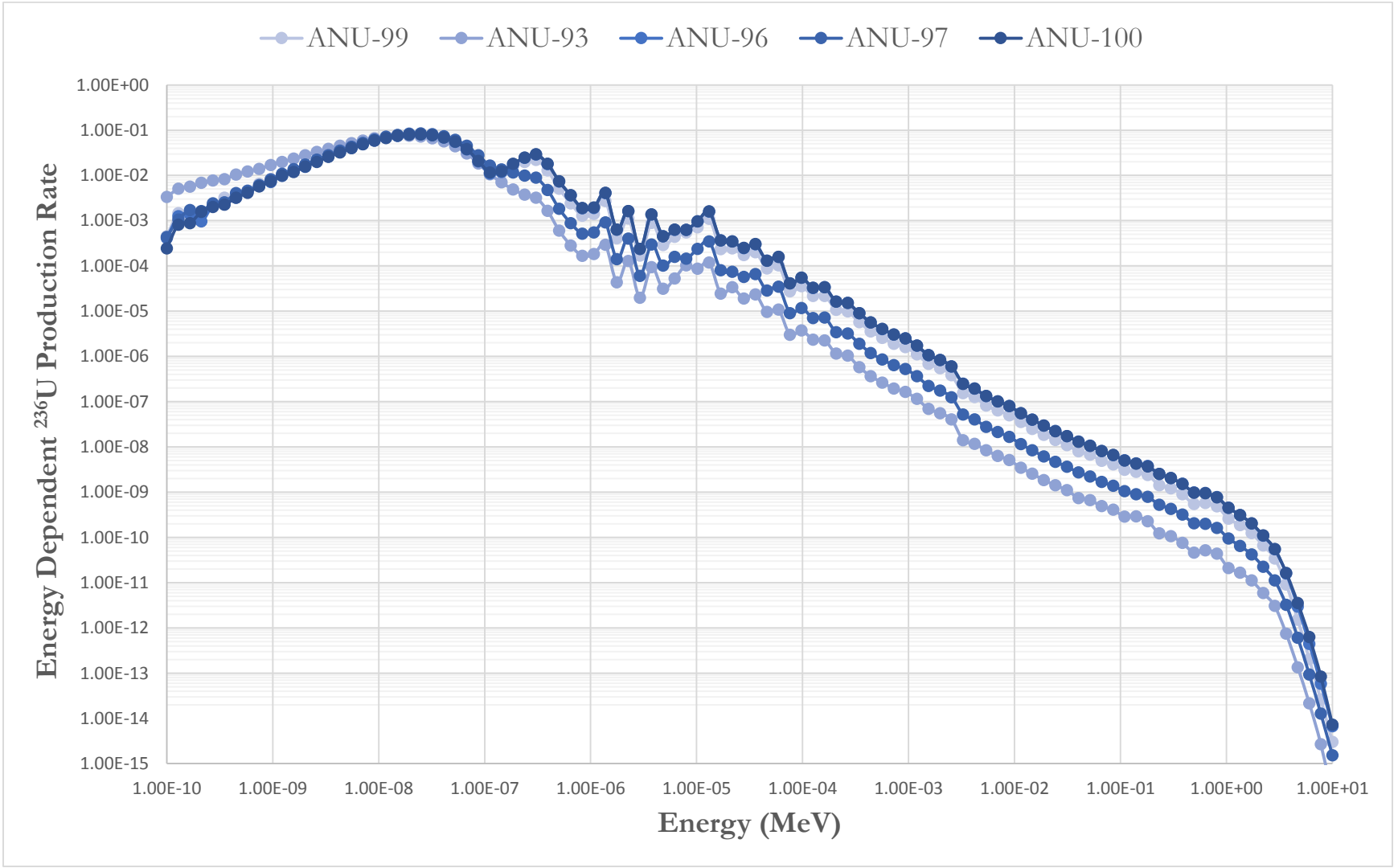

Figure IV.14: The energy dependent ^{236}U production rate as a function of incident neutron energy for select UOC samples.

IV.4.5. Model Assumptions

So far the sensitivities of the elemental parameters (concentrations, isotopic distributions, etc.) have been evaluated in terms of the ^{236}U production model. Uncertainties associated with the elemental parameters can include measurement errors/bias either through differing methodologies or sample preparations. Lack of measurement data available or UOC history (mining / processing history) can also lead to measured elemental concentrations that are not representative of the sample. Therefore, the potential variations of the elemental parameters can be used to evaluate the uncertainty associated with the model. In addition to this type of uncertainty, several key assumptions were used to build the production model.

Certain assumptions of the model, such as geometry and equilibrium were used to reduce the complexity of the model. While potentially more parameters could have been included, increasing complexity, the model would risk overfitting the measurements. In other words, the model would predict the ^{236}U content very accurately for one specific UOC sample set, while failing significantly with any additional UOC samples. Since the model will ultimately be used to assess an unknown UOC sample, it is useful to reduce the complexity. It is still important to evaluate the bias associated with using specific assumptions in the model.

IV.4.5.1. Geometry

The geometry of the ore in the MCNP model was by the far the most significant assumption used. While the effects of the geometry assumption is somewhat mitigated by neutron path length in uranium ores, it still adds a degree of bias in the model. Two key parameters are associated with the geometry of the MCNP model: the neutron leakage term (in terms of surface to volume ratios of the UOC) and the homogeneity of the uranium mineralization.

IV.4.5.2. Neutron Leakage

The neutron leakage term is the loss term associated with neutrons leaving the geometry of the uranium mineralization. Consequently, the leakage term is related to the ratio of surface area to volume (SA/V) of the UOC geometry. As the SA/V ratio increases, the average path length the neutron has to travel to leave the geometry decreases (increasing probability of escape). As the geometry becomes infinite (i.e. no surface area), the ratio will approach zero.

The sensitivity of the leakage term to the production model was evaluated by varying the SA/V ratio between the two bounding cases (infinite and borehole geometries) for various UOC samples. The results of the study can be seen in Figure IV.15, with the $^{236}U/^{238}U$ ratio for each case normalized to the respective infinite geometry. The variation in ^{236}U production relative to the surface area to volume ratio seems to be independent of the UOC sample. Changes in the elemental concentrations, and therefore the energy dependent neutron flux, does not significantly affect the neutron leakage from the geometry.

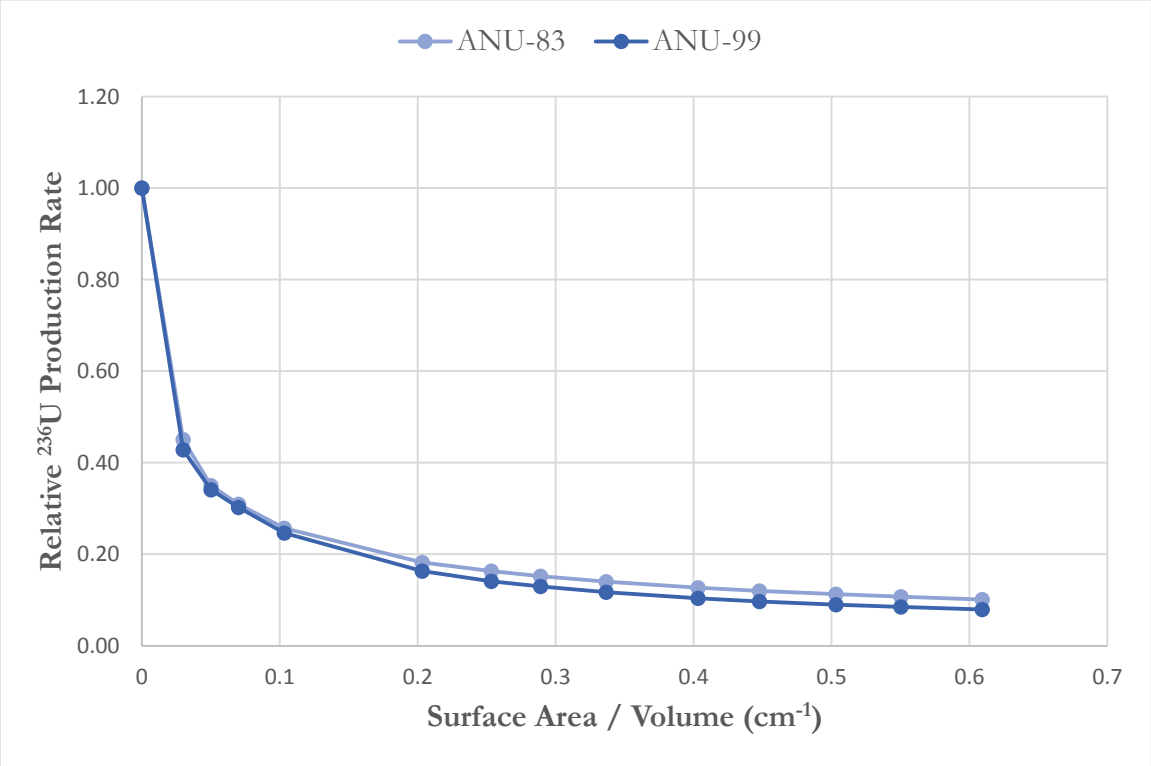

Figure IV.15: The relationship between modeled production rates relative to the surface area / volume ratio, normalized to infinite sphere geometry.

A relationship seems to exist between the measured results of the UOC samples when compared to the model sensitivity of the SA/V ratio. The UOC samples can be grouped into two subsets: one set that is better represented by the borehole geometry and the other set

under an infinite geometry. The sample set represented by the infinite geometry (see Figure IV.6) include both reference standards. As discussed previously, the reference standards both incorporate uranium mined and milled extensively from a geographically broad source. Measured elemental and isotopic concentrations of the samples would represent a homogenous mixture of the mined majority of the ore body. As the volume of ore that is mined and milled increases, the neutron leakage term approached zero (and therefore can appropriately be modeled as an infinite geometry). Conversely, several samples in the borehole geometry can be speculated (through the low uranium concentration and level of impurities) to have been obtained as crushed uranium ore through aliquots of drill cores. Typically samples obtained through these methods are more representative of smaller scale and/or exploratory mining. The elemental and isotopic concentrations of the samples under this scenario would only be characteristic of the size of the drilled rock core. In this case, neutron leakage outside the geometry does not contribute to the measured production of ^{236}U and should be taken into consideration (borehole geometry).

The significance shown on the origin of the UOC samples brings forth an important point. The history of UOC samples (specifically mining / milling operations and procedures) in open source literature seems to be scarce. A combination of issues with proprietary information and the general availability for uranium ores both contribute to this deficiency. Commonly, mining operations are concerned with the release of information about their procedures and so therefore limit the open source literature. The availability of uranium ore (commercial sensitivities, etc.) can also play a role in the level of characterization. The number of samples available significantly influences the choice on whether or not to use a given sample (specifically is a sample has an unknown geological context and characterization). For example, the only initial characterization of the UOC samples used in this study typically consisted only of a general location. Further information on the samples had to be deduced from other open literature sources based on past and present operations in the area. With better origin characterizations of UOC samples, the bias in the model associated with neutron leakage can be minimized.

IV.4.5.3. Homogenous Distribution

Measurements of the elemental concentrations for a given UOC sample are representative of a homogenous distribution (through the milling/processing of the ore). However, the uranium mineralization in the uranium ore body can consist of a heterogeneous sample matrix. The model assumes that due to the mean free path of neutrons in the ore, a simulation of a homogenous mixture is valid. Simulations were conducted on the model to assess the effects that a heterogeneous distribution (specifically the grain size and grain concentration/density of the uranium) had on the overall ^{236}U production. This would allow any potential bias and uncertainty associated with a homogenous assumption to be evaluated

A VBA script was used to randomly model dense uraninite grains (8.5 g cm^{-3}) in a less dense (2.5 g cm^{-3}) ore matrix. The VBA random number generator was used to quasi-randomly assign a grain position within the main ore geometry. Each grain position was modeled as a sphere with grain sizes representative of the diameter (ranging from 10 – 80 μm). The grain diameter was randomly sampled from 10 – 80 μm, keeping a constant uranium concentration characteristic of uraninite. This process was repeated until the total uranium concentration was equal to that reported for the given UOC sample. The neutron source was biased to randomly sample from the uraninite locations. Due to the relatively high computation power required with this model, only two UOC samples were evaluated in this study. Figure IV.16 shows the variation of the estimated ^{236}U production relative to the homogenous/heterogeneous distribution of the uranium in the ore.

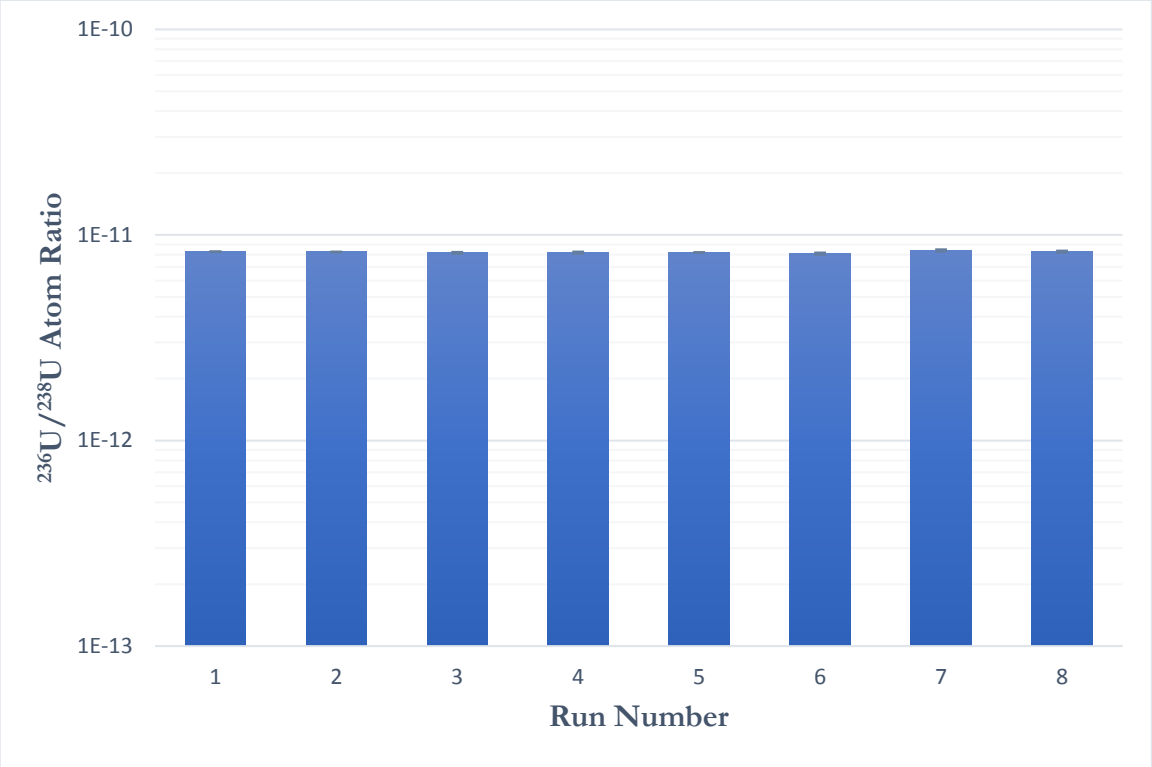

Figure IV.16: Fluctuations in ^{236}U production for random uraninite distributions evaluated over 8 simulations (error bars are representative of counting statistics).

The fluctuations seen in ^{236}U production (Figure IV.16) range by approximately 1% between runs, which is within the counting statistical error. The results are in good agreement with the assumption that a heterogeneous distribution of micro grain structures does not impact neutron transport. The neutron mean free path in ores (~30 cm) allows the assumption of a homogenous distribution of elemental concentrations. The larger impact the distribution has on the model would is through the (α,n) reactions (see section 4.1.2). One assumption that was not investigated in this sensitivity test was the distribution of initial neutron source within the uraninite grains. The neutron source was evenly distributed (by uranium mass) throughout the uraninite grain in the model. In reality, the distribution of (α,n) neutrons would be near the surface interface; whereas the fission neutrons would be distributed throughout the volume of the uraninite. The small grain volumes considered should not cause significant bias with this assumption; however, this can be tested in future work.

IV.4.6. Ore Age

Uranium mineralization in ore bodies has been shown to primarily occur, depending on the genetic origins, during specific geologic time periods. The time periods of uranium mineralization can be directly related to the type of formation process. For example, non-redox formations typically occurred before the oxygenation of the atmosphere. Principally, five geologic time periods have been shown to form major uranium concentrations in ore bodies: 2800 – 2200 M years, 2000 – 1500 M years, 1300 – 1100 M years, 500 – 400 M years, and 300 M years to recent[21]. These time periods are shown in Table IV.7 with the most commonly associated genetic type of uranium ore deposit.

Table IV.7: Common Genetic origins for uranium ores associated with the mineralization age.

Genetic Origin	**Mineralization Age (MY)**
Quartz-Pebble Conglomerate	2800 – 2200
Unconformity / Vein	2000 – 1500
Breccia-Complex	1300 – 1100
Black Shales	500 – 400
Sedimentary	300

The ^{236}U production model assumes that the timescale of the uranium mineralization relative to the decay constant of ^{235}U is large enough to assume equilibrium. It is by this assumption that the following equation (relating the $^{236}U/^{238}U$ atom ratio to the current ^{236}U production) can be used:

$$\lim_{t \to \infty} \frac{^{236}U}{^{238}U} = \frac{P_{236_U} \lambda_{235_U}{}^{-1}}{^{238}U}$$

As the ore deposit is a dynamic environment, the elemental composition and isotopics over time will change (which can be difficult to estimate). However, the previous equation only needs the static (time independent) calculation of the production rate. While this assumption

is most likely valid for long mineralization ages, it is possible for the assumption to create a bias in younger ore deposits. To determine the time dependence on the estimation of ^{236}U content, the limit was removed in the previous equation:

$$N_{236} \approx \sum_{t_1}^{t_9} P_{t_n}(e^{-\lambda_{235} t_{n-1}} - e^{-\lambda_{235} t_n})\, \lambda_{235}{}^{-1}$$

where t_1 to t_9 are the time periods used in this study (see Table IV.7) with the oldest age being 1500 MY and the youngest age being 5 MY respectively. As MCNPX is a time independent code, the approximation was needed to solve for time dependence. To approximate the integral, time steps were used so that the code could independently solve the static production rate for each time step. As the difference in time periods approaches zero ($\lim_{t_n - t_{n-1} \to 0}$), the approximation will approach the correct solution. Due to the relatively small changes in production rate for small time steps (and realistic computing limits), the size of the time step is limited. The time dependent production rate evaluated changes in the uranium isotopics (and through secular equilibrium, changes in uranium daughter products) relative to the time period. Changes in the elemental concentrations with time were improbable to estimate with any degree of confidence and so was not considered for the time dependence study. The uranium isotopics were adjusted by the following equations for each time period:

$$N_{238}(t_n) = N_{238}(t_0)\, e^{\lambda_{238} t_n}$$

$$N_{235}(t_n) = N_{235}(t_0)\, e^{\lambda_{235} t_n}$$

$$N_{234}(t_n) = N_{234}(t_0)(e^{\lambda_{238} t_n} - e^{-\lambda_{234} t_n})$$

The ^{236}U production rate was found for several UOC samples at time periods ranging from 5 MY to 1500 MY, using the respective isotopics for uranium and daughter products. The cumulative contribution to the $^{236}U/^{238}U$ atomic ratio was calculated for each bounding time period (for example 0 – 5 MY) and normalized to that of the equilibrium estimation. The results of the study is shown in Figure IV.17 for 4 samples, chosen to represent the most variation in ^{236}U content.

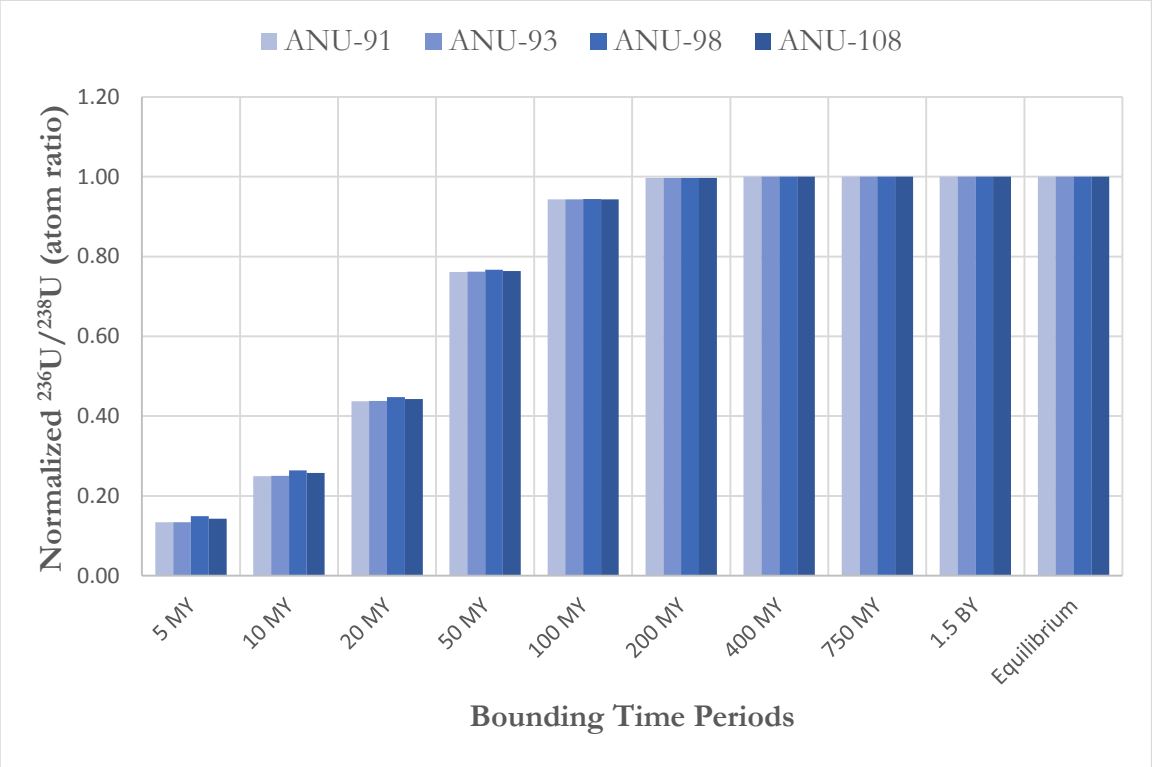

Figure IV.17: The cumulative contribution to the $^{236}U/^{238}U$ atomic ratio for consecutive bounding time periods normalized to the equilibrium estimation.

The results show that ^{236}U content produced in older time periods (for example, 750 - 1500 MY) contribute insignificantly to the current ^{236}U concentration. This result is not surprising, due to the small rate of decay of ^{235}U relative to the older time periods. What is important to note, is how rapid the time dependent contributions become insignificant. Figure IV.17 can be used to estimate the bias for potentially young uranium mineralization when using the equilibrium assumption. For relatively young ores (5 – 50 MY), the assumption will overestimate the ^{236}U from as much as 24 to 87% depending on the age. However, the vast majority of uranium mining (either prospective or operational) does not utilize uranium mineralization below 300 MY. This is due to the rarity of uranium ore bodies younger than 300 MY and the economic viability of such a mining operation (not long enough to have an economical ore grade). Therefore the equilibrium assumption in the model is valid and

should be used to reduce computational time, unless special circumstances dictate otherwise (prior knowledge of mineralization age).

V. DATA ANALYSIS METHODOLOGY

The main goal of this research is a feasibility study on using ^{236}U as a distinctive and unalterable "fingerprint" for identifying the original source of uranium involved in a proliferation or safeguards-violation scenario. This is fundamentally an inversion problem, since it solves for the parameters of nuclide production (cause) from the ^{236}U content (effect). When measuring a specific uranium isotopic concentration, ideally an inference could be made on the unknown parameter set distribution. A possible solution to the inversion problem can be found through the use of statistical analysis methods, which include a broad range of tools to analyze data and update models. Specifically for the current research, Bayesian analysis was chosen due to the ability to represent uncertainties in the parameter set and also to incorporate prior information related to the ore deposit.

Bayesian analysis utilizes probability modeling (applying a probability distribution on a random variable) on both the unexplained outcomes and influential parameters. Although the parameters (i.e. REE content) influencing ^{236}U production are approximated deterministically, they can be modeled as having a given probability distribution to allow for the incorporation of the available information on the parameters and on the uncertainty contained in that information. Once the parameters can be expressed though probability distributions, the inversion of said probabilities can be found through Bayes' theorem. If A and E are events and event E is possible [i.e. $P(E) \neq 0$], then the inversion of the probabilities are related as follows:

$$P(A|E) = \frac{P(E|A)P(A)}{P(E|A)P(A) + P(E|A^c)P(A^c)}$$

where $P(A|E)$ and $P(E|A)$ are conditional probabilities such that the probability of the first event is conditional on the second. Bayes and Laplace went further with the inversion theorem by considering that the uncertainty on the parameters θ could be modeled through a probability distribution $\pi(\theta)$ referred to as a prior distribution. An interference can then be based on the distribution of θ conditional on an observation x, $\pi(\theta|x)$, referred to as a posterior distribution:

$$\pi(\theta|x) = \frac{f(x|\theta)\pi(\theta)}{\int f(x|\theta)\pi(\theta)d\theta}$$

The underlying structure of all Bayesian analysis relies on the posterior distribution, which can be found up to a constant of proportionality from both the parametric statistical model, $f(x|\theta)$, and a prior distribution on the parameter set, $p(\theta)$. The constant of proportionality is simply the marginal distribution of the Bayes' theorem (i.e. the denominator), which does not depend on the parameters. The posterior distribution is simply the update of the prior distribution from the incorporation of measurement data, such as the uranium isotopic concentration. From a statistical viewpoint, measurements and parameters have little difference mathematically through use of probability inversions. By allowing both the ^{236}U production (outcome) and the parameter vectors to have probability distributions, Bayes' theorem actualizes information on an unknown parameter based on an observation of ^{236}U. For example, generalizing the parameter for ore classification (OB) i.e. volcanic, the following updated probability distribution of ore classification can be found for a given ^{236}U measurement:

$$P(OB|^{236}U) = \frac{f(^{236}U|OB)p(OB)}{\sum f(^{236}U|OB)p(OB)}$$

The main tool of the Bayesian method is the posterior distribution, incorporating both the requirements of the likelihood principle (section V.1.1) and the inversion of the probability distributions. To calculate an estimate of a parameter from the posterior distribution, an estimator (rule for calculating an estimate from the distribution) is needed. There are many estimators, both point and interval, which can be utilized for a given data set. To optimize the specific estimator, use of a loss / utility function can be employed. The loss function $L(\theta, \hat{\theta})$ is a function that evaluates the cost or error associated with using a given estimator $\hat{\theta}$ to assess the parameter. By minimizing the loss function for the data set, the estimation of the posterior distribution can be optimized.

V.1. Bayesian Inference

The determination of three factors are needed for Bayesian inference:

- The distribution of the observed data given the model parameters, $f(x|\theta)$
- The prior distribution for the parameters, $\pi(\theta)$
- The loss associated with the estimation, $L(\theta, \hat{\theta})$

Each of these factors can be derived numerous ways and can contain partially subjective considerations. The following sections will describe the methods used to determine the factors and the potentially more rigorous derivations that can be used in future work.

V.1.1. Data Model

In order to make probability statements about θ given the observable x, a model providing the joint probability distribution for θ and x is needed. Bayes' theorem shows that for a given probability model, the data x only affects the posterior distribution through the sampling distribution (or data distribution) $f(x|\theta)$. The sample distribution (when viewed as a probability density) is a function of x for a fixed θ. When the data is actually measured ($x = x_{meas}$). The likelihood function utilizes these measurements to find the values of θ that are most likely to have generated x_{meas}:

$$l(\theta|x_{meas}) \equiv f(x_{meas}|\theta)$$

The sampling density and the likelihood function are different mathematical objects, with different properties. As a sampling density, $f(x|\theta)$, θ is fixed and x is variable. As a likelihood function, $l(\theta|x)$, x is fixed and θ is allowed to vary [77]. Therefore, when computing the posterior distribution the likelihood function is used to condition against the measured (known) data set:

$$\pi(\theta|x) = \frac{l(x|\theta)\pi(\theta)}{\int l(x|\theta)\pi(\theta)d\theta}$$

It can be shown by using the above equation that the shape of the likelihood function that is important, not the constants of proportionality. Multiplying the likelihood by any constant

(not related to θ) is irrelevant, as it will cancel out when computing the posterior distribution. This leads to the likelihood principal: which states that for a given sample of data, any two probability models that have the same likelihood function yield the same inference for θ [77]:

$$l_1(\theta|x) = K\, l_2(\theta|x)$$

To find the likelihood functions, a full probability model (a joint probability distribution for all observable and parameter qualities in the problem). After which when a measurement is made, the likelihood of the parameter distribution for the fixed measurement can be made.

Two main statistical approaches are available, nonparametric and parametric. Nonparametric attempts to incorporate as much complexity of the underlying distribution of the outcome, by using an infinite-dimensional parameter space [78]. Parametric represents the observation distribution through a density function, where only the parameter θ (finite dimensionality) is unknown [78]. The focus for this research will be solely on a parametric probability model. Nonparametric models typically are more complex and require larger data sets due to the infinite dimensionality of the problem. Due to the limited measurement data that exists for ^{236}U, parametric models are thought to better estimate the posterior distributions. The use of parametric models in this work does not exclude the use of a nonparametric models in future work. If the influencing factors change, or if can be shown that nonparametric models better represent the data, then future work can utilize a nonparametric scheme.

Parametric probability models can now be defined as consisting of the estimated ^{236}U concentration, distributed by a model such that $f(^{236}U|\theta)$ where only the parameter θ is unknown and has a finite vector space [78]. The MCNP production model can be used to estimate the parametric probability distribution for a given parameter. The production model can be supplemented by measurement data when available; however, is not restricted for missing measurement sets.

V.1.2. Prior Distribution

The choice in prior distribution is a critical (and controversial) point of Bayesian analysis. The difficulty can come from a sense of arbitrariness in the choice of a prior, where ungrounded prior distributions can produce unjustified posterior inferences [78]. One approach that has

been taken is for personal prior elicitation. This method calls for the elicitation of subjective distributions with normal error structure, which describes a way to quantify expert knowledge [79]. This approach can be classified as an informative prior, as it provides definitive information about a parameter. An informative prior can also be based on previous data, which allows iteration on the posterior as well as addition of multiple data sets.

Informative priors are inherently problem-specific, and in some cases not feasible (lack of data, difficulty/cost in obtaining data, etc.). The alternative is to find physical rules or methods to provide vague/general information about a parameter, known as an "uninformative" prior. An example of such a prior can be through a uniform distribution which gives the same likelihood to each value of the parameter. Criticisms with uniform distributions is through potential variance under re-parameterization (change of variable). In other words, when the specific parameter a prior uniform distribution is applied to can affect the outcome. Numerous methodologies exist to better define a uninformative prior, however this research focuses on the structural methods of the Jeffrey's noninformative prior compared to a uniform distribution.

The Jeffrey's noninformative prior is a prior distribution that is proportional to the square root of the determinant of the Fisher information (a measure of the degree of information that a random variable explains about an unknown parameter). A key feature of this distribution is through the invariance under re-parameterization. The Fisher information is given by:

$$I(\theta) = -E\left[\frac{\partial^2 \log P(x|\theta)}{\partial^2 \theta}\right]$$

where E is the expectation operator, and $I(\theta)$ is the Fisher information for a one dimensional parameter (for multivariate parameters, the fisher information matrix is a generalization of the previous equation). The prior can be found as a determinate of the Fisher information:

$$\pi^*(\theta) \propto [\det I(\theta)]^{1/2}$$

V.1.3. Bayesian Point Estimation

When the prior distribution is available, the posterior distribution can be derived given observational data with a likelihood distribution. The posterior distribution can therefore be considered to contain all available information on parameter θ (integration of prior information and information contained in the data set). Bayesian inference can be based entirely on the posterior distribution, which describes the properties of the parameter. However, many scenarios exist where a point estimation of a parameter is more useful than a distribution Bayesian point estimation calculates the point estimate of the parameter by minimizing a loss function (represents a cost or error when the parameter takes on a given value). The minimization of a loss function describes the optimal point on the posterior distribution that has minimal error with deviations of the real parameter value. The selection of the best point estimator is based on the context of a particular applied problem. Knowledge of the expected loss can sometimes be hard to estimate, and therefore the optimal loss function is difficult to determine. Classical loss terms, which are well documented and mathematically accessible, can be used alternatively. For example, minimization of the squared-error loss function:

$$L(\theta, \hat{\theta}) = (\theta - \hat{\theta})^2$$

results in the posterior mean for the point estimate. Other common examples of Bayesian point estimators are utilize the central tendency statistics. The posterior median which minimizes the expected loss for the absolute-value loss function:

$$L(\theta, \hat{\theta}) = |\theta - \hat{\theta}|$$

The posterior mode (MAP) which minimizes the expected loss for a 0 – 1 loss function:

$$L(\theta, \hat{\theta}) = \begin{cases} 1 - \hat{\theta} & \theta \in \Phi_0 \\ \hat{\theta} \end{cases}$$

While these loss functions are simple to manipulate, other approaches may better represent the Bayesian risk associated with the posterior distribution. While this work solely utilizes the

classical loss terms, future studies should evaluate alternative approaches such as a parametrized class of loss functions or a partial ordering of loss functions.

V.1.4. Markov Chain Monte Carlo

One of the difficulties of Bayesian analysis is typically the quantities of interest require integrating over a potentially high dimension parameter space $\theta \in \Theta$. Analytical integration severely restricts the type of models that can be implemented (i.e. the likelihood and prior distribution is constrained to analytically solvable forms). Numerical methods can provide an alternative to an analytical solution by approximating the posterior distribution through different techniques. Markov chain Monte Carlo (MCMC) is one set of techniques that can be used to sample a multivariate distribution when direct integration is difficult. The general process involves constructing a Markov chain on the state space (i.e. the parameter space) which has a steady state distribution approximating the posterior distribution. MCMC is therefore a strategy for generating samples mimicking samples drawn from the posterior distribution.

Markov chains are random sequences that undergoes transitions from states that are independent of the history of the transitions and only are influenced by the previous state (stationary transition probability) [80]. The Monte Carlo characteristic of MCMC derives from randomly sampling within each state of the Markov chain. A MCMC approach will therefore randomly wander around the target distribution via a set of proposal distributions $\sim g(\theta^*|\theta)$ which aims to identify regions of high probability density. A MCMC chain converges to the target distribution if the following essential properties are true: irreducibility, where for any state of the chain there is a positive probability or transitioning to all other states; and aperiodicity, where the chains should not be cyclical. The Metropolis-Hastings (MH) algorithm satisfies both conditions, and is one of the more popular methods of MCMC (used as a basis for numerous other MCMC techniques) [81]. The general MH algorithm is as follows:

- Initialize $\theta^{(0)}$ starting from some prior distribution $p(\theta)$
- Define a proposal distribution with a pdf $g(\theta^*|\theta)$ for all $\theta^*, \theta \in \Theta$.

- At iteration t, generate a new candidate θ^* by sampling from the proposal distribution:

$$\theta^* \sim g\left(\theta^* \middle| \theta^{(t-1)}\right).$$

- Calculate the Hastings acceptance ratio for the candidate state:

$$\alpha_t = min\left[1, \frac{p(\theta^*|^{236}U)}{p\left(\theta^{(t-1)}\middle|^{236}U\right)} * \frac{g\left(\theta^{(t-1)}\middle|\theta^*\right)}{g\left(\theta^*\middle|\theta^{(t-1)}\right)}\right]$$

- Generate a random value $\omega \in [0,1]$

$$\textbf{If } \omega \leq \alpha_t, \textbf{ Then } \theta_t = \theta^*. \textbf{ Else}, \theta_t = \theta^{(t-1)}.$$

- Repeat for specified number of iterations.

The acceptance ratio allows the Metropolis-Hastings algorithm to be used when dealing with unnormalized posteriors (i.e. unknown marginalization), since only the ratios of the densities is needed. The ratio of sampling probabilities between proposed and previous state accounts for asymmetry in the proposal distribution. The acceptance ratio, in the context of this research, will result in a Markov process that will explore the state space defined by the posterior distribution $p(\theta|^{236}U)$.

V.2. Bayesian Inference

The founding principle of Bayesian statistics (as previously discussed) is to represent the uncertainty associated with a given parameter with a probability distribution. Bayesian inference uses the components of Bayes' theorem (see section 3.1) to update the probability distribution of an unknown parameter. The selection of the parameter of interest is dictated by the user and ultimately the motivation behind Bayesian analysis. Parameters can be chosen to represent a particular variable (i.e. gadolinium content), vector of variables, or particular variable distributions (i.e. UOC classification). Therefore, Bayesian inference techniques can be utilized to derive an estimated variable distribution or for model test (subsets of variable distributions representing a particular classification). The goal of this work was to evaluate different analysis methods for ^{236}U signatures in UOC, particularly utilizing Bayesian techniques. This is not an exhaustive testing of all statistical methods, but rather feasibility

testing of a select few promising approaches. Model testing was done (utilizing a selection of prior and null distributions) for UOC classification based on mineralization and deposition. Parameter estimation was also explored through latent variables produced by a variety of regression techniques.

V.2.1. Model Selection

Bayesian model testing is no different than any other Bayesian inference technique. It still utilizes Bayes' theorem to update the posterior distribution, except the measured ^{236}U through the model will update a given model (M_n) of the form:

$$P(M_1|^{236}U) = \frac{f(^{236}U|M_1)p(M_1)}{\sum f(^{236}U|M_n)p(M_n)}$$

where the probability of a model (M_n) is derived by conditioning on the subset of parameters such that $P(\theta \in M_n|x)$. The solution of the marginal distribution (denominator) is dependent on the models completely representing the parameter vector space. Similarly to a comparative forensics approach, if a potential model is missing from the analysis the results can be biased towards a false positive. Two methods can be used to account for the potential bias: use of a null model and use of a Bayes' factor. A null model is used to characterize the full range of ^{236}U variation that might not be represented completely by the set of models considered. The Bayes' factor is a ratio of the maximum likelihood estimates (the maximum value for the likelihood function) of two selected models. Consequently, the prior and marginal distributions are factored out of the ratio and the probability of one model relative to another can be found.

V.2.1.1. Uranium Mineralization

The primary uranium mineralogy can be useful to know for an unknown UOC sample in a nuclear forensics scenario. Estimation of the uranium mineralogy can sometimes be complicated or nearly impossible due to the processing mechanisms for UOC. The uranium mineralogy for a given UOC sample potentially could be inferred from the ^{236}U content through Bayesian inference. The feasibility on such an analysis scheme was tested through a suite of minerals shown in Table V.1. The elemental concentrations of select minerals was

obtained in Uranium Ore Deposits [82], with additional parameters estimated based on the previous work. Appropriate variations were added to the parameters (representing elemental content variation for a given mineral) and ran through the production model to produce a respective ^{236}U distribution.

Table V.1: A suite of uranium minerals, a brief description of the elemental characteristics, and the mean $^{236}U/^{238}U$ ratio produced in the model.

Mineral	**Description**	**$^{236}U/^{238}U$ (atom ratio)**
UO_2	pure uranium oxide	1.19E-10
Uraninite	oxidation of UO2, also containing lead oxides and trace REE	1.19E-10
Coffinite	uranium-bearing silicate mineral	1.25E-10
Brannerite	multiple oxides containing calcium, titanium and iron	3.53E-11
Davidite-Ce	rare earth oxide mineral with Ce end member	2.82E-12
Davidite-La	rare earth oxide mineral with La end member	2.77E-12
Carnotite	potassium uranium vanadate	8.37E-11
Autunite	hydrated calcium uranyl phosphate	1.59E-10
Thorinite	mixture of uranium / thorium oxides	7.35E-11

A singular ^{236}U value would ideally be used for the analysis, however a distribution would more likely better represent the AMS measurement. This is due to the bias and uncertainty that can be observed in AMS measurements depending on the system (see chapter 3). For this work, a normal distribution was estimated for the ^{236}U measurements taken from the reported standard deviations. This type of distribution is only representative of counting statistics, where bias associated between systems can be accounted for in future revisions.

Two different distributions were evaluated for use as a null model in this work. The first distribution consisted of a uniform distribution bounded by the minimum and maximum ^{236}U

concentrations seen from a variety of UOC measurements. The second distribution was found through randomly sampling the range of elemental concentrations independently and running through the production model. The modeled distribution of ^{236}U isotopic ratios would ideally represent the entire range of concentrations, assuming a large number of samples were performed. Both normalized null distributions are shown in Figure V.1.

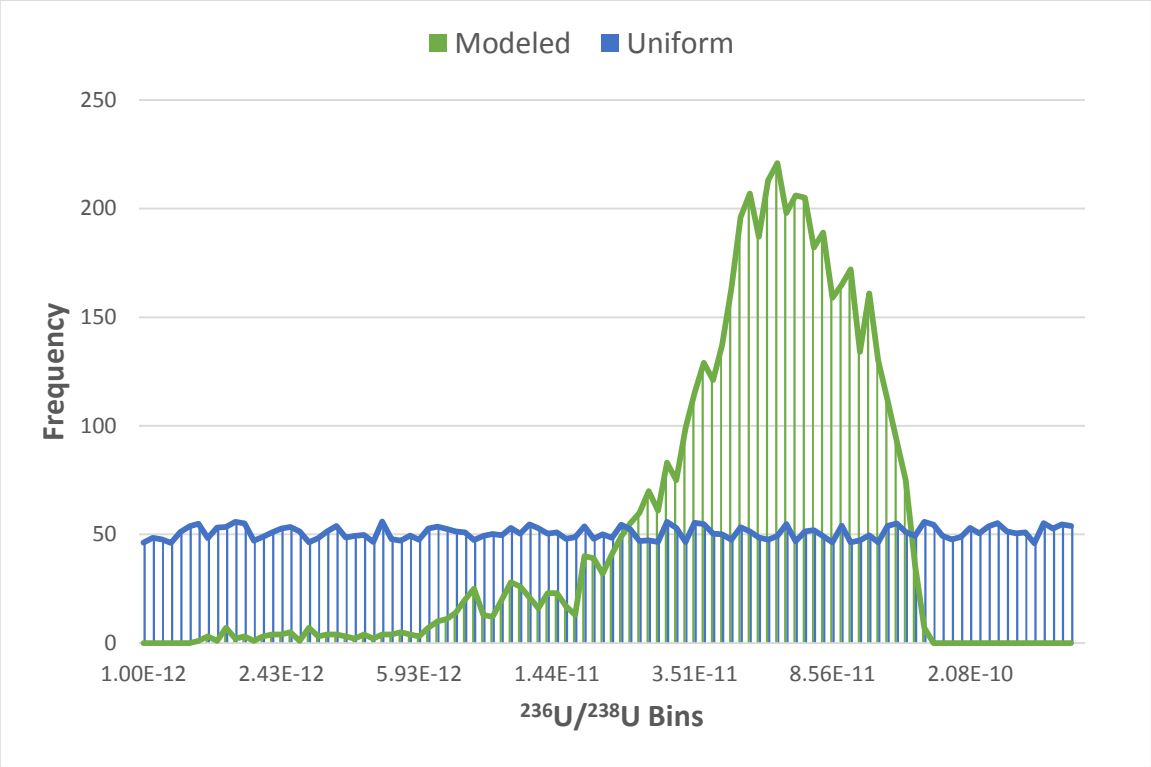

Figure V.1: A 5000 point histogram of the modeled and uniform null distributions with 102 $^{236}U/^{238}U$ bins.

The difference between uniform and modeled null models can be evaluated using the histogram distributions shown in Figure V.1. The objective of the null model in this research is to reduce the analysis sensitivity on missing ^{236}U distributions (not contained in the model set). Commonly, a uniform distribution is used to equally represent the distribution range.

However, with ill-posed problems (specifically non-uniqueness of ^{236}U signatures) the true distribution of ^{236}U possibilities can be misrepresented by a uniform distribution. This is the case for this model, as is shown for the distribution of the modeled null model. By using the modeled null model, larger penalties are created for deviations closer to the center of data (the ^{236}U signature has to be relatively close to the evaluated model), while lower penalties are assessed for signatures on the exterior of the distribution. The effects of using both distributions will be tested against the measured UOC data set.

A script was developed in MATLAB R2014b [83] code was developed to solve the posterior distribution (more specifically the maximum likelihood function) for each model (see Appendix VI.3). The code randomly sampled from the ^{236}U distribution, with a respective weight function (based on the normal distribution). A weighted value for each model was calculated every iteration, approximating the maximum likelihood estimator $\hat{l}$:

$$\lim_{n\to\infty} \hat{l}(H_1|^{236}U) = \frac{1}{n}\sum_{i=1}^{n} f(^{236}U_i|H_1)p(H_1)\omega_1$$

Several estimators can be used to evaluate the posterior distribution (see section 3.1.3), but this study utilized the maximum likelihood estimator. The results of the study is shown in Table V.2, with the previously measured mineralogy included for select samples. The measured uranium mineralogy for the UOC samples was estimated through open literature, and therefore not necessarily a true representation of the sample.

Table V.2: The estimated uranium mineralogy using Bayesian inference compared against the true mineralogy highlighted in yellow (Uniform NULL assumption).

Mineralogy	ANU-103	ANU-99	ANU-101	ANU-98
UO2	0%	0%	1%	0%
Uraninite	0%	0%	1%	0%
Coffinite	0%	0%	1%	0%
Brannerite	0%	2%	41%	1%
Davidite	**76%**	0%	0%	0%
Carnotite	0%	0%	13%	0%
Autunite	0%	0%	0%	0%
Thorinite	0%	0%	31%	0%
NULL	23%	**98%**	12%	**99%**

Mineralogy	ANU-91	ANU-104	ANU-105	ANU-97
UO2	11%	0%	0%	0%
Uraninite	11%	0%	0%	0%
Coffinite	8%	0%	0%	0%
Brannerite	0%	0%	0%	**85%**
Davidite	0%	**100%**	**80%**	0%
Carnotite	37%	0%	0%	0%
Autunite	2%	0%	0%	2%
Thorinite	27%	0%	0%	0%
NULL	4%	0%	20%	6%

The samples containing davidite showed a good agreement with the Bayesian analysis, with an average likelihood of 85% (with no significant difference between the lanthanum and cerium forms). Davidite (a rare earth oxide) has a high concentration of REE, which has been previously shown to have a high influence with ^{236}U content. Consequently, all the samples that were estimated to have davidite as the primary uranium mineralization was able to be predicted through the Bayesian model selection. However, with only three davidite

samples tested, this is not an exhaustive test of the estimation capability. Distinguishing davidite as the primary uranium mineralization though does show promise, and future studies should investigate further.

Unfortunately, none of the other estimated mineralization from the samples agreed with the model selection analysis. The replacement of the uniform null distribution with the modeled null distribution did not have a significant impact on the sensitivity of the analysis, with no real reduction in false negatives. The specificity of the analysis was improved with use of the modeled null distribution, by reducing the likelihood of false positives.

The main limitation in the analysis is the incomplete modeling of the mineralogy distributions, specifically the pitchblende distributions. The distributions represent the theoretical chemical formulation, and the impact impurities have has not been evaluated on the uranium mineralogy. Also uranium ore deposits typically include mixtures of primary and secondary mineralization, and the impact of a mixture effect on the analysis was not evaluated. However, with the choice of the modeled null distribution, the selection of false positives was limited for the majority of the cases tested. In a nuclear forensics scenario, limitation of false positives is a critical factor for any type of analysis. A more thorough evaluation for the capabilities of ^{236}U concentration in predicting uranium mineralogy needs to be performed with a larger sample size.

V.2.1.2. Uranium Deposition

Uranium ore deposits can be classified by several ways, including by geologic setting and depositional scheme. While the characteristics that dictate that uranium ore classification might not be influential to the model (i.e. the host rock matrix), similar processes can influence sensitive parameters for ^{236}U production. Classification by uranium deposition currently is more feasible for analysis (relative to geologic setting) due to the larger groupings and the control parameters. Specifically, the major controls on deposition of uranium are commonly redox, pH, ligand concentration, and temperature. The same parameters control both the alpha target and REE concentrations (which have high influences on ^{236}U

production). Bayesian analysis was used to assess the probability of an unknown UOC sample to be classified using a depositional scheme.

The model based ^{236}U distribution was found by grouping known UOC samples into either: low-temperature redox, high-temperature redox, or non-redox depositions. The ^{236}U for each sample was previously calculated in the model through normal distributions in the elemental concentrations (average and standard deviation found in the measurements). A joint probability distribution of the grouped UOC samples was used to estimate the likelihood for each model. The high-temperature and low-temperature redox distributions were approximated by grouping the individual distributions of the ANU UOC samples by their respective deposition mode. Figure V.2 shows the joint probability distribution of ^{236}U for high temperature redox. Additionally, the same two null models as the uranium mineralogy analysis.

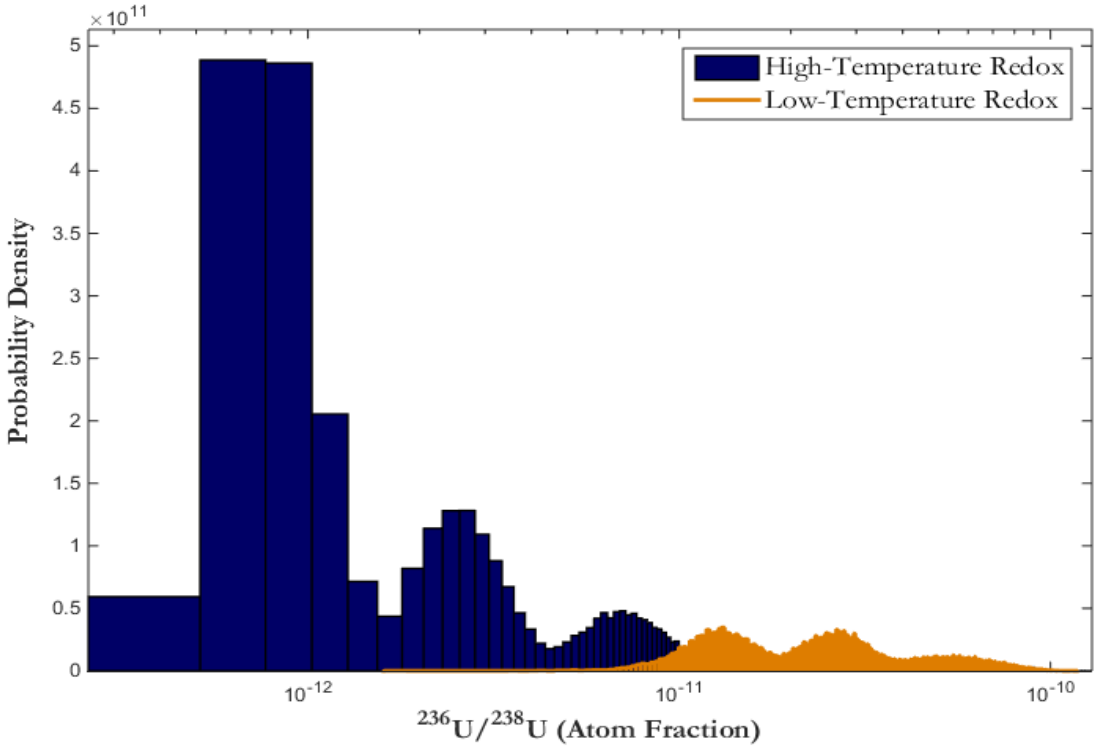

Figure V.2: The joint probability distributions of the high-temperature and low-temperature uranium depositions, included is the uniform null distribution.

The same script was used (with minor modifications) utilizing MATLAB R2014b [83] to solve the posterior distribution for each model given a ^{236}U measurement. Similarly, the code randomly sampled from the ^{236}U distribution, with a respective weight function (based on the normal distribution). A weighted value for each model was calculated every iteration, approximating the maximum likelihood estimator. The results are shown for each UOC measurement utilizing an uniform null distribution in Table V.3.

Table V.3: Bayesian model comparison of the predicted uranium deposition with the true deposition method highlighted in yellow for UOC samples (uniform null distribution).

Sample I.D.	High-Temp Redox	Low-Temp Redox	Null
ANU-92	0%	0%	**100%**
ANU-93	**55%**	35%	10%
ANU-94	**80%**	8%	11%
ANU-97	0%	0%	**100%**
ANU-98	8%	**73%**	19%
ANU-99	**78%**	11%	11%
ANU-103	**81%**	0%	19%
ANU-104	**63%**	24%	12%
ANU-105	**81%**	0%	19%
ANU-91	0%	0%	**100%**
ANU-96	39%	**52%**	9%
ANU-100	38%	**53%**	9%
ANU-101	41%	**50%**	9%
ANU-102	24%	**66%**	10%
ANU-267	37%	**54%**	9%

A known bias in this analysis is due to using the UOC samples both for model fitting and testing. While a distinction was made to use the model data for distribution fitting and the measurements data for testing, similar governing parameters are associated with both. The

analysis is only relevant for samples with similar elemental distributions as those that were used, although the null model attempts to mitigate this bias. Still, the degree to which the code was able to distinguish the uranium deposition scheme is promising. Future work should investigate this analysis methodology further to reduce the associated bias. Specifically, larger sample sizes would allow a more thorough estimation of each model distribution. Different classification schemes can also be evaluated for use in this methodology. The impact of the analysis by changing the null distribution from uniform to modeled is shown in Table V.4. The number of false positives is reduced from one to zero, increasing the specificity of the analysis. However the sensitivity of the analysis is also reduced, with the number of true positives being reduced from 73% to 67%.

Table V.4: Bayesian model comparison of the predicted uranium deposition with the true deposition method highlighted in yellow for UOC samples (modeled null distribution).

Sample I.D.	High-Temp Redox	Low-Temp Redox	Null
ANU-92	0%	0%	**100%**
ANU-93	**62%**	35%	3%
ANU-94	**70%**	6%	24%
ANU-97	0%	0%	**100%**
ANU-98	4%	44%	**52%**
ANU-99	**68%**	8%	24%
ANU-103	**92%**	0%	8%
ANU-104	**52%**	19%	29%
ANU-105	**90%**	0%	10%
ANU-91	0%	0%	**100%**
ANU-96	37%	**51%**	12%
ANU-100	36%	**52%**	12%
ANU-101	40%	**51%**	8%
ANU-102	10%	30%	**60%**
ANU-267	34%	**50%**	16%

V.2.2. Parameter Estimation

The previous Bayesian analysis methods have all utilized single, discrete parameter testing (i.e. model selection). The single parameter, whether uranium mineralogy or deposition, has contained a set of distributions that describe ^{236}U production. This type of analysis can be prone to inadequate grouping, where the estimated parameter distribution in not representative of the real distribution. Another source of bias can occur when the parameter set is not mutually exclusive and/or exhaustive. Consequently, the analysis can fail for unknown samples falling outside the fitted sample distribution (although false positives are mitigated by an appropriate null model).

One solution is to use continuous parameter estimation, specifically by solving for the elemental posterior distributions for an unknown ^{236}U measurement. Ideally, this approach resolves the issues associated with a small fitting sample size (e.g. inadequate grouping, exhaustive parameter set, etc.) by utilizing the continuous range of elemental concentrations. The potential bias can therefore be reduced but at a cost of increasing the complexity (computation time) of solving a high dimensional integration. The solution of the posterior distribution is not trivial, and therefore numerical techniques are needed for approximation. Two numeric Monte Carlo Markov Chain techniques were evaluated to approximate the posterior distribution for a given ^{236}U measurement: Metropolis-Hastings and Gibbs sampling. Gibbs sampling follows the same principals as the MH algorithm (see section 3.1.4), but the variable conditional distributions (i.e. the distribution of one variable while keeping the others constant) are adopted for the proposal distributions. Implementing the conditional distributions for the proposal allows the acceptance ratio to always be one, resulting in all samples being accepted. The benefit of Gibbs sampling is the convergence efficiency is generally improved with respect to MH, although Gibbs sampling doesn't allow for parameters to evolve jointly (i.e. can be inefficient for highly correlated parameters). The full conditional distributions need to be known, however, in order to utilize the Gibbs algorithm:

1. Establish random variables as X_1, X_2, and X_3 using the PLSR technique.

2. Set variables to the initial vectors $x_1^{(0)}, x_2^{(0)}$, and $x_3^{(0)}$ obtained by sampling from prior distributions (for this case uniform distributions).
3. At iteration i, sample the posterior distribution:

$$P\left(X_1 = x_1 \middle| X_2 = x_2^{(i-1)}, X_3 = x_3^{(i-1)}, {}^{236}U\right).$$

4. Set new vector values $x_1^{(i)}$ by sampling from the updated posterior distribution.
5. Repeat previous steps 3 and 4 by sweeping remaining latent variables:

$$P\left(X_2 = x_2 \middle| X_1 = x_1^{(i)}, X_3 = x_3^{(i-1)}, {}^{236}U\right)$$

$$P\left(X_3 = x_3 \middle| X_1 = x_1^{(i)}, X_2 = x_2^{(i)}, {}^{236}U\right)$$

6. Continue for a user defined number of iterations.

In general, a given parameter is sampled from the conditional distribution (initially the prior distribution) with the remaining parameters being constant. The algorithm then sweeps through each variable in the iteration, updating the distribution with the most recent available samples. The weight of the sampled parameter distribution is assigned based on the distribution of the ^{236}U measurement. This process continues until the distribution of the samples converge to the posterior joint distribution. Consequently, the number of parameters, and the degree of correlation, greatly affects the computation time of Gibbs sampling. It has been shown in the previous sections that not all the parameters have the same influence on ^{236}U production. In fact, some of the parameters have a high degree of collinearity, which does not add any additional information to the solution. Regression techniques were evaluated to fully describe the conditional distributions and to reduce the dimensionality of the parameters (although at the cost of increasing the uncertainty in the analysis).

V.2.2.1. Regression Analysis

Regression analysis is a technique for estimating the relationships among variables. Specifically for interest in this work is the ability to model the relationship between dependent variables (uranium isotopics) and explanatory parameters (elemental concentrations, etc.). A

linear regression technique is considered for this analysis; however, nonlinear regression potentially could model the data better. The two linear regression methods evaluated are the Principal Component Regression (PCR) and Partial Least Square Regression (PLSR) models. Both models represent the relationship between the dependent variable y_i and the vector of regressors x_{i1} - x_{ip} in the following linear form:

$$y_i = B_1 x_{i1} + \cdots + B_p x_{ip} + \varepsilon_i$$

The regressors can be a direct function of the parameters for the MCNP model, or a subset of principal components/latent variables (which are often used to reduce the data set or when the explanatory variables are collinear). Principal components and latent variables are used for PCR and PLSR respectively, and reduce the parameter dimensionality to reduce computation time for the analysis. Scoping work was performed to evaluate both regression analysis techniques. Both techniques construct a new variable vector as a linear combination of the parameter; however, PLSR was found to be the more appropriate method for data reduction. PCR components are constructed to explain the variability in the parameter set without considering the related variability in ^{236}U concentration, while PLSR takes into account this additional variability. For small parameter variations (e.g. gadolinium concentration) that result in large ^{236}U variations, PLSR is the better regression technique.

The Bayesian linear regression will combine Bayes' theorem with the PLSR model shown previously:

$$P(\boldsymbol{X}|^{236}U) = \frac{f(^{236}U|\boldsymbol{X},\boldsymbol{\beta},\sigma^2)p(\boldsymbol{X},\sigma^2)}{\int f(^{236}U|\boldsymbol{X},\boldsymbol{\beta},\sigma^2)p(\boldsymbol{X},\boldsymbol{\beta},\sigma^2)\partial\boldsymbol{X}\partial\boldsymbol{\beta}\partial\sigma^2}$$

where $\boldsymbol{X},\boldsymbol{\beta}$ are the latent variable and regression coefficient vectors respectively. The error term is assumed to be distributed as $\varepsilon_i \sim N(0,\sigma^2)$. The solution of the posterior distribution for a given ^{236}U concentration is the distribution of the latent variables in the vector space. Transformation of the vector back to the scale of the parameter set can then be used to

estimate the elemental concentration distributions, assuming the number of latent variables are sufficient.

V.2.2.2. Cross-Validation of PLSR (Partial Least Squares Regression)

The choice of number of latent variables to use is dependent on several factors, one being the percent variation explained in ^{236}U concentrations. A data set (referenced from here on as the training data set) is needed for PLSR to optimize the model parameters (score and loading factors) to fit the parameter and ^{236}U variation as well as possible. A problem can occur when the number of latent variables becomes large, where the model is likely to fit the training data, but fail to represent newly introduced test data. Cross-validation was therefore used to assess the ability of PLSR to generalize the independent data set with a defined number of latent variables. The data was broken up into a training set (used to optimize the model) and a test set (used to evaluate the model), where the number of latent variables can be evaluated. For this research, the available data was not large enough to break up into two equivalent sized groups. Leave-one-out cross-validation (LOOCV) was therefore used, which employs one observation as the test set and the remaining data as the training set (iterated for all combinations). LOOCV can also be used to evaluate observations that could potentially be outliers in the data set. A particular case can be seen by utilizing LOOCV when evaluating the percent variance explained in Y ($^{236}U/^{238}U$ ratio) relative to the number of latent variables used shown in Figure V.3.

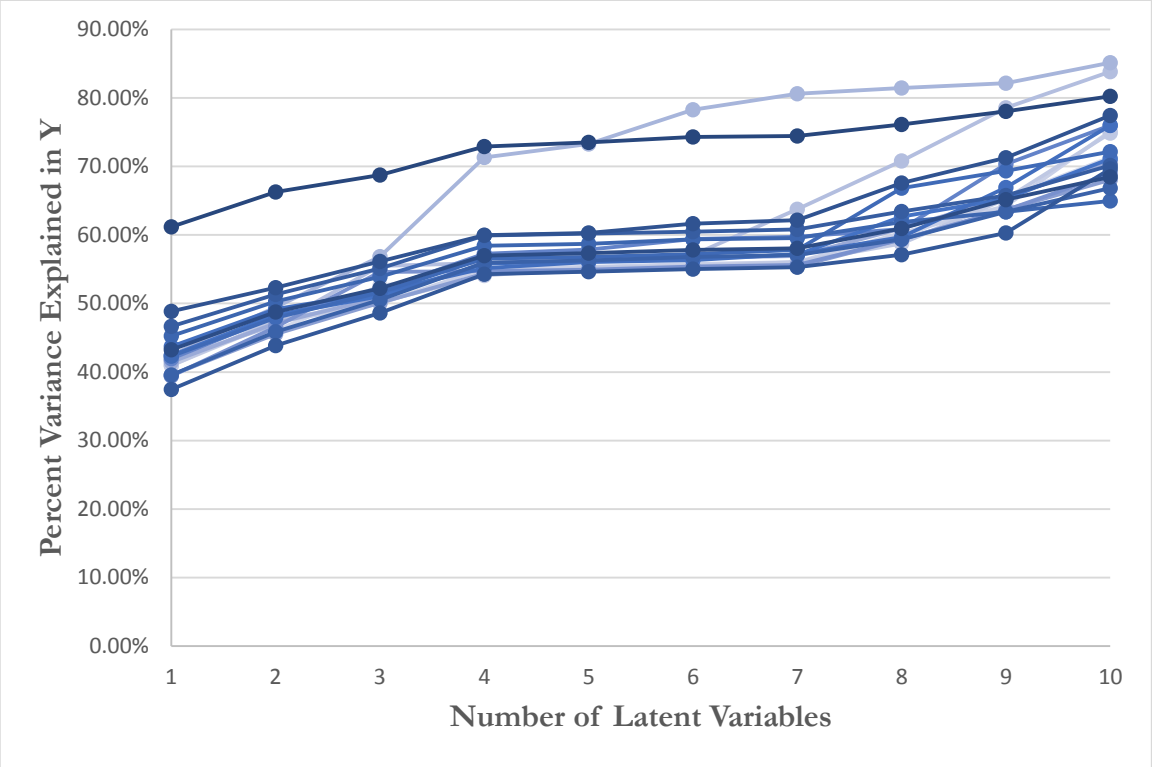

Figure V.3: The percent variance explained in Y ($^{236}U/^{238}U$ ratio) relative to the number of latent variables used; each line is a unique LOOCV case.

For two of the LOOCV cases, the explained variance increases significantly when leaving that particular observation out of the training set. By including those particular data points in the set, the number of latent variables needed to reach the same variance increases from 4 to 10 which can be significant. As the main goal for the regression analysis was to reduce the computation time for calculating the posterior distribution, a smaller set of latent variables was desired. A low percent change in explained variance was seen with additional increases past three latent variables, and as a result was used for all subsequent regression analysis. The distribution of the residuals is shown in Figure V.4, with two estimated fits for the distribution. The normal fit uses a normal distribution and includes all the residuals. The estimate of the mean and standard deviation for the normal fit is approximately 0.0 and 8.2 x 10^{-12} respectively. The variance in the residuals is one of the limiting factors for Bayesian parameter estimation using regression analysis.

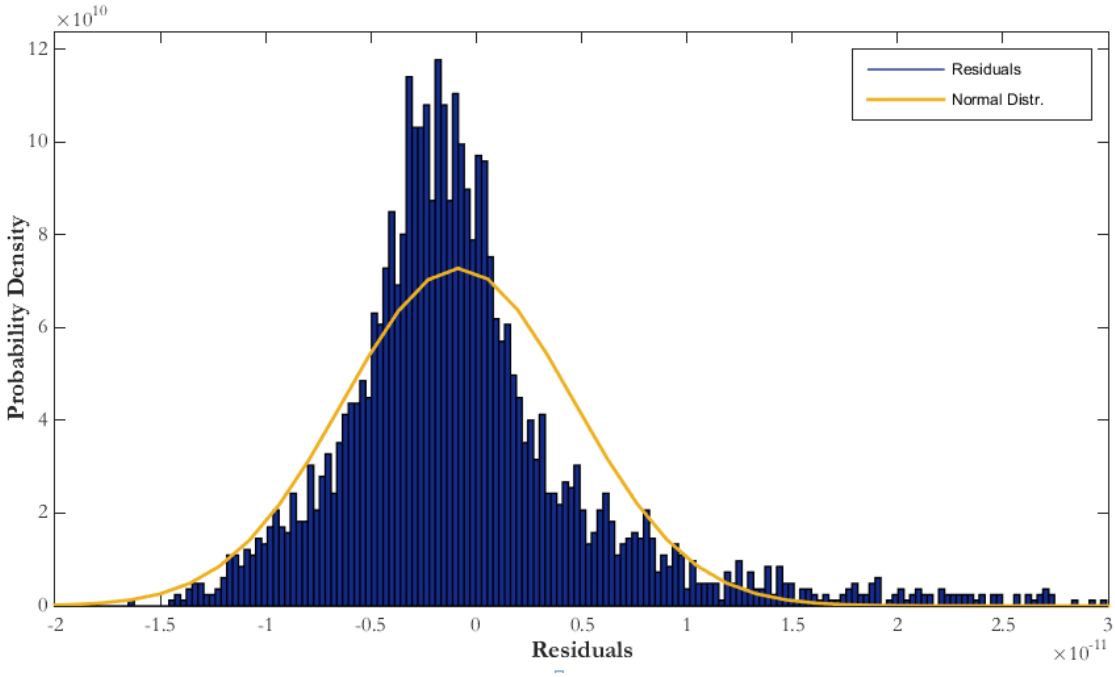

Figure V.4: The residuals distribution of measured to predicted $^{236}U/U$ ratios with the utilization of three latent variables.

V.2.2.3. Gibbs Sampling Utilizing PLS Regression

Utilizing three component PLSR on the sample test data (random elemental concentrations sampled from uniform prior distributions) led to the following regression model:

$$Y = B_0 + B_1X_1 + B_2X_2 + B_3X_3 + \varepsilon$$

where ε is i.i.d. $\sim N(0, \sigma_\varepsilon^2)$ and $Y \sim N(^{236}U, \sigma_{meas}^2)$. The following likelihood function can then be derived from the linear regression:

$$l(^{236}U|X_1, X_2, X_3, \tau) \sim N(B_0 + B_1X_1 + B_2X_2 + B_3X_3, \sigma_{meas}^2 + \sigma_\varepsilon^2)$$

the following prior distributions were assumed for the parameters:

$$\sigma_{meas}^2 + \sigma_\varepsilon^2 = {}^1/_\tau \quad \text{where} \quad \tau \sim gamma(\alpha, \beta)$$

$$X_1 \sim Unif(min, max)$$

$$X_2 \sim Unif(min, max)$$

$$X_3 \sim Unif(min, max)$$

Using the likelihood function and the proposed priors, the posterior distribution can be evaluated up to a constant of proportionality (assuming mutually independent parameters):

$$P(X_1, X_2, X_3, \tau|^{236}U) \propto l(^{236}U|X_1, X_2, X_3, \tau)P(X_1)P(X_2)P(X_3)P(\tau)$$

The joint posterior distribution is difficult to directly sample from; however, the conditional distributions of the parameters (in this case, but not always) can be found. The following steps are used to reduce the joint posterior distribution to a conditional distribution for each parameter, and simplify to a common distribution (e.g. normal, gamma, etc.) which can be easily sampled from:

$$\ln\left(P(X_1, X_2, X_3, \tau|^{236}U)\right) \propto \ln\left(l(^{236}U|X_1, X_2, X_3, \tau)\right) + \sum_{i=1}^{3} \ln(P(X_i)) + \ln(P(\tau))$$

$$\propto -\frac{1}{2}\ln(\tau^{-1}) - \frac{(^{236}U - B_0 + B_1X_1 + B_2X_2 + B_3X_3)^2}{2 * (\tau^{-1})} + (\alpha - 1)\ln\tau - \beta\tau - \frac{1}{2}\ln\alpha + \alpha\ln\beta$$

The conditional distribution for X_1 can be found by setting all other variables to constants, so therefore:

$$\ln P(X_1|X_2, X_3, \tau, ^{236}U) \propto -\frac{(^{236}U - B_0 + B_1X_1 + B_2X_2 + B_3X_3)^2}{2 * (\tau^{-1})}$$

This is just a quadratic function of X_1:

$$\ln P(X_1|X_2, X_3, \tau, ^{236}U) \propto -X_1^2\left(\frac{B_1^2}{2 * (\tau^{-1})}\right) - X_1\left(\frac{2B_1(^{236}U - B_0 + B_2X_2 + B_3X_3)}{(\tau^{-1})}\right)$$

By taking the exponential and equating to a normal distribution (up to a constant of proportionality):

$$-\left[X_1^2\left(\frac{B_1^2}{2*(\tau^{-1})}\right)+X_1\left(\frac{2B_1(^{236}U-B_0+B_2X_2+B_3X_3)}{(\tau^{-1})}\right)\right]\propto-\left[\frac{(X_1-\mu)^2}{2\sigma^2}\right]$$

So the conditional distribution of X_1 is a normal distribution of the form:

$$p(\beta_1X_1|X_2,X_3,\sigma_\varepsilon,{}^{236}U)\sim N\left(\frac{^{236}U-B_0-B_2X_2-B_3X_3}{B_1},\frac{\tau^{-1}}{B_1^2}\right)$$

The same format was followed for the remaining latent variables. The conditional distribution on the error variance was found from the joint posterior with fixed latent variables:

$$\ln P(\tau|X_1\ldots,U)\propto(\alpha-1)\ln\tau-\beta\tau+\frac{1}{2}\ln\tau-\frac{\tau}{2}(^{236}U-B_0+B_1X_1+B_2X_2+B_3X_3)^2$$

This conditional distribution is representative of a gamma distribution with the following parameters:

$$p(\tau|X_1,X_2,X_3,{}^{236}U)\sim gamma\left(\alpha+\frac{1}{2},\beta+\frac{1}{2}(^{236}U-(B_0+B_1X_1+B_2X_2+B_3X_3)\right)$$

A Gibbs sampler for the regression model was implemented through a script utilizing MATLAB R2014b, which applied the conditional distributions previously solved. The full code can be found in Appendix VI.3. The chain ran for 5000 iterations, with a burn-in of 1000 iterations. A trace plot is shown in Figure V.5 of the uranium posterior scores for ANU sample 103, after the burn-in period. The trace plot indicates that the Markov chains for the three latent variables are indeed aperiodicity, as no cyclical patterns are detected.

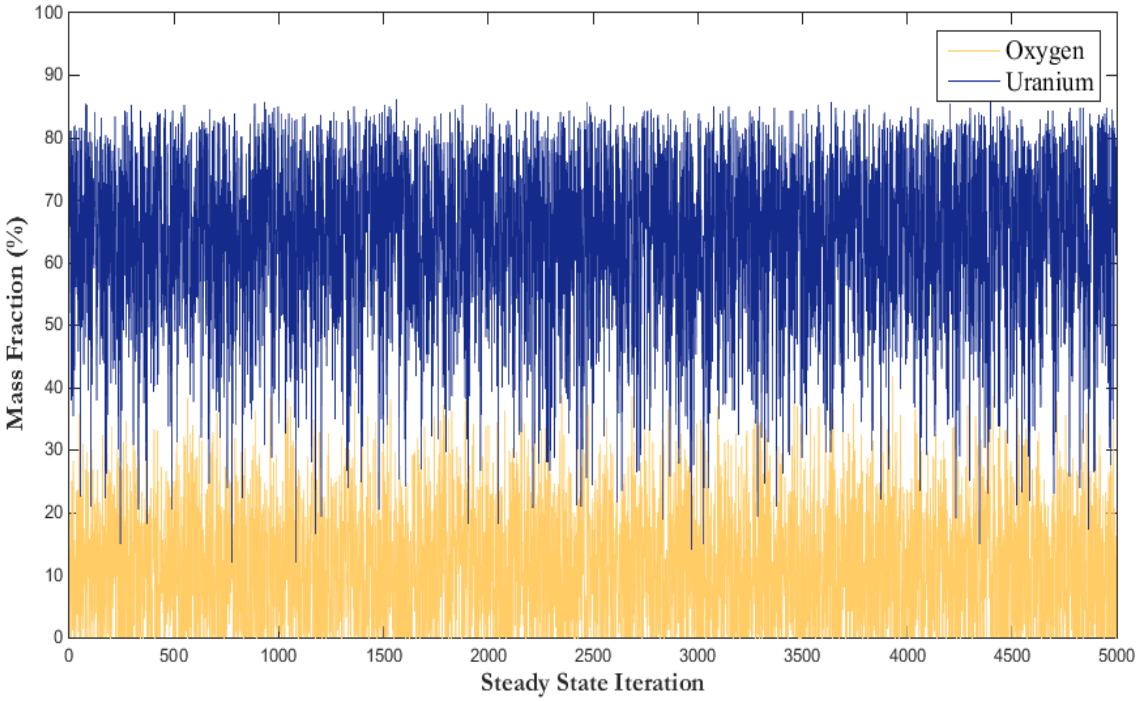

Figure V.5: Steady state Gibbs sampling sequence of the uranium posterior distribution for ANU-103 with a 1000 iteration burn-in.

Gibbs sampling was performed for the ANU samples utilizing a three latent variable set. The conditional distributions were produced from regression (PLSR) of those latent variables and assuming an uniform prior distribution for each. The MCMC distribution matrix for the latent variables was then transformed back to the actual parameters, producing a simulated solution for the posterior distribution. The predicted distributions of uranium for ANU samples 103 and 97 are shown in Figure V.6 and Figure V.7 respectively. Using the posterior mean (minimization of the squared loss function) for the two distributions results in a uranium concentration of 2% with a measured concentration of 1.9%, and 64% with a measured concentration of 69% for ANU samples 103 and 97 respectively. The results indicate a well-defined distinction between samples with high and low uranium concentrations for the majority of cases. However, this does not preclude samples with a predicted uranium distribution such as Figure V.6 from having a real uranium concentration in a higher range.

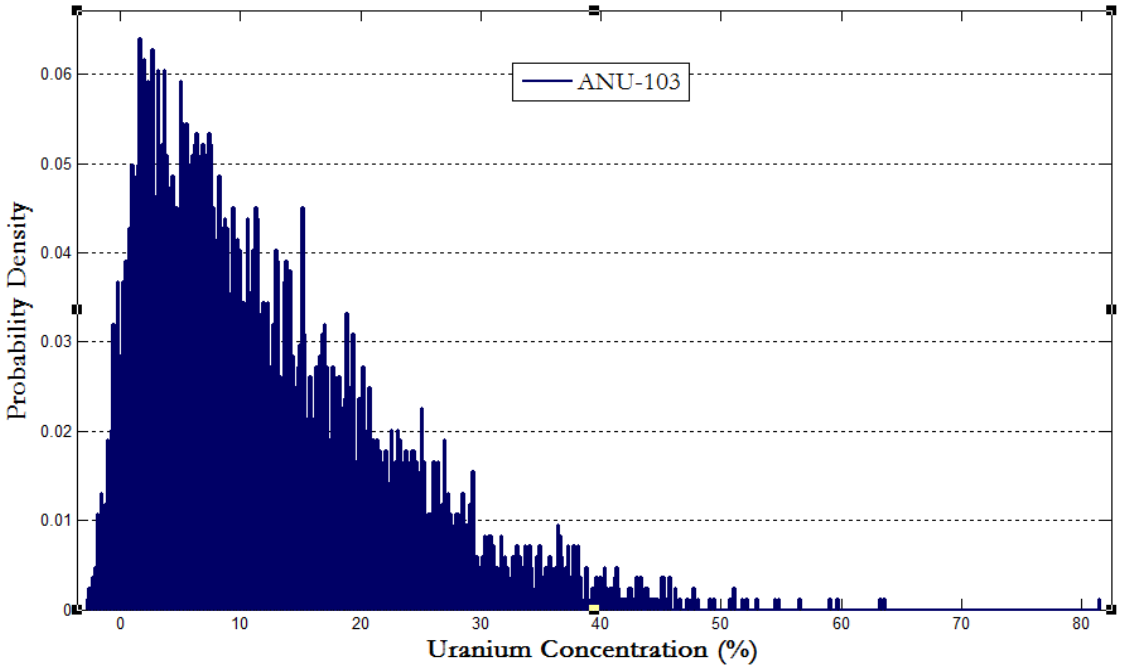

Figure V.6: The posterior distribution of uranium solved utilizing Gibbs sampling for UOC sample ANU-103, with a measured concentration of 2 weight percent.

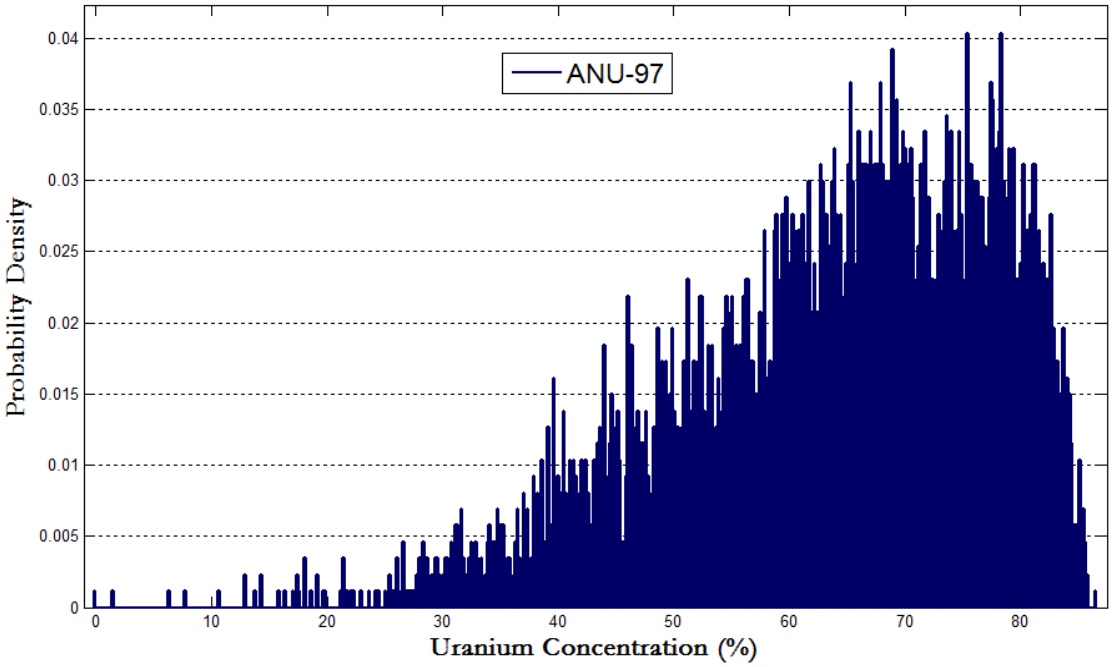

Figure V.7: The posterior distribution of uranium solved utilizing Gibbs sampling for UOC sample ANU-97, with a measured concentration of 69 weight percent.

The results of Gibbs sampling using regression analysis is limited by the variance in the residuals (error distribution in Figure V.4). This effectively increases the variance in the measured ^{236}U, decreasing the possibility of distinction between posterior distributions. This especially evident in the gadolinium posterior distributions which does not change significantly between sample cases.

V.2.2.4. Secondary Stage Metropolis-Hastings

To remove the error variance in the regression analysis, the MCNP production model needs to be utilized in a Metropolis-Hastings algorithm. The problem with sampling from the model is the computation time needed for convergence. One idea is to use Gibbs sampling as the proposal distribution for a secondary stage Metropolis-Hastings algorithm. Utilizing the regression conditional distributions for the proposal distribution can allow for a faster convergence. This is accomplished through tuning the proposal distribution to sample along a regression predicted posterior distribution. A schematic of the two stage Metropolis-Hastings algorithm is shown in Figure V.8.

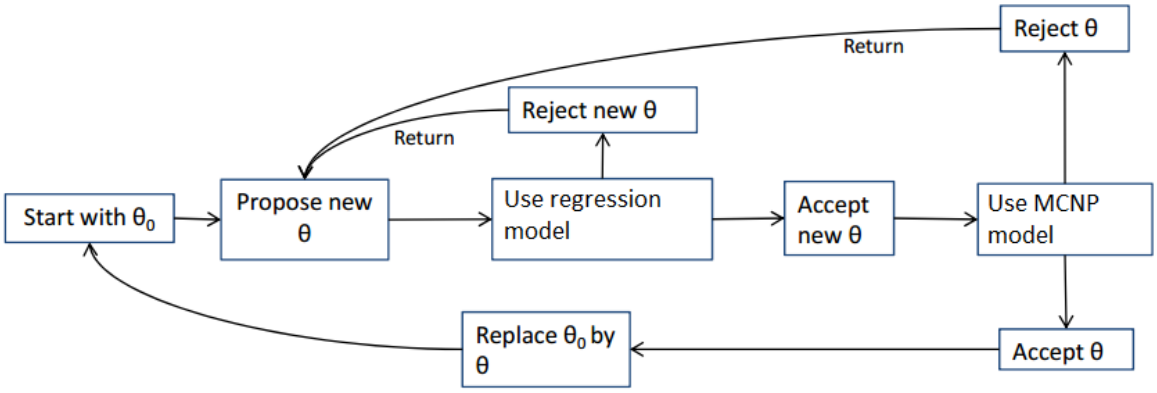

Figure V.8: A schematic of the two stage Metropolis-Hastings algorithm, utilizing both the regression model and the MCNP model.

The secondary stage Metropolis-Hastings analysis represents a complete coupling of the measurement data, SOURCES 4C source model, the MCNP production model, and analysis algorithm. The complete VBA code is shown in the Appendix VI.2, but the algorithm is

taken from Figure V.8. The estimated uranium posterior distributions for UOC sample ANU-267 is shown in Figure V.9 utilizing both the Gibbs sampling with regression (orange) and the two stage Gibbs / Hastings (blue) algorithm.

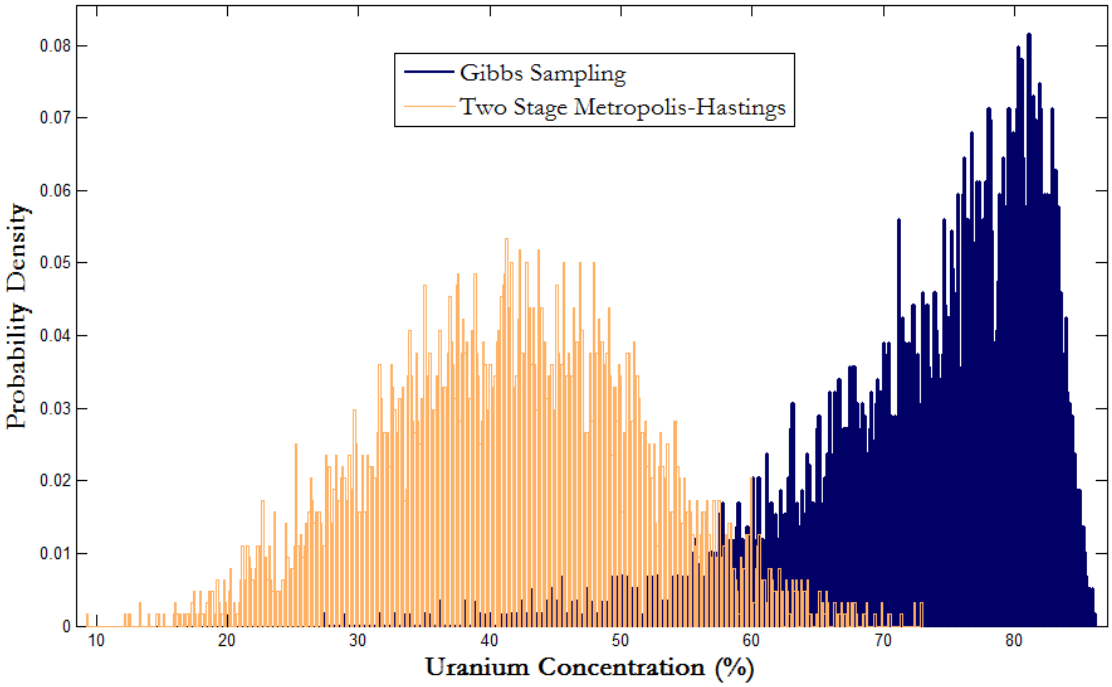

Figure V.9: The posterior distribution of uranium solved utilizing Gibbs sampling with regression (orange) and the two stage Gibbs / Hastings (blue) for UOC samples ANU-267.

As expected, the posterior distribution is highly dependent on the variance of the error distribution. The error in the Gibbs sampling is a combination of measurement error associated with AMS, the estimated error in the MCNP production model, and the residual error in the regression analysis. These sources of error lead to a large variance in the posterior solution distribution for a given parameter, which can be seen in Figure V.9. The use of the two stage algorithm removes the error associated with the regression analysis (effectively decreasing the error variance) which then reduces the variance in the solution of the uranium posterior distribution. Using the posterior mean (minimization of the squared loss function) for the two distributions results in a uranium concentration of 73% with standard deviation

of 9% for Gibbs with regression and 42% with a standard deviation of 10% for the two stage Metropolis Hastings algorithm. The measured uranium concentration for the UOC sample was approximately 43%, which indicates a significant improvement between the two algorithms. However, the UOC sample chosen had minimal error in the production model and a high error in the regression prediction, which the two stage algorithm ultimately removes. Samples that do not meet these criteria will most likely not have as significant improvements in the calculated distributions (i.e. error remains consistent between methods). It is interesting to note that the standard deviation slightly increased for the Metropolis-Hastings method when, with a reduced error term, was predicted to decrease. The most likely cause is the physical limit on uranium concentration, which can artificially reduce the standard deviation for distributions with high uranium means.

The approach towards the measured concentrations seems to be promising, however more work needs to be done to reduce the computation time and benchmarking of additional UOC samples. Improvements can be made to the calculated posterior distributions by increasing both the burn-in and iteration numbers. Another improvement would be in direct use of the parameters (instead of using regression analysis as a pseudo proposal distribution), however both methods can increase the computation time needed. One challenge for future work will be to reduce the computational time, through either changes in the model or in the sampling scheme. The accuracy of the Metropolis-Hastings method will also always be limited by the error of both the production model and the AMS measurements for the parameters.

VI. CONCLUSIONS AND RECOMMENDATIONS

Nuclear forensics generally utilizes two broad classes of signature (characteristics intrinsic to the uranium origin): comparative and predictive. Predictive signatures are drawn upon when representative data for a set of suitable reference samples are unavailable. However, the majority of work in the area has focused on expanding the comparative capabilities of UOC signatures (more measurements, more samples, etc.). The use of predictive signatures for UOC samples is significantly limited. This work examined the feasibility of using predictive signatures for UOC forensics analysis, specifically by utilizing ^{236}U concentrations. The examined technique involves the measurement of the ^{236}U isotopic ratio of UOC samples using AMS systems. The results are then analyzed through Bayesian methods to update a likelihood distribution of ^{236}U isotopics calculated utilizing a Monte Carlo production model to determine specific ore deposit parameters (e.g., mineralization, deposition, elemental distributions). These parameters can be used to narrow the deposit location for an unknown uranium ore. The feasibility of the complete system (AMS measurements, production modeling, and data analysis) was evaluated for available UOC samples with diverse backgrounds (i.e., differing mineralogy and depositional classification).

The complete system is very dependent on the AMS system capabilities for ^{236}U measurements. Specifically, the abundance sensitivity is a significant factor on whether measurements can be used for nuclear forensics analysis. The sensitivity limit for CAMS ^{236}U measurements is approximately 1×10^{-11}, which can misrepresent UOC samples containing low uranium or high REE concentrations. The use of time-of-flight measurements can reduce this limit (as seen in the ANU system); however, the reduction of beam efficiency for ^{236}U counts introduces a bias that has not been accounted for. The current AMS capabilities dictate the use of time-of-flight measurements to assess the complete range of ^{236}U, however the bias between systems needs to be investigated before implementation.

The production model was evaluated against specific UOC samples to assess predictive capabilities, given elemental concentration measurements. The model agreed well for the AMS measurement test cases with the exception of four samples. The measured elemental data for the specific UOC samples are most likely not representative of the deposit (through

high milling/processing). The methods utilized to acquire the samples were not available in the literature. The variations of this process (ore pulp vs. yellowcake, sampling area, etc.) could potentially influence the predictive ability of the model. Future work should utilize well characterized samples to assess the bias associated with the processing of the UOC. An investigation of better characterized samples and a larger sample size would allow a better assessment of the model capabilities.

Data analysis was performed using Bayesian methods, due to the ability to represent uncertainty in the parameter distributions and the incorporation older data/measurements through prior distributions. This latter characteristic confirmed the choice of Bayesian analysis for this feasibility study, as nuclear forensics scenarios generally incorporate multiple signatures for analysis. Both model selection and parameter estimation was evaluated to determine the potential capabilities of ^{236}U signatures. In all, analysis of the ^{236}U signature has the potential capability to determine the following parameters. While each of these capabilities shows promise, work needs to be performed to validate the techniques by utilizing a larger and better characterized data set.

1. Identification of the uranium mineralogy shows promise, especially for the uranium minerals containing high concentrations of REE (e.g. davidite). More work needs to examine real variations within each uranium mineral group, to better estimate the likelihood for a given ^{236}U ratio. The use of an informed prior would also better incorporate knowledge of uranium mineralogy distributions for ore deposits.

2. Identification of the uranium ore deposit can also be found, assuming an appropriate grouping structure. The depositional classification, as variations in deposition will influence elemental concentrations. The samples used to estimate the distributions was limited, and a larger sample size would be needed to utilize this analysis. The IAEA classification was not explored in this study, due to low sample size and indirect influences on sensitive parameters of the model.

3. Inferences on elemental distributions were investigated utilizing a combination of regression analysis and Gibbs sampling. Specifically, the REE distribution analysis was able to distinguish between samples with low and high concentrations. The analysis was limited by the accuracy of the production model to represent variations in ^{236}U concentrations. The computation time also limited the sampling efficiency of the analysis, and introduced the need for regression analysis. While the use of regressors decreased computational time, it also introduced additional error that was not accounted for.

The feasibility of coupling a complete system for predictive signatures has been shown to be possible, specifically with ^{236}U concentrations. The integrated system is an improvement on previous methods for predictive signatures on UOC samples, and provides a methodology for ^{236}U analysis in a nuclear forensics scheme. The openness of the analysis allows further improvements to be dictated by the user, specifically on the desired parameter estimation. The addition of other data is made possible within the Bayesian scheme, as the prior distribution for a given parameter can be updated with comparative measurement signatures.

REFERENCES

1. (IAEA), I.A.E.A. *Illicit Trafficking Database (ITDB)*. 2012; Available from: http://www-ns.iaea.org/security/itdb.asp.

2. Keegan, E., Richter, S., Kelley, I., Wong, H., Gadd, P., et al., *The provenance of Australian uranium ore concentrates by elemental and isotopic analysis.* Applied Geochemistry, 2008. **23**(4): p. 765-777.

3. Švedkauskaitė-LeGore, J., Rasmussen, G., Abousahl, S., van Belle, P., *Investigation of the sample characteristics needed for the determination of the origin of uranium-bearing materials.* Journal of Radioanalytical and Nuclear Chemistry, 2008. **278**(1): p. 201-209.

4. Badaut, V., M. Wallenius, and K. Mayer, *Anion analysis in uranium ore concentrates by ion chromatography*. Journal of Radioanalytical and Nuclear Chemistry, 2009. **280**(1): p. 57-61.

5. Varga, Z., M. Wallenius, and K. Mayer, *Origin assessment of uranium ore concentrates based on their rare-earth elemental impurity pattern*, in *Radiochimica Acta International journal for chemical aspects of nuclear science and technology*. 2010. p. 771.

6. Švedkauskaite-LeGore, J., Mayer K., Millet, S., Nicholl, A., Rasmussen, G., Baltrunas, D., *Investigation of the isotopic composition of lead and of trace elements concentrations in natural uranium materials as a signature in nuclear forensics*, in *Radiochimica Acta*. 2007. p. 601.

7. Varga, Z., Wallenius, M., Mayer, K., Keegan, E., Millet, S., *Application of Lead and Strontium Isotope Ratio Measurements for the Origin Assessment of Uranium Ore Concentrates.* Analytical Chemistry, 2009. **81**(20): p. 8327-8334.

8. Brennecka, G., *Uranium Isotope Variations in Nature: Mechanisms, Applications, and Implications*. 2011, Arizona State University.

9. Hutcheon, I., M. Kristo, and K. Knight, *Nonproliferation Nuclear Forensics*, in *Uranium: Mineralogy, Geochemistry and the Environment*. 2013, Mineralogical Association of Canada Short Course Winnipeg MB.

10. Murphy, M., Stirling, C., Kaltenbach, A., Turner, S., Schaefer, B., *Fractionation of 238U/235U by reduction during low temperature uranium mineralisation processes.* Earth and Planetary Science Letters, 2014. **388**(0): p. 306-317.

11. Berkovits, D., Feldstein, H., Ghelberg, S., Hershkowitz, A., Navon, E., Paul, M., *^{236}U in uranium minerals and standards.* Nuclear Instruments and Methods in Physics Research Section B: Beam Interactions with Materials and Atoms, 2000. **172**(1–4): p. 372-376.

12. Buchholz, B., Brown, T., Hamilton, T., Hutcheon, I., Marchetti, A., et al., *Investigating uranium isotopic distributions in environmental samples using AMS and MC-ICPMS*. Nuclear Instruments and Methods in Physics Research Section B: Beam Interactions with Materials and Atoms, 2007. **259**(1): p. 733-738.

13. Wilcken, K., Fifield, L., Barrows, T., Tims, S., Gladkis, L., *Nucleogenic 36Cl, 236U and 239Pu in uranium ores*. Nuclear Instruments and Methods in Physics Research Section B: Beam Interactions with Materials and Atoms, 2008. **266**(16): p. 3614-3624.

14. Fabryka-Martin, J.T., *Production of radionuclides in the earth and their hydrogeologic significance, with emphasis on chlorine-36 and iodine-129*. 1988, The University of Arizona.

15. Fabryka-Martin, J.T. and D.B. Curtis, *Alligator Rivers Analogue Project Final Report, Geochemistry of 239Pu, 129I, 99Tc, and 36Cl*. 1992.

16. X-5 Monte Carlo Team, "**MCNP** - A General N-Particle Transport Code, Version 5" Volume I: **Overview and Theory**, LA-UR-03-1987 *MCNPX_2.3.0_Manual.pdf*.

17. Phillips, F.M., W.D. Stone, and J.T. Fabryka-Martin, *An improved approach to calculating low-energy cosmic-ray neutron fluxes near the land/atmosphere interface*. Chemical Geology, 2001. **175**(3–4): p. 689-701.

18. Cornett, R., Fabryka-Martin, J., Cramer, J., Andrew, H., Koslowsky, V., *^{36}Cl production and mobility in the Cigar Lake uranium deposit*. Nuclear Instruments and Methods in Physics Research Section B: Beam Interactions with Materials and Atoms, 2010. **268**(7–8): p. 1189-1192.

19. Gindler, J.E., National Research Council, *The Radiochemistry of Uranium*. 1962: Los Alamos National Laboratory.

20. Langmuir, D., *Aqueous environmental geochemistry*. 1997, Upper Saddle River, N.J.: Prentice Hall.

21. Gupta, C., *Chemical Metallurgy*. 2003: Wiley-VCH.

22. Plant, J., *Uranium ore deposits - products of the radioactive Echo Bay U-Ni-Ag-Cu deposits, North West Territories, Canada*. Economic Geology, 1999. **68**: p. 635-656.

23. Dahlkamp, F.J., *Genesis of Uranium Deposits. An Appraisal of the Present State of Knowledge*, in *Ore Genesis*, G.C. Amstutz, et al., Editors. 1982, Springer Berlin Heidelberg. p. 644-654.

24. Wolery, T.J., *EQ3/6, a software package for geochemical modeling of aqueous systems: Package overview and installation guide (Version 7.0)*, in *Other Information: PBD: 14 Sep 1992*. 1992. p. Medium: ED; Size: 70 p.

25. Abdelouas, A., W. Lutze, and E. Nuttall, *Uranium contamination in the subsurface; characterization and remediation.* Reviews in Mineralogy and Geochemistry, 1999. **38**(1): p. 433-473.

26. Keith, C., *Sorption of Neptunium on Graphite under Potential Repository Conditions.* Proceedings of the 14th International High Level Radioactive Waste Management Conference, 2013.

27. Chen, J.H., R. Lawrence Edwards, and G.J. Wasserburg, *238U,234U and232Th in seawater.* Earth and Planetary Science Letters, 1986. **80**(3–4): p. 241-251.

28. Stirling, C.H., Andersen, M., Potter, E., Halliday, A., *Low-temperature isotopic fractionation of uranium.* Earth and Planetary Science Letters, 2007. **264**(1–2): p. 208-225.

29. Sakanoue, M., K. Konishi, and K. Komura, *Stepwise determinations of thorium, protactinium, and uranium isotopes and their applications in geochronological studies.* Radioactive Dating and Methods of Low-Level Counting, 1968: p. 313 - 329.

30. Lively, R., Harmon, R., Levinson, A., Bland, C., *Disequilibrium in the 238uranium series in samples from yeelirrie, Western Australia.* Journal of Geochemical Exploration, 1979. **12**(C): p. 57-65.

31. Kaufman, A., T.-L. Ku, and S. Luo, *Uranium-series dating of carnotites: concordance between 230Th and 231Pa ages.* Chemical Geology, 1995. **120**(1–2): p. 175-181.

32. Bigeleisen, J., *Temperature dependence of the isotope chemistry of the heavy elements.* Proceedings of the National Academy of Sciences of the United States of America, 1996. **93**(18): p. 9393-9396.

33. Buerger, S., Boulyga, S., Cunningham, J., Koepf, A., Poths, J., *The range of variation of uranium isotope ratios in natural uranium samples and potential application to nuclear safeguards.* IAEA symposium, 2010.

34. Richter, S. and S.A. Goldberg, *Improved techniques for high accuracy isotope ratio measurements of nuclear materials using thermal ionization mass spectrometry.* International Journal of Mass Spectrometry, 2003. **229**(3): p. 181-197.

35. Böhlke, J., Laeter, J., Bievre, P., Hidaka, H., Peiser, H., et al., *Isotopic compositions of the elements, 2001.* Journal of Physical and Chemical Reference Data, 2005. **34**(1): p. 57-67.

36. Dahlkamp, F.J., *Classification of uranium deposits.* Mineralium Deposita, 1978. **13**(1): p. 83-104.

37. Agency, I.A.E., *Methods of Exploitation of Different Types of Uranium Deposits*. 2000: The Agency.

38. McKay, A.D., Y. Miezitis, and A.G.S. Organisation, *Australia's uranium resources, geology and development of deposits.* Canberra: AGSO--Geoscience Australia, 2001.

39. Mashkovtsev, G.A., *Uranium deposits: main types and concepts for detection.*, in *Changes and Events in Uranium Deposit Development, Exploration, Resources, Production and the World Supply-Demand Relationship*. 1995, International Atomic Energy Agency and OECD Nuclear Energy Agency: Vienna. p. 297 - 306.

40. Kreuzer, O.P., Markwitz, V., Porwal, A., McCuaig, T., *A continent-wide study of Australia's uranium potential: Part I: GIS-assisted manual prospectivity analysis.* Ore Geology Reviews, 2010. **38**(4): p. 334-366.

41. Gabelman, J.W., *Classification of uranium deposits.* Ore Geology Reviews, 1988. **3**(1–3): p. 13-29.

42. *Radionuclides in the Environment*. 2010: Wiley. 522.

43. Wilcken, K.M., Barrows, T., Fifield, L., Tims, S., Steier, P., *AMS of natural 236U and 239Pu produced in uranium ores.* Nuclear Instruments and Methods in Physics Research Section B: Beam Interactions with Materials and Atoms, 2007. **259**(1): p. 727-732.

44. Gosse, J.C. and F.M. Phillips, *Terrestrial in situ cosmogenic nuclides: theory and application.* Quaternary Science Reviews, 2001. **20**(14): p. 1475-1560.

45. Measday, D.F., *The nuclear physics of muon capture.* Physics Reports, 2001. **354**(4–5): p. 243-409.

46. Hadermann, J. and K. Junker, *Emission of neutrons following muon capture in heavy nuclei.* Nuclear Physics A, 1976. **271**(2): p. 401-411.

47. Koning, A.J. and D. Rochman, *Modern Nuclear Data Evaluation with the TALYS Code System.* Nuclear Data Sheets, 2012. **113**(12): p. 2841-2934.

48. Stone, J., Evans, J., Fifield, L., Allan, G., Cresswell, R., *Cosmogenic Chlorine-36 Production in Calcite by Muons.* Geochimica et Cosmochimica Acta, 1998. **62**(3): p. 433-454.

49. Southon, J. and M. Roberts, *Ten years of sourcery at CAMS/LLNL – Evolution of a Cs ion source.* Nuclear Instruments and Methods in Physics Research Section B: Beam Interactions with Materials and Atoms, 2000. **172**(1–4): p. 257-261.

50. Kilius, L.R., J.C. Rucklidge, and A.E. Litherland, *Background reduction for heavy element accelerator mass spectrometry.* Nuclear Instruments and Methods in Physics Research Section B: Beam Interactions with Materials and Atoms, 1988. **31**(3): p. 433-441.

51. Steier, P., Golser, R., Kutschera, W., Liechtenstein, V., Priller, A., et al., *Heavy Ion AMS with a "Small" Accelerator.* Nuclear Instruments and Methods in Physics Research Section B: Beam Interactions with Materials and Atoms, 2002. **188**: p. 283 - 287.

52. Berggren, A.-M., G. Possnert, and A. Aldahan, *Enhanced beam currents with co-precipitated niobium as a matrix for AMS measurements of 10Be.* Nuclear Instruments and Methods in Physics Research Section B: Beam Interactions with Materials and Atoms, 2010. **268**(7–8): p. 795-798.

53. Betz, H.-D., *Charge States and Charge-Changing Cross Sections of Fast Heavy Ions Penetrating Through Gaseous and Solid Media.* Reviews of Modern Physics, 1972. **44**(3): p. 465-539.

54. Tumey, S. *CAMS Nuclear Forensics*. 2014 [cited 2015; Available from: https://cams.llnl.gov/cams-competencies/forensics/nuclear-forensics.

55. Brown, T., Marchetti, A., Martinelli, R., Cox, C., Knezovich, J., Hamilton, T., *Actinide measurements by accelerator mass spectrometry at Lawrence Livermore National Laboratory.* Nuclear Instruments and Methods in Physics Research Section B: Beam Interactions with Materials and Atoms, 2004. **223–224**: p. 788-795.

56. ATSDR, *Toxicological Profile for Uranium.* Washington: US Public Health Services, 1999. **398**.

57. Jurečič, S., Benedik, L., Planinsek, P., Necemer, M., Kump, P., Pihlar, B., *Analysis of uranium in the insoluble residues after decomposition of soil samples by various techniques.* Applied Radiation and Isotopes, 2014. **87**(0): p. 61-65.

58. Martinelli, R., Hamilton, T., Brown, T., Marchetti, A., Williams, R., et al., *Isolation and Purification of Uranium Isotopes for Measurement by Mass-Spectrometry (233, 234, 235, 236, 238U) and Alpha-Spectrometry (232U).* Lawrence Livermore National Laboratory UCRL-TR-232228, 2006.

59. Orabi, A.H., *Determination of uranium after separation using solvent extraction from slightly nitric acid solution and spectrophotometric detection.* Journal of Radiation Research and Applied Sciences, 2013. **6**(2): p. 1-10.

60. Horwitz, E., Dietz, M., Chiarizia, R., Diamond, H., *Separation and preconcentration of uranium from acidic media by extraction chromatography.* Analytica Chimica Acta, 1992. **266**(1): p. 25-37.

61. UTEVA. *Eichrom Technologies*. 2013 June 2015]; Available from: http://www.eichrom.com/products/info/uteva_resin.aspx.

62. BIO-RAD, *AG 1, AG MP-1 and AG 2 Strong Anion Exchange Resin*. Bio-Rad Laboratories, 2000.

63. Stone, J., Fifield, K., Beer, J., Vonmoos, M., Obrist, C., et al., *Co-precipitated silver–metal oxide aggregates for accelerator mass spectrometry of 10Be and 26Al*. Nuclear Instruments and Methods in Physics Research Section B: Beam Interactions with Materials and Atoms, 2004. **223–224**(0): p. 272-277.

64. ESRL. *The Measurements: Accelerator Mass Spectroscopy for 14C after the Stable Isotope Lab*. [cited 2015; Available from: http://www.esrl.noaa.gov/gmd/ccgg/isotopes/accelerator.html.

65. Chadwick, M., Herman, M., Oblozinsky, P., Dunn, M., Danon, Y., et al., *ENDF/B-VII.1 Nuclear Data for Science and Technology: Cross Sections, Covariances, Fission Product Yields and Decay Data*. Nuclear Data Sheets, 2011. **112**(12): p. 2887-2996.

66. Liu, B., Phillips, F., Fabryka-Martin, J., Fowler, M., Stone, W., *Cosmogenic 36Cl accumulation in unstable landforms: 1. Effects of the thermal neutron distribution*. Water Resources Research, 1994. **30**(11): p. 3115-3125.

67. Lal, D., *Production of 3He in terrestrial rocks*. Chem. Geol. Isot. Geos. Section, 1987(66): p. 89 - 98.

68. Cerling, T.E. and H. Craig, *Geomorphology and In-Situ Cosmogenic Isotopes*. Annual Review of Earth and Planetary Sciences, 1994. **22**(1): p. 273-317.

69. Charalambus, S., *Nuclear transmutation by negative stopped muons and the activity induced by comsic-ray muons*. Nuclear Physics, 1971. **A166**: p. 145 - 161.

70. Hayakawa, S., *Cosmic-Ray Physics*. 1969, New York: John Wiley and Sons. 774.

71. Wilson, W., Perry, R., Charlton, W., Parish, T., Estes, G., et al., *SOURCES 4C : a code for calculating ([alpha],n), spontaneous fission, and delayed neutron sources and spectra*. 2002. Medium: ED; Size: 127 p.

72. Deer, W.A., *An introduction to the rock-forming minerals / W.A. Deer, R.A. Howie, J. Zussman*, ed. J. Zussman and R.A. Howie. 1992, Harlow, England : New York, NY: Longman Scientific & Technical ; Wiley.

73. Weaver, C.E. and L.D. Pollard, *The Chemistry of Clay Minerals. Developments in Sedimentology, .* Vol. 15. 1973, New York: Elsevier Scientific Publishing Company.

74. Frondel, C., *Systematic mineralogy of uranium and thorium*, in *Bulletin*. 1958.

75. IAEA, *World Distribution of Uranium Deposits (UDEPO)*, ed. I.A.E.A. (IAEA). 2009.

76. Rosman, K.J.R. and P.D.P. Taylor, *Isotopic Compositions of the Elements 1997 (technical report)*. Pure Applied Chemistry, 1998. **70**(1): p. 217 - 235.

77. Christensen, R., Johnson, W., Branscum, A., Hanson, T., *Bayesian Ideas and Data Analysis: An Introduction for Scientists and Statisticians*. 2011: CRC Press.

78. Robert, C., *The Bayesian Choice: A Decision-Theoretic Motivation*. 1994, New York: Springer-Verlag.

79. Kadane, J., Dickey, J., Winkler, R., Smith, W., Peters, S., *Interactive Elicitation of Opinion for a Normal Linear Model*. Journal of the American Statistical Association, 1980. **75**(372): p. 845-854.

80. Charles, J.G., *Introduction to Markov Chain Monte Carlo*, in *Handbook of Markov Chain Monte Carlo*. 2011, Chapman and Hall/CRC.

81. Lai, T.L., *Introduction to Hastings (1970) Monte Carlo Sampling Methods Using Markov Chains and Their Applications*, in *Breakthroughs in Statistics*, S. Kotz and N. Johnson, Editors. 1997, Springer New York. p. 235-256.

82. Dahlkamp, F.J., *Uranium Ore Deposits*. 1993: Springer Berlin Heidelberg.

83. *MATLAB and Statistics Toolbox Release 2014b*, in *The MathWorks, Inc.*: Natick, Massachusets, United States.

APPENDIX

VI.1. ANU Sample Compositions

UOC Sample	Na_2O	MgO	Al_2O_3	K_2O	SiO_2	CaO	Fe_2O_3	TiO_2
ANU-083	4.85	1.79	9.65	0.66	61.88	4.67	7.01	0.73
ANU-084	1.41	4.25	6.44	4.40	63.67	8.58	10.42	0.63
ANU-085	1.10	0.00	8.92	2.44	84.90	0.69	1.03	0.87
ANU-086	0.72	0.78	0.96	0.55	70.84	17.76	4.77	1.19
ANU-087	0.73	11.97	11.07	0.43	69.08	2.46	2.59	1.37
ANU-088	5.06	1.98	11.25	0.78	69.08	3.84	5.95	0.81
ANU-089	0.59	4.76	11.35	1.39	74.38	0.64	5.29	0.87
ANU-091	0.86	0.20	0.24	0.00	24.60	1.44	1.03	0.84
ANU-092	1.12	0.06	0.72	0.00	37.96	2.13	1.12	0.48
ANU-093	1.34	5.13	12.60	3.61	61.42	0.81	11.24	1.04
ANU-094	0.83	1.21	22.22	5.91	62.13	0.82	2.95	1.58
ANU-095	0.64	0.10	11.19	2.48	83.27	0.43	0.63	0.34
ANU-096	0.84	0.42	0.00	0.00	12.68	1.46	0.41	0.39
ANU-097	0.80	0.61	2.96	0.00	14.07	1.88	1.09	0.63
ANU-098	1.00	4.00	3.56	0.00	26.93	9.49	1.23	1.14
ANU-099	1.06	0.24	1.81	0.69	47.62	0.65	22.29	1.05
ANU-100	0.87	3.04	3.01	0.00	2.35	7.73	1.20	1.28
ANU-101	1.11	6.03	0.22	0.00	32.33	14.73	2.11	0.96
ANU-102	0.43	0.31	0.34	0.12	77.76	1.24	1.90	0.87
ANU-103	0.90	0.11	0.03	0.20	23.22	0.63	24.74	47.66
ANU-104	0.71	1.31	2.23	0.29	33.49	1.23	23.03	35.56
ANU-105	0.95	0.80	0.75	0.70	15.51	0.63	19.90	57.31
ANU-107	0.60	0.65	7.72	1.74	87.39	0.47	0.74	0.50
ANU-108	1.66	0.26	1.58	0.00	16.13	1.31	1.06	1.01
ANU-109	1.25	0.22	1.63	0.00	13.77	1.15	0.92	1.00
ANU-110	3.61	2.63	13.98	3.28	65.65	3.98	5.20	1.20
ANU-111	2.13	0.33	12.44	4.15	77.01	0.70	2.20	0.79
ANU-223	0.71	0.18	0.00	0.00	3.88	3.81	0.49	0.44
ANU-267	0.45	0.14	2.65	0.71	45.69	0.65	0.71	0.57

UOC Sample	Be (ppm)	V (ppm)	Cr (ppm)	Cu (ppm)	Sr (ppm)	Zr (ppm)	Sm (ppm)
ANU-083	389	1712	634	333	413	369	0
ANU-084	33	901	534	358	184	116	4
ANU-085	21	675	255	70	25	88	13
ANU-086	13	817	203	214	5812	620	6655
ANU-087	23	1011	2575	351	40	132	6
ANU-088	261	1471	401	285	224	196	1
ANU-089	23	1189	187	565	14	157	5
ANU-091	7	855	185	592	18	29	18
ANU-092	211	496	285	40	336	28	1
ANU-093	60	527	286	27	64	399	14
ANU-094	48	768	481	1068	64	1714	12
ANU-095	18	551	280	168	73	278	10
ANU-096	6	604	328	103	34	5	1487
ANU-097	27	838	214	2027	60	56	167
ANU-098	0	483	421	0	212	532	232
ANU-099	36	9236	249	8001	102	14	401
ANU-100	14	462	145	195	27	5	1370
ANU-101	11	2341	605	2657	258	13	17
ANU-102	14	865	428	3896	87	8	23
ANU-103	18	8852	14564	1938	1654	1664	225
ANU-104	21	8783	3821	2408	1419	185	169
ANU-105	14	15637	6182	1789	989	111	231
ANU-107	20	700	386	3433	77	336	0
ANU-108	23	1539	170	1987	42	1462	899
ANU-109	27	1618	269	144	40	1578	827
ANU-110	20	756	315	142	201	331	0
ANU-111	49	637	5	226	103	129	20
ANU-223	6	586	116	37	170	263	1590
ANU-267	38	593	483	37320	612	62	74

UOC Sample	Eu (ppm)	Gd (ppm)	Dy (ppm)	Pb (ppm)	Th (ppm)	U (ppm)
ANU-083	1	54	12	421	30	76846
ANU-084	3	26	0	431	2	1318
ANU-085	0	40	4	253	74	236
ANU-086	1723	3813	1189	514	20752	233
ANU-087	4	17	5	213	25	2297
ANU-088	2	21	2	333	18	10725
ANU-089	1	28	13	145	32	6199
ANU-091	5	105	209	1352	152	627434
ANU-092	1	25	3	107	1	500023
ANU-093	1	15	6	216	13	24635
ANU-094	10	29	17	293	26	20414
ANU-095	2	22	6	1630	23	6631
ANU-096	617	1854	746	85	937	745022
ANU-097	61	386	792	84	18	692433
ANU-098	28	129	78	17730	349046	98930
ANU-099	112	448	200	14149	28	203206
ANU-100	630	1849	745	81	795	709583
ANU-101	2	64	11	5013	2	371615
ANU-102	12	58	2	3013	29	147194
ANU-103	78	746	2279	284	1852	19944
ANU-104	24	334	871	600	649	17827
ANU-105	27	565	1596	750	1266	28497
ANU-107	0	49	0	189	33	1465
ANU-108	57	67	87	1246	2754	679196
ANU-109	55	28	112	1196	2196	705940
ANU-110	1	35	4	483	9	3652
ANU-111	2	43	0	366	20	1876
ANU-223	209	1565	2231	9638	157794	634162
ANU-267	13	60	27	1345	13	425531

VI.2.MCNP and SOURCES 4C Coupling (VBA)

```
Sub Input ()
Const ForReading = 1, ForWriting = 2, ForAppending = 8
Const TristateUseDefault = -2, TristateTrue = -1, TristateFalse = 0
Set mydoc = Sheets(1)

'Load Input
folder1 = mydoc.Cells(2, 2)
batname1 = mydoc.Cells(3, 2)
refname1 = mydoc.Cells(4, 2)

folder2 = mydoc.Cells(2, 4)
batname2 = mydoc.Cells(3, 4)
refname2 = mydoc.Cells(4, 4)

FileNumber = mydoc.Cells(6, 2)

' Sources 4C Batch File
CreateObject("Scripting.FileSystemObject").CreateTextFile folder2 & "\" & batname2 'Create a
file
Set batopen = CreateObject("Scripting.FileSystemObject").GetFile(folder2 & "\" & batname2). _
      OpenAsTextStream(ForAppending, TristateUseDefault)

strFirstFile = mydoc.Cells(9, 2)
Set wbk = Workbooks.Open(strFirstFile)
Set MaterialsW = wbk.Sheets("W.F.")
Set MaterialsA = wbk.Sheets("A.F.")
Set SecEq = wbk.Sheets("S.E.")

II = 0
Do While II < FileNumber
   Name = MaterialsW.Cells(1, 4 + II)
   II = II + 1
   stringline = "copy " & folder2 & "\" & Name & " E:\Sources\tape1"
   batopen.WriteLine stringline
   stringline = "start /wait /d E:\Sources sources4c.exe"
   batopen.WriteLine stringline
   stringline = "copy E:\Sources\outp2 " & folder2 & "\" & Name & "o.txt"
   batopen.WriteLine stringline
Loop

' Make Sources Input Files
II = 0
Do While II < FileNumber
```

```
   Name = MaterialsW.Cells(1, 4 + II)
   CreateObject("Scripting.FileSystemObject").CreateTextFile folder2 & "\" & Name 'Create a
file
   Set inputopen = CreateObject("Scripting.FileSystemObject").GetFile(folder2 & "\" & Name). _
         OpenAsTextStream(ForAppending, TristateUseDefault)
   stringline = Name
   inputopen.WriteLine stringline
   stringline = "1 2 1"
   inputopen.WriteLine stringline
   CC = 0
   JJ = 0
   Do While CC < 31
      af = MaterialsA.Cells(2 + CC, 4 + II)
      If af > 0.0005 Then
         JJ = JJ + 1
      End If
      CC = CC + 1
   Loop
   stringline = JJ & " 0"
   inputopen.WriteLine stringline
   NN = 0
   Do While NN < 31
      num = MaterialsA.Cells(2 + NN, 1)
      af = MaterialsA.Cells(2 + NN, 4 + II)
      If af > 0.0005 Then
         stringline = num & " " & af
         inputopen.WriteLine stringline
      End If
      NN = NN + 1
   Loop
   stringline = "20 10.0 0.0"
   inputopen.WriteLine stringline
   stringline = "12"
   inputopen.WriteLine stringline

   NN = 0
   Do While NN < 12
      num = SecEq.Cells(2 + NN, 2)
      af = SecEq.Cells(2 + NN, 4 + II)
      stringline = num & " " & af
      inputopen.WriteLine stringline
      NN = NN + 1
   Loop
   CC = 0
   JJ = 0
```

```
   Do While CC < 8
      af = MaterialsA.Cells(37 + CC, 4 + II)
      If af > 0 Then
         JJ = JJ + 1
      End If
      CC = CC + 1
   Loop
   stringline = JJ & " 4000"
   inputopen.WriteLine stringline
   NN = 0
   Do While NN < 8
      num = MaterialsA.Cells(37 + NN, 3)
      af = MaterialsA.Cells(37 + NN, 4 + II)
      If af > 0 Then
         stringline = num & " " & af
         inputopen.WriteLine stringline
      End If
      NN = NN + 1
   Loop
   II = II + 1
Loop

Dim RetVal
RetVal = Shell("cmd.exe /c" & folder2 & "\" & batname2, 1)

II = 0
' Make MCNP Batch File
CreateObject("Scripting.FileSystemObject").CreateTextFile folder1 & "\" & batname1 'Create a
file
Set batopen = CreateObject("Scripting.FileSystemObject").GetFile(folder1 & "\" & batname1). _
      OpenAsTextStream(ForAppending, TristateUseDefault)
II = 0
Do While II < FileNumber
   inputname = MaterialsW.Cells(1, 4 + II)
   stringline = "mcnp5 i=" & inputname & ".inp" & " o=" & inputname
   batopen.WriteLine stringline
   II = II + 1
Loop

'Make MCNP Input File
II = 0
Do While II < FileNumber
   inputname = MaterialsW.Cells(1, 4 + II)
   CreateObject("Scripting.FileSystemObject").CreateTextFile folder1 & "\" & inputname &
".inp" 'Create a file
```

```
   Set inputopen = CreateObject("Scripting.FileSystemObject").GetFile(folder1 & "\" &
inputname & ".inp"). _
         OpenAsTextStream(ForAppending, TristateUseDefault)
   Set refread = CreateObject("Scripting.FileSystemObject").OpenTextFile(folder1 & "\" &
refname1, ForReading, False)
   Set refread2 = CreateObject("Scripting.FileSystemObject").OpenTextFile(folder2 & "\" &
inputname & "o.txt", ForReading, False)
   check = 0
   Do While Not refread.atendofstream
      stringline = refread.Readline
      Select Case Left(stringline, 3)
         Case "m1 "
            check = 1
         Case "c  "
            check = 0
         Case "SP3"
            check = 2
      End Select
      If check = 0 Then
         inputopen.WriteLine stringline
      ElseIf check = 1 Then
         JJ = 0
         inputopen.WriteLine stringline
         Do While JJ < 30
            cs = MaterialsW.Cells(2 + JJ, 3)
            ar = MaterialsW.Cells(2 + JJ, 4 + II)
            elem = MaterialsW.Cells(2 + JJ, 2)
            stringline = "       " & cs & "       -" & ar & "      $ " & elem
            If ar > 0 Then
               inputopen.WriteLine stringline
            End If
            JJ = JJ + 1
         Loop
         JJ = 0
         Do While JJ < 3
            cs = MaterialsW.Cells(53 + JJ, 3)
            ar = MaterialsW.Cells(53 + JJ, 4 + II)
            stringline = "       " & cs & "       -" & ar
            inputopen.WriteLine stringline
            JJ = JJ + 1
         Loop
      Else
         JJ = 0
         inputopen.WriteLine stringline
         Do While JJ < 14
```

```
            stringline = refread2.Readline
            JJ = JJ + 1
         Loop
         Do While JJ < 35
            stringline = refread2.Readline
            Total = Right(stringline, 9)
            stringline = "       " & Total
            inputopen.WriteLine stringline
            JJ = JJ + 1
         Loop
      End If
   Loop

   UU = MaterialsW.Cells(57, 4 + II)
   stringline = "FM4 " & UU & " 3 102"
   inputopen.WriteLine stringline
   stringline = "M3 92235.70c 1"
   inputopen.WriteLine stringline
   II = II + 1

Loop

End Sub

Sub Output()

strFirstFile = mydoc.Cells(10, 2)
Set wbk = Workbooks.Open(strFirstFile)
Set Results = wbk.Sheets("Results")
Set Data = wbk.Sheets("Data")

'Output Sources 4C total neutron yield
II = 0

Do While II < FileNumber
   inputname = Data.Cells(3 + II, 1)
   Set refread = CreateObject("Scripting.FileSystemObject").OpenTextFile(folder2 & "\" &
inputname & "o.txt", ForReading, False)
   JJ = 0
   Do While JJ < 62
      stringline = refread.Readline
      JJ = JJ + 1
   Loop
      stringline = refread.Readline
      Total = Right(stringline, 9)
```

```
      Data.Cells(3 + II, 6) = Total
      II = II + 1
Loop

'Output MCNP Tally
II = 0

Do While II < FileNumber
   inputname = Data.Cells(3 + II, 1)
   Set refread = CreateObject("Scripting.FileSystemObject").OpenTextFile(folder1 & "\" &
inputname, ForReading, False)
   check = 0
   Do While Not refread.atendofstream
      stringline = refread.Readline
      Select Case Left(stringline, 5)
         Case " mult"
            check = 1
      End Select
      If check = 1 Then
         stringline = refread.Readline
         OUT = Right(stringline, 18)
         TALLY = Left(OUT, 11)
         STD = Right(OUT, 6)
         Results.Cells(3 + II, 5) = TALLY
         check = 0
      End If
   Loop
   II = II + 1
Loop

End Sub
```

VI.3.Two Stage Gibbs / Hastings (Matlab)

```
% Set up Latent Variables using PLS Regression
X = Elem;
Y = U236;
[n,p] = size(X);
[Xloadings,Yloadings,Xscores,Yscores,beta,PctVar] = plsregress(X,Y,Lat);
XLt = Xloadings.';
YLt = Yloadings.';

% Preallocating variables
XS(1,1:Lat) = 0;
```

```
XSprop(1,1:Lat) = 0;
MCNP(1:4,1:5000) = 0;
Xnew(1:5000,1:p) = 0;
Xnew2(1:5000,1:p) = 0;
Err(1:n,1) = 0;
px(1:p,1:50) = 0;
py(1:p,1:50) = 0;
Xprop(1,1:p) = 0;

% Estimating Error Distribution
for I = 1:n
Err(I,1) = Y(I,1) - ([1 X(I,:)]*beta);
end
[~,SigErr] = normfit(Err);
Sig = sqrt(SigErr^2 + Sig236^2);

% Set up Uniform Samples for Latent Variables
XS(1,1:Lat) = mean(Xscores(:,1:4));

% Gibbs Sampler (Burn in)
for I = 1:5000 %burn in of 10000
   for J = 1:Lat
                    mu = (Unk236 - mean(Y)) -((XS(1,1:Lat) * YLt) - (XS(1,J)*YLt(J,1)));
      mu = mu / YLt(J,1);
                    sigma = sqrt(Sig^2 / YLt(J,1)^2);
                    ii = 0;
      while ii == 0
         XS(1,J) = normrnd(mu,sigma,1,1);
         if (min(Xscores(:,J)) <= XS(1,J))&&(XS(1,J) <= max(Xscores(:,J)));
            ii = 1;
         end
      end
   end
end

% Gibbs Sampler (Steady State)
for I = 1:5000 %5000 iterations
   for J = 1:Lat
                    mu = (Unk236 - mean(Y)) -((XS(1,1:Lat) * YLt) - (XS(1,J)*YLt(J,1)));
      mu = mu / YLt(J,1);
                    sigma = sqrt(Sig^2 / YLt(J,1)^2);
                    ii = 0;
      while ii == 0
         XS(1,J) = normrnd(mu,sigma,1,1);
         if (min(Xscores(:,J)) <= XS(1,J))&&(XS(1,J) <= max(Xscores(:,J)));
```

```
            ii = 1;
          end
        end
    end
    Xnew(I,:) = (XS(1,:) * XLt) + mean(X);
end

% Calculate Initial Acceptance
Accept(2,1) = (XS(1,:) * YLt) + mean(Y);
Accept(2,1) = normpdf(Accept(2,1),Unk236,Sig236);

% Create PDFs for elemental dist. based on Gibbs
for J = 1:p
    [~,edges,bin] = histcounts(Xnew(:,J),50);
    count = accumarray(bin,1);
    for I = 1:50
        px(J,I) = (edges(I) + edges(I+1))/2;
    end
    py(J,:) = count;
end
Xtemp(1,:) = Xnew(Samp,:);

% Create Excel COM server
Excel = actxserver('Excel.Application');

% Open Excel Files
workbook = Excel.Workbooks.Open('E:\MCNP\Work\Met\VBA(Met).xlsm');

% Metropolis Hastings for REE
for I = 1:5000
    for J = 1:p
        if J == 17
            Xprop(1,J) = normrnd(Xtemp(1,J),0.02);
        elseif J == 18
            Xprop(1,J) = normrnd(Xtemp(1,J),0.02);
        else
            Xprop(1,J) = randpdf(py(J,:),px(J,:),[1,1]);
        end
    end

    % Write material data
    xlswrite1('E:\MCNP\Work\Met\VBA(Met).xlsm', Xprop(1,:).','W.F.', 'D2:D21');
    workbook.Save

    % Run VBA macros
```

```
   Excel.Run('Sources4c');
   system('E:\MCNP\Work\Met\Met.bat');
   Excel.Run('OutputResults');

   % Read Results into matlab
   MCNP(2:3,I) = xlsread1('E:\MCNP\Work\Met\VBA(Met).xlsm','AR','B3:B4');
   MCNP(1,I) = Xprop(1,20)/100;
   MCNP(4,I) = (1.68551484185288E-07 * MCNP(2,I) * MCNP(3,I)) / MCNP(1,I);

   % Calculate acceptance ratio and modify parameters
   Accept(1,1) = normpdf(MCNP(4,I),Unk236,Sig236);
   AR = Accept(1,1) / Accept(2,1);
   W = rand();
   if W <= AR
      Accept(2,1) = Accept(1,1);
      Xtemp = Xprop;
      Xnew2(I,:) = Xprop(1,:);
   else
      Xnew2(I,:) = Xtemp(1,:);
   end
end

% Quit Excel and Delete Handles/Variables
Excel.Quit
delete(Excel)
clear Excel workbook status Xtemp Accept Xprop MCNP px py
```